Thesis for the degree
Doctor of Philosophy

Submitted to the Scientific Council of the
Weizmann Institute of Science
Rehovot, Israel

By
Eran Sagi

עבודת גמר (תזה) לתואר
דוקטור לפילוסופיה

מוגשת למועצה המדעית של
מכון ויצמן למדע
רחובות, ישראל

מאת
ערן שגיא

פאזות טופולוגיות בנוכחות אינטראקציות חזקות
Strongly interacting topological phases

Advisor:
Prof. Yuval Oreg

מנחה:
פרופ' יובל אורג

June 2018

תמוז תשע"ח

Abstract

In this thesis, we develop and apply non-perturbative approaches for the study of fractional topological phases. Such phases present a considerable challenge due to their inherent strongly interacting nature, and are indeed not well understood theoretically. In fact, tractable models of fractional phases (beyond the quantum Hall regime) are scarce. Throughout this thesis, we make heavy use of the coupled-wire approach, where the available tools for interacting one-dimensional systems are applied to higher dimensional ones by breaking them into arrays of weakly coupled wires.

We start by using the coupled-wire approach to construct analytically tractable models for a large set of two-dimensional fractional topological insulators. In particular, this approach allows us to write tractable models of exotic non-Abelian phases. We then extend the coupled-wire approach to three-dimensions and use it to propose models of fractional strong topological insulators. Using these models, we study non-trivial properties of the surface once it is gapped by various mechanisms. In addition, we use the coupled-wire approach to construct fractional chiral superconductors, constituting the fractional analogs of the $p + ip$ superconductor. Such phases give rise to a non-trivial conformal field theories on the edge, as well as non-Abelian bulk excitations. We further introduce a generalized coupled-layer approach to realize strongly interacting topological phases in three-dimensions. We do this by leveraging the recently discovered duality between the Dirac theory in two-dimensions and QED_3, the theory of quantum electrodynamics, as well as the phenomenon of spontaneous interlayer coherence.

In addition to the above fundamental theoretical results, we also focus on more experimentally realistic proposals. First, we propose an experimental configuration which effectively realizes fractional quantum Hall physics with a torus topology, giving rise to a topological ground state degeneracy. We suggest an experiment where imprints of this fundamental degeneracy can be probed. Finally, we propose path for experimentally realizing effective interacting spin models, and in particular spin-liquid phases, using topological semiconductor nanowires in a Cooper boxes.

תקציר

בתזה זו, אנו מפתחים כלים אנליטיים לא הפרעתיים למטרת חקר פאזות טופולוגיות שבריות. פאזות אלה מהוות אתגר משמעותי עקב הימצאות אינטראקציות חזקות בבסיסן, ואכן, ההבנה התיאורטית שלהן לוקה בחסר. למעשה, מודלים פתירים עבור פאזות אלה (למעט מערכות המאופיינות באפקט הול הקוונטי) הינם מצרך נדיר. בתזה זו, אנו משתמשים באופן נרחב בשיטת החוטים המצומדים, בה מערכות רב-מימדיות ממודלות על ידי מערך של חוטים המצומדים באופן חלש. במודלים אלה, כלים שפותחו עבור מערכות חד-מימדיות בעלות אינטראקציות חזקות משמשים לחקר מערכות רב-מימדיות.

תחילה, אנו משתמשים בשיטת החוטים המצומדים לתכנון מודלים עבור מבודדים טופולוגיים שבריים דו-מימדיים. בפרט, גישה זו מאפשרת לנו לתכנן מודלים עבור פאזות לא-אבליות. בהמשך, אנו מכלילים את שיטת החוטים המצומדים לתלת-מימד, ומציגים מודלים עבור מבודדים טופולוגים חזקים שבריים. בעזרת מודלים אלה, אנו חוקרים תופעות לא טריוויאליות הקורות על השפה בנוכחות פער אנרגיה הנוצר על ידי מנגנונים שונים. בנוסף, אנו משתמשים בשיטת החוטים המצומדים לבניית מודלים עבור מוליכי על כיראליים שבריים, המהווים את האנלוג השברי של מוליכי-על מסוג $p + ip$. פאזות אלה מאופיינות על ידי תורות שדה קונפורמיות לא טריוויאליות על השפה, ועירורים לא אבליים הרחק ממנה. כמו כן, אנו משתמשים בשיטת שכבות מצומדות לצורך חיזוי פאזות טופולוגיות בעלות אינטראקציות חזקות בתלת-מימד. אנחנו עושים זאת תוך שימוש בדואליות שהתגלתה לאחרונה בין תורת דיראק הדו-מימדית לתורה המתארת אלקטרודינמיקה קוואנטית, QED_3, ובתופעת הקוהרנטיות הבין-שכבתית.

בנוסף לתוצאות אלה, אנו מתמקדים בתחזיות הקרובות יותר לניסויים. תחילה, אנו מציעים מערכת הממשת את הפיסיקה של אפקט הול הקוונטי על טופולוגיה של טורוס, בו קיים ניוון טופולוגי של מצב היסוד. כמו כן, אנו מציעים ניסוי החושף אותות של ניוון יסודי זה. לבסוף, אנו מציעים מימוש ניסיוני של מודלי-ספין בעלי אינטראקציות חזקות, המתארים בין היתר נוזלי-ספין (spin-liquids), בעזרת חוטים מוליכים למחצה בקופסאות קופר.

Acknowledgements

First of all, I would like to thank my advisor, Yuval Oreg, for his guidance over these years, and for introducing me to the field of condensed matter physics. The long hours we spent discussing physics were truly a pleasure, and were indispensable in allowing me to develop a deeper understanding of the problems we were facing.

Secondly, I was fortunate to closely collaborate with Ady Stern, Erez Berg, David Mross, Raul Santos, and Zohar Nussinov over these years. I want to thank each of them–it was a pleasure having the opportunity to be exposed to so many different ideas and approaches to physics, and I can genuinely say that I have learned a lot from each of these collaborations.

I would also like to acknowledge my fellow students. The fruitful discussions and long coffee breaks have made these years much more enjoyable, and led to many great insights.

Finally, I want to thank my wife Carmel, for the support and understanding throughout these years, as well as her ability to put things in perspective for me.

List of Abbreviations

TI Topological Insulator

FTI Fractional Topological Insulator

CI Chern Insulator

FCI Fractional Chern Insulator

IQHE Integer Quantum Hall Effect

FQHE Fractional Qunatum Hall Effect

FCSC Fractional Chiral Superconductors

SPT Symmetry Protected Topological phases

SET Symmetry Enriched Topological phases

CFT Conformal Field Theory

MZM Majorana Zero Mode

List of Publications

1. E. Sagi, A. Stern, and D. F. Mross, Composite Weyl semimetal as a parent state for three dimensional topologically ordered phases, arxiv: 1806.01860

2. E. Sagi, H. Ebisu, Y. Tanaka, A. Stern, and Y. Oreg, Spin liquids from Majorana Zero Modes in a Cooper Box, arxiv: 1806.03304

3. E. Sagi, A. Haim, E. Berg, F. von Oppen, and Y. Oreg, Fractional chiral superconductors, Phys. Rev. B 96, 235144 (2017)

4. E. Sagi and R. A. Santos, Supersymmetry in the Fractional Quantum Hall Regime, Phys. Rev. B 95, 205144 (2017)

5. H. Ebisu, E. Sagi, Y. Tanaka, and Y. Oreg, Generalized parafermions and non-local Josephson effect in multi-layer systems, Phys. Rev. B 95, 075111 (2017)

6. E. Sagi and Z. Nussinov, Emergent quasicrystals in strongly correlated systems, Phys. Rev. B 94, 035131 (2016)

7. E. Sagi and Y. Oreg, From an array of quantum wires to three-dimensional fractional topological insulators, Phys. Rev. B 92, 195137 (2015)

8. E. Sagi, Y. Oreg, A. Stern, B. I. Halperin, Imprint of topological degeneracy in quasi-one-dimensional fractional quantum Hall states, Phys. Rev. B 91, 245144 (2015)

9. E. Sagi and Y. Oreg, Non-Abelian topological insulators from an array of quantum wires, Phys. Rev. B 90, 201102(R) (2014)

Contents

8   Spin liquids from Majorana Zero Modes in a Cooper Box   94

9   Discussion   103

References   105

A   Appendix: Fractional chiral superconductors   116

**B   Appendix: Composite Weyl semimetal as a parent state for three dimensional
topologically ordered phases   126**

C   Appendix: Spin liquids from Majorana Zero Modes in a Cooper Box   136

Chapter 1

Introduction

Historically, phases of matter have been classified through the celebrated Landau paradigm, which distinguishes phases according to the concepts of the order parameter and spontaneous symmetry breaking. Despite its success, it has been recognized in the past few decades that the Landau paradigm fails to provide a complete description of all phases, with the missing components being topological properties of the quantum wavefunction.

This became apparent with the observation of integer and fractional quantum Hall states [1, 2], and later, with the discovery of $\mathbb{Z}_2$ topological insulators in two-dimensions (2D) and three-dimensions (3D) [3–15]. The above are examples of what is now collectively called *topological phases of matter*. More recent evidence for observations of topological phases include topological superconducting phases [16–25], topological crystalline insulators [26–34], topological semimetallic phases [35–45], spin liquids [46], and others.

One can roughly group gapped topological phases into two categories: "integer" and "fractional" phases (in analogy to the integer and fractional quantum Hall states). In the former, the phases can generically be understood in the absence of interactions. They are associated with a topological index in the bulk, and protected gapless edge modes (related by the bulk-edge correspondence). The presence of symmetries constraints the form of the Hamiltonian and therefore the single particle wavefunctions, resulting in diverse topological characteristics depending on the symmetries of the system. This leads to the notion of symmetry protected topological phases (SPTs). In fact, non-interacting SPTs protected by time-reversal, particle-hole, and chiral symmetries have been fully classified [47, 48]. Beyond this celebrated periodic table, topological phases protected by other symmetries, such as lattice symmetries [26–34], have also been thoroughly studied.

Interactions affect the above picture in two major ways: first, they can reduce the non-interacting classification by producing paths in parameter space that connect topologically distinct states without closing the gap, thus making them topologically equivalent. Second,

they can generate strongly interacting topological phases which cannot exist in the absence of interactions.

Indeed, fractional phases (also known as or topologically ordered phases), are examples of states that cannot be understood in the absence of interactions. These states are usually characterized by remarkable properties such as fractionalization of quantum numbers, anyonic excitations, and a ground state degeneracy determined by the topology of the underlying space. Since interactions stabilize these phases, their study generally requires non-perturbative methods, making their analysis highly non-trivial. Indeed, solvable models giving rise to such phases of matter are scarce.

A relatively recent approach is the coupled-wire approach [49–72]. In this approach, a 2D or 3D topologically ordered phase is constructed from coupled 1D gapless systems, each of which is described by a conformal field theory (CFT). Since the conformal algebra is infinite in $1+1$-dimensions, it supplies us with many analytical tools, making gapless one-dimensional (1D) systems tractable even in the presence of strong interactions. Within the coupled-wire approach, this machinery plays a central role in allowing us to write exactly solvable or analytically tractable model systems realizing fractional phases in higher dimensions. Throughout this thesis, we extensively use the coupled-wire approach to study of fractional phases in two- and three-dimensions.

The structure of this thesis is as follows: Chapter 2 presents the main tool used throughout this thesis - the coupled-wire approach - and its application for the study of fractional quantum Hall states. Chapter 3 is based on the results of Ref. [54], where we demonstrate how the coupled-wire approach can be used to construct fractional Chern and topological insulators in 2D. Chapter 4 presents the results of Ref. [63], in which we propose an experimental realization of effective fractional quantum Hall states with a torus topology, and suggest imprints of the resulting topological ground state degeneracy. Chapter 5 discusses the results of Ref. [58], where we extend the coupled-wire approach to three-dimensions and use it to construct three-dimensional fractional topological insulators. Chapter 6 is based on the results of Ref. [71], in which we use the coupled-wire approach to propose a fractional chiral superconductor phase, constituting the fractional analog of the $p+ip$ superconductor. Chapter 7 introduces the results of Ref. [73], where we leverage the recently discovered duality between a two-dimensional Dirac cone and QED_3 to propose the emergence of a strongly correlated 'composite Weyl semimetal', as well as topologically ordered phases, in three-dimensions. Chapter 8 presents the results of Ref. [74], where we propose a path for experimentally realizing interacting spin models from topological semiconductor nanowires in Cooper boxes. Finally, in chapter 9 I will discuss the main results of this thesis and their possible extensions.

Chapter 2

Methods: The coupled-wire approach

In this section, I will present the coupled-wire approach, which will be used extensively throughout this thesis. To be specific, I will demonstrate how the coupled-wire approach is used to study quantum Hall states [49, 50, 75, 76].

2.1 Integer quantum Hall states

Consider a two dimensional system of spinless electrons with an external magnetic field. We decompose the plane on which the electrons reside into an array of N weakly coupled wires, making it a highly anisotropic 2D system. As we will see, within this approach, by bosonizing the wire degrees of freedom, we can explicitly write model Hamiltonians for fractional quantum Hall states.

We choose a gauge in which the vector potential $\mathbf{A}$ points in the $\hat{x}$ direction. In the absence of coupling between the wires, the spectrum is now made shifted parabolas. We define $2k_\phi$ as the shift between two adjacent parabolas due to the magnetic field, and k_F^0 as the Fermi-momentum in the absence of an external magnetic field. The spectrum of the j'th wire is given by

$$E_j(k_x) = \frac{\left(k_x - 2k_\phi j\right)^2}{2m},$$

where m is the effective mass of the electrons. We start by linearizing the spectrum, and describing the low-energy physics in terms of $2N$ chiral boson fields $\phi_{R/L}^j$, such that

$$\psi_{R/L}^j \propto e^{i\left(\phi_{R/L}^j + k_{R/L}^j x\right)}, \tag{2.1}$$

where $\psi_{R/L}^j$ is the fermion annihilation operator of the right/left moving component of wire

number j, and $k^j_{R/L}$ is the corresponding Fermi-momentum. The boson fields satisfy

$$\left[\phi_{R/L}(x), \phi_{R/L}(x') \right] = \pm i\pi \text{sign}(x - x'),$$

thus ensuring that the electron operators defined in Eq. 2.19 satisfy the fermionic anti-commutation relations.

The low-energy excitations are given by the quadratic Hamiltonian

$$H_x = \frac{v}{2\pi} \sum_j \int dx \left[\left(\partial \phi_R^j \right)^2 + \left(\partial \phi_L^j \right)^2 \right]$$

in the absence of interactions. The density operators (measuring density deviations from the homogeneous ground state) are given by $\rho^j_{R/L}(x) = \pm \frac{1}{2\pi} \partial_x \phi^j_{R/L}$. Therefore, density-density interactions leave the Hamiltonian quadratic in terms of the ϕ-fields, making the bosonization approach extremely useful in studying 1D interacting systems.

Within our construction, the quantum Hall filling factor is given by

$$\nu = \frac{k_F^0}{k_\phi}. \tag{2.2}$$

Given a filling factor ν, the Fermi momenta take the form

$$k^j_{R/L} = k_\phi \left(2j \pm \nu \right) + \beta, \tag{2.3}$$

where β is a gauge dependent parameter, which we simply set to zero.

To construct Abelian quantum Hall states, we identify a set of mutually (and self) commuting cosine terms that do not break translational invariance (i.e., conserve momentum), and are capable of completely gapping out the bulk. By an analysis of the gapless modes that remain near the edges and the properties of the bulk excitations, we will then be able to identify various QHE states. Notice that once we linearize the spectrum, the only remnants of the original model are the Fermi-momenta (Eq. 2.3), which dictate the allowed cosine terms coupling different chiral modes (through momentum conservation). In the quantum Hall case, these are determined by the filling factor (which in turn is a function of the magnetic field and the density of electrons). In other systems studied in this thesis, it will generally be a function of different model parameters, such as the spin-orbit coupling.

The simplest quantum Hall system corresponds to $\nu = 1$, in which case adjacent parabolas cross at the chemical potential (that is, $k_R^j = k_L^{j+1}$). In this case, simple tunneling operators between the wires conserve momentum, and can gap out the spectrum, leaving only a single

free chiral mode on each edge. To be specific, the terms we consider are

$$H_{\nu=1} = t \sum_{j=1}^{N-1} \int dx \cos\left(\phi_R^j - \phi_L^{j+1}\right).$$ (2.4)

These terms are relevant, and therefore gap out the bulk degrees of freedom. If the system contains N wires, the two modes $\phi_{L,1}$ and $\phi_{R,N}$ remain free, and represent the chiral edge modes of the $\nu = 1$ IQHE.

The generalization to any other IQHE states is simple. Indeed, for $\nu = n$, with n being an integer, the terms which conserve momentum are n'th-nearest neighbor tunneling operators of the form

$$H_{\nu=n} = t \sum_{j=1}^{N-n} \int dx \cos\left(\phi_R^j - \phi_L^{j+n}\right).$$ (2.5)

We now have n chiral modes on each edge: $\phi_L^1, \phi_L^2, \cdots, \phi_L^n$ and $\phi_R^N, \phi_R^{N-1}, \cdots, \phi_R^{N-n+1}$, as expected for the $\nu = n$ IQH state.

2.2 Laughlin states

The simplest fractional states belong to the so-called Laughlin series, occuring at filling factors of the form $\nu = 1/m$, with m being an odd integer. As opposed to the integer case, multi-electron processes are required in order to form a set of commuting terms which conserve momentum and can gap the bulk. In order to identify this set of terms, it is convenient to define a new set of chiral fields through the transformation

$$\eta_{R/L}^j = \frac{m+1}{2}\phi_{R/L}^j + \frac{1-m}{2}\phi_{L/R}^j.$$ (2.6)

This mapping should be accompanied by a transformation of the momenta

$$q_{R/L}^j = \frac{m+1}{2}k_{R/L}^j + \frac{1-m}{2}k_{L/R}^j.$$ (2.7)

In terms of the fermions, the mapping takes the form

$$\tilde{\psi}_{R/L}^j = \left(\psi_{R/L}^j\right)^{\frac{m+1}{2}} \left(\psi_{L/R}^j\right)^{\frac{1-m}{2}},$$ (2.8)

where $\tilde{\psi}_{R/L}^j \propto e^{i\left(\eta_{R/L}^j + q_{R/L}^j x\right)}$, a negative exponent should be understood as an Hermitian conjugation, and the multiplication of identical Fermion operators should be taken with an ap-

propriate point splitting. Note that while this transformation is very simple in the bosonic language, it is non-linear in terms of the fermions.

The η-fields satisfy the commutation relations

$$\left[\eta_{R/L}(x), \eta_{R/L}(x')\right] = \pm i\pi m \operatorname{sign}(x - x'),$$

ensuring that the transformed $\tilde{\psi}$-fields satisfy the fermionic anti-commutation relations as well.

It can now be checked that the momenta q form a pattern identical to the $\nu = 1$ case. Similar to the previous section, this means that operators of the form

$$H_{\nu=1/3} = u \sum_{j=1}^{N-1} \int dx \cos\left(\eta_R^j - \eta_L^{j+1}\right) \tag{2.9}$$

conserve momentum and can gap out the bulk in the strong coupling limit. In terms of the original fermions, this term results from a hopping process accompanied by particle-hole excitations. Notice that the above terms are actually irrelevant in the weak coupling limit. They can however flow to the strong coupling limit if the amplitude u is made large enough. Alternatively, forward scattering interactions can alter the Luttinger-liquid fixed point and make them relevant.

Once the bulk is gapped, the two modes $\eta_{L,1}$ and $\eta_{R,N}$ remain decoupled, and we get a single chiral η-mode on each edge, which satisfy the chiral Luttinger liquid structure of the Laughlin-edge modes

$$\left[\eta_\sigma(x), \partial \eta_\sigma(x')\right] = 2\pi\sigma i m \delta(x - x'). \tag{2.10}$$

To make contact with more conventional notations (see, e.g., [77]), we define the (bosonized) quasiparticle operators

$$\chi_i = \frac{\eta_i}{m}, \tag{2.11}$$

which satisfy

$$\left[\chi_\rho(x), \partial \chi_\rho(x')\right] = \frac{2\pi i}{m}\delta(x - x').$$

In terms of these, the electron operators take the well-known form $\tilde{\psi} = e^{im\chi}$.

If the cosines flow to the strong coupling limit, the low energy bulk excitations are local kink excitations where the argument $\eta_i^R - \eta_{i+1}^L$ jump by 2π from one minimum of the cosine to another - i.e., configurations satisfying

$$\partial_x\left(\eta_i^R - \eta_{i+1}^L\right) = \pm 2\pi\delta(x - x_0) \tag{2.12}$$

where x_0 is the location of the kink.

Using the definition of the η-fields, the total charge operator is given by

$$
\begin{aligned}
Q &= e \sum_{i=1}^{N} \int dx \frac{1}{2\pi} \partial_x \left(\phi_i^R - \phi_i^L \right) \\
&= \frac{e}{m} \sum_{i=1}^{N} \int dx \frac{1}{2\pi} \partial_x \left(\eta_i^R - \eta_i^L \right) \\
&= \frac{e}{m} \sum_{i=1}^{N} \int dx \frac{1}{2\pi} \partial_x \left(\eta_i^R - \eta_{i+1}^L \right).
\end{aligned}
$$

Therefore, the kink configuration in Eq. 2.12, is associated with a charge of $\pm e/m$, as expected from Laughlin quasiparticles. One can additionally study the mutual statistics of two kink excitations and find that it is identical to that of a Laughlin quasiparticles [50].

In the analysis of the $v = 1/m$ state, we used a transformation to the new $\tilde{\psi}$ fields, whose momentum structure resembles that of electrons in a $v = 1$ state. This allowed us to repeat the construction of the $v = 1$ case and stabilize a Laughlin state. In what follows we turn to study hierarchical multi-component FQH states, and demonstrate that similar transformations map them to non-interacting IQH states of the form $v = n$.

2.3 Hierarchical quantum Hall states

In this section we describe hierarchical Abelian states defined by a $n \times n$ K-matrix with odd (even) diagonal (off-diagonal) entries. The charge vector $\mathbf{Q}$ in this case is a vector of dimension n with all entries equal 1. The corresponding filling factor is given by [77]

$$
v = \mathbf{Q}^T K^{-1} \mathbf{Q}. \tag{2.13}
$$

For convenience, we artificially group the wires into sets of n wires (and assume we have N such groups). Accordingly, we denote the chiral boson fields as $\phi_{R/L}^{j,l}$, where $j = 1 \ldots N$, and $l = 1 \ldots n$. The associated momentum values take the form $k_{R/L}^{j,l} = k_\phi \left(2 \left[(j-1)n + l \right] \pm v \right)$. For convenience, we define n-dimensional vectors containing the n chiral field for each value of j:

$$
\overrightarrow{\phi}_{R/L}^{j} = \begin{pmatrix} \phi_{R/L}^{j,1} \\ \phi_{R/L}^{j,2} \\ \vdots \\ \phi_{R/L}^{j,n} \end{pmatrix}. \tag{2.14}
$$

To follow the same logic as before, we would like to map this state to an integer quantum Hall state with filling n (which has n edge modes, as required). This can be done through a simple generalization of Eq. 2.6:

$$\overrightarrow{\eta}_{R/L}^{\,j} = \frac{K+1}{2}\,\overrightarrow{\phi}_{R/L}^{\,j} + \frac{1-K}{2}\,\overrightarrow{\phi}_{L/R}^{\,j}. \tag{2.15}$$

In terms of these fields the momentum structure indeed corresponds to a state with filling $\nu = n$, such that terms of the form

$$H_{\nu = \mathbf{Q}^T K^{-1} \mathbf{Q}} = u \sum_{j=1}^{N-1} \sum_{l=1}^{n} \int dx \cos\left(\eta_R^{j,l} - \eta_L^{j+1,l} \right) \tag{2.16}$$

gap out the bulk in the strong coupling limit. Again, these terms describe hopping terms with particle-hole excitations in terms of the original electrons. The fields $\overrightarrow{\eta}_L^{\,1}$ and $\overrightarrow{\eta}_R^{\,N}$ remain free, and satisfy the commutation relations

$$\left[\eta_L^{1,l}(x), \partial \eta_L^{1,l'}(x') \right] = -2i\pi K_{l,l'} \delta(x - x'). \tag{2.17}$$

$$\left[\eta_R^{N,l}(x), \partial \eta_R^{N,l'}(x') \right] = 2i\pi K_{l,l'} \delta(x - x'). \tag{2.18}$$

These are the low energy degrees of freedom constituting the edge theory. As the above fields all carry a charge of 1 electron, the n electron operators on the edges take the form

$$\Psi_l = e^{i\eta^l}. \tag{2.19}$$

Again, to make contact with more conventional notations, we can define the quasiparticle fields χ on the first edge according to

$$\vec{\chi} = K^{-1}\vec{\eta}.$$

Their commutation relations take the form

$$\left[\chi_l(x), \partial \chi_{l'}(x') \right] = \pm 2i\pi K_{l,l'}^{-1} \delta(x - x'),$$

and in terms of them, the electron operator is

$$\Psi_l = e^{i\sum_{l'} K_{ll'} \chi_{l'}}.$$

The cosine terms in Eq. 2.16, again give rise to kink excitations of the form

$$\partial_x \left(\vec{\eta}_j^R - \vec{\eta}_{j+1}^L \right) = 2\pi \hat{e}_j \delta(x - x_0), \tag{2.20}$$

where $\hat{e}_j$ is a unit vector whose j'th entry is 1 and the rest vanish. The total charge can now be written as

$$\begin{aligned} Q &= \frac{e}{2\pi} \sum_j \int dx \vec{Q}^T \partial_x \left(\vec{\phi}_j^R - \vec{\phi}_j^L \right) \\ &= \frac{e}{2\pi} \sum_j \int dx \vec{Q}^T K^{-1} \partial_x \left(\vec{\eta}_j^R - \vec{\eta}_{j+1}^L \right). \end{aligned}$$

Therefore, the charge associated with the kink excitation, Eq. 2.20 takes the form $e\vec{Q}^T K^{-1} \hat{e}_j$. Combinations of these charges take the form $e\vec{Q}^T K^{-1} l$, which indeed reproduces the expected charges in hierarchical states.

2.4   Non-Abelian states

To discuss generalizations to non-Abelian quantum Hall states, it is useful to first take a slightly broader view of the approach presented so far. The constructions of Abelian quantum Hall states can be described as follows: first, within each wire (or more generally, each unit cell), we applied a transformation that defines new set of boson fields η, which behave like the chiral Luttinger liquid degrees of freedom we expect to find on the edge after we gap out the bulk.

Then, using these new degrees of freedom, we couple a right moving operator η_j^R of one unit cell with the left mover η_{j+1}^L of the next unit cell (see the upper part of Fig. 2.1 for a schematic depiction). This leaves the left (right) moving sector of the first (last) wire gapless. By construction, the edge modes are the expected chiral Luttinger liquid degrees of freedom.
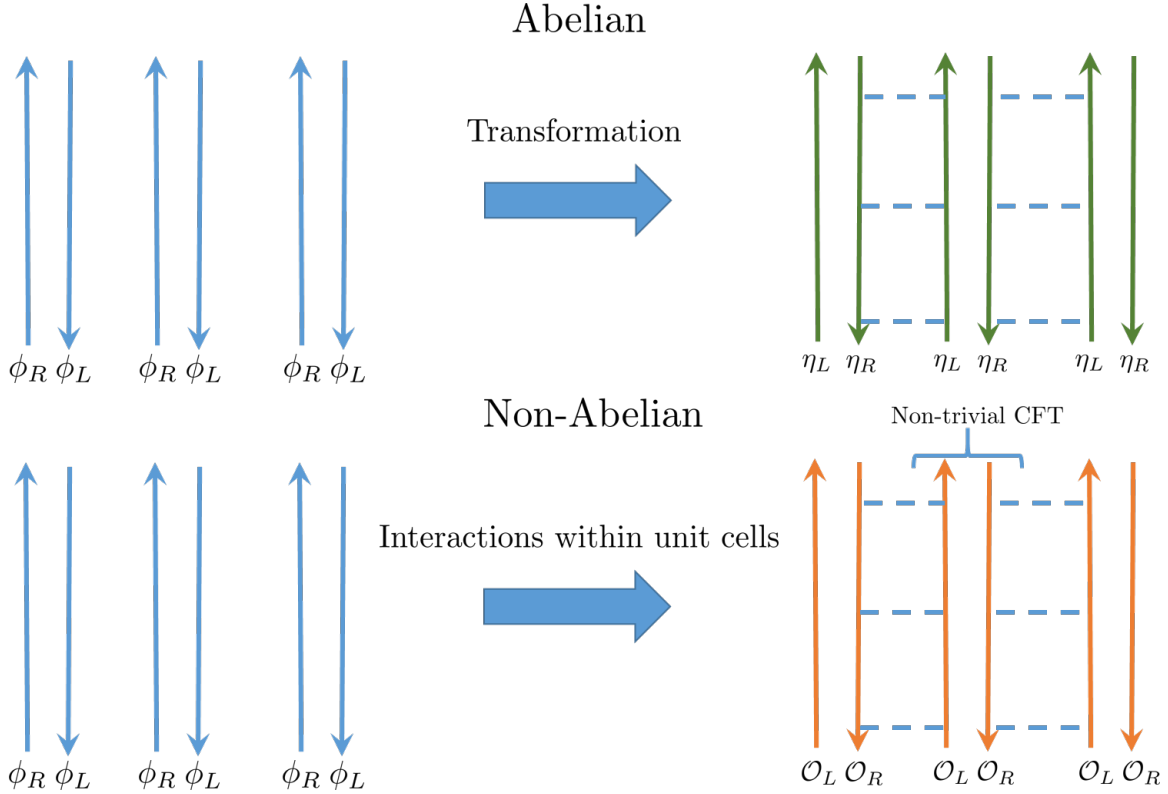
Figure 2.1: A schematic depiction of the coupled-wire approach for realizing Abelian and non-Abelian topological states.

To generalize the coupled-wire approach to non-Abelian states, we need to generate gapped systems with more general chiral CFTs on the edges. To do that, we generalize the above strategy: first, we write interacting terms within each unit cell, in such a way that each unit cell is described by a new fixed point, described by the CFT which is the non-chiral version of the CFT expected to reside on the edge of the sample. Identifying fields $\mathcal{O}_j^R$ ($\mathcal{O}_j^L$) belonging to the right (left) moving sectors of this CFT, one can then write terms of the form

$$\sum_j \int dx \left[\mathcal{O}_j^{R\dagger} \mathcal{O}_{j+1}^L + \text{h.c.} \right], \tag{2.21}$$

thereby gapping the bulk and leaving behind a chiral version of the CFT on each edge. This process is presented schematically in the lower part of Fig. 2.1.

Indeed, this approach was used by Teo and Kane [50] to realize the non-Abelian Moore-Read and Read-Rezayi states, and will be used in this thesis to construct novel non-Abelian phases of matter.

Chapter 3

Non-Abelian topological insulators from an array of quantum wires

This chapter describes the results of our first project, presented in Ref. [54]. In this project, we demonstrate that the coupled-wire approach can be useful in studying 2D fractional states beyond the quantum Hall regime. In particular, we focused on constructing tractable models for fractional Chern and topological insulators.

3.1 Introduction

Prior to this work, it was demonstrated [49, 50, 75, 76] that integer and fractional quantum Hall states may be elegantly understood through tractable coupled-wire models. The wire degrees of freedom are described through the bosonization formalism, allowing one to treat interaction effects analytically. Indeed, this approach allows one to treat inter-wire multi-electron terms that stabilize strongly interacting FQH states.

The purpose of this work is to demonstrate that the coupled-wire approach can be used to construct tractable models for fractional phases beyond the quantum Hall regime. In particular, we focused on two types of 2D phases: fractional Chern insulators (FCIs) and fractional topological insulators (FTIs).

An FCI is the fractional analog of a Chern insulator – a material experiencing the IQHE without a net magnetic field. The possibility of an FCI has been discussed quite extensively in the literature (see Ref. [78] for a review). Indeed, numerical investigations of lattice models with nearly flat bands presented strong evidence for FCI states (see, e.g., [79–84]). In this work we use the coupled-wire approach to present an alternative analytic approach to the subject, which in particular does not require the presence of flat bands.

Using an analogy between a magnetic field and a spin-orbit coupling, we then generalize the above model to a time-reversal invariant FTI. Such phases have indeed been discussed previously (see, e.g., Refs. [85–92]), yet analytically tractable models remain scarce.

3.2   Wire construction of a Chern insulator

The existence of edge modes [93] in the QHE can be understood in various ways. In particular, one can understand them by studying the classical circular trajectories of electrons in a magnetic field, which turn into chiral "skipping orbits" near the edge. As we argue, it is possible to construct a similar semi-classical theory for a specific set of Chern insulators as well. Consider a system consisting of electrons and holes (whose masses differ in sign). In the presence of a magnetic field, their classical trajectories are curved in opposite directions. If, however, the electrons and the holes experience opposite magnetic fields, their trajectories will be curved in the same direction. One can imagine constructing a Chern-insulator by separating the plane into regions which contain only holes and only electrons. If the magnetic field is opposite in the two regions, the classical trajectories will be similar to those of electrons in a uniform magnetic field. This suggests that, upon quantization, this system should have a non-zero Chern number despite the fact that the total magnetic flux vanishes, making the system a Chern insulator.

Motivated by the above semi-classical picture, we have designed the wire construction shown in Fig. 3.1a. Each unit cell consists of four wires. We tune the wires' chemical potentials such that wires 1 and 2 of each unit cell are near the bottom of the band, and wires 3 and 4 are near the top. Thus, we have alternating pairs of wires that contain electrons and holes. A positive (negative) magnetic field is introduced between the pairs of electron (hole) wires. Indeed, this is an anisotropic version of the semi-classical picture we described above.

It is convenient to choose a gauge in which the vector potential A points in the $\hat{x}$ direction. We start by tuning the wires' bands such that all their crossing points match in energy. In this case, the energy spectra are similar to those depicted in Fig. 3.1b. In analogy to the quantum Hall case presented in the previous section, we define k_F^0 as the Fermi momenta in the absence of an external magnetic field, and $k_\varphi = \frac{eBa}{2\hbar c}$ as the shift of the parabolas due to the magnetic fields (see Fig. 3.1b). It is also useful to define the filling fraction as $\nu = \frac{k_F^0}{k_\varphi}$. In the scenario described above, where the crossing points match in energy, it is easy to verify that the filling factor is $\nu = 1$.

If neighboring wires of the same type are weakly tunnel coupled (with an amplitude t), a gap opens between parabolas 1 and 2, and parabolas 3 and 4. The spectrum in this case is depicted in Fig. 3.1c. Introducing coupling between the electrons and holes *inside* a unit cell

(a)   (b)   (c)   (d)
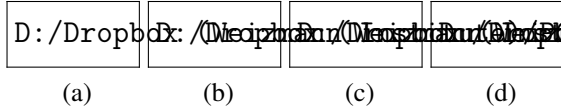
Figure 3.1: (Color Online) (a) Physical scheme of the Q1D model we study. Blue wires contain electrons, and red wires contain holes. The black arrows represent the magnetic field through the system. (b) The energy spectrum of the wires (as a function of k_x) near zero energy without tunneling between the wires ($t, t', t'' = 0$). The wires are tuned such that the four parabolas cross each other at zero energy, and the chemical potential is set to be zero. The spectra in blue, dashed blue, dashed red, and red correspond to wires 1, 2, 3, and 4 in a unit cell, respectively. (c) The energy spectrum when t is switched on. A gap opens near $k_x = 0$. (d) The spectrum when t' is switched on as well. This gives an additional gap at $k_x > 0$. Free chiral modes are left on wires 1 and 4. Finally, if one switches on t'', there are free chiral modes at the edge of the system, which suggests that there is a non-zero Chern number.

(t'), an additional gap opens at $k_x > 0$, and we obtain the spectrum depicted in Fig. 3.1d. In the absence of additional terms, each four-wire unit cell contains a chiral mode on each of its edges. Switching on small tunneling between different unit cells (t''), the gapless modes associated with adjacent unit cells gap out, leaving behind chiral modes on the edges of the system. The coupling between the edges decays exponentially with the sample width, and in the thermodynamic limit we expect to find truly gapless edge states. The observation of gapless edge states indicates that there is a non-zero Chern number $C = \pm 1$.

3.3   Fractional Chern Insulators

The wire construction prompts us to add interactions and use the bosonization technique, in analogy to the QHE case (see Chapter 2). This allows us to generalize the above results to fractional Chern insulator (FCI) states. In the presence of interactions, multi-electron processes may open a gap even if the Fermi point of the left movers is not equal to the Fermi points of the right movers [49, 94–96].

To understand the required conditions for a gap opening due to multi-electron scattering processes, it is useful to present the spectra of Fig. 3.1b in an alternative way. Instead of plotting the entire spectrum, we display in Fig. 3.2a the Fermi momenta as a function of the wire index. A cross ($\otimes$) denotes the Fermi point of a right mover, and a dot ($\odot$) denotes the Fermi point of a left mover. Before analyzing the fractional case, it is useful to revisit the simple $\nu = 1$ case. We will see that the main results of the previous section arise naturally through the bosonization framework.

Linearizing the spectrum around the Fermi-points of each wire, and using the standard

bosonization procedure, we again define the two chiral bosonic fields, ϕ_i^R and ϕ_i^L, for each wire. In terms of these, the fermionic operators are given by $\psi_i^R \propto e^{i\left(k_i^R x + \phi_i^R\right)}$, and $\psi_i^L \propto e^{i\left(k_i^L x + \phi_i^L\right)}$.

Without interactions, a momentum conserving single-electron tunneling between the wires (denoted in Fig. 3.2a by an arrow) is possible only when the left and right movers from adjacent wires are at the same point in k-space. These single-electron tunneling operators between adjacent wires (denoted in Fig. 3.2a by green, red, and dashed red arrows) take the form

$$t\,\psi_{1(3)}^{R\dagger}\,\psi_{2(4)}^{L} + \text{h.c.} \propto t \cos\left(\phi_{1(3)}^{R} - \phi_{2(4)}^{L}\right),$$
$$t'\,\psi_{2}^{R(L)\dagger}\,\psi_{3}^{L(R)} + \text{h.c.} \propto t' \cos\left(\phi_{2}^{R(L)} - \phi_{3}^{L(R)}\right),$$
$$t''\,\psi_{4}^{R(L)\dagger}\,\psi_{1'}^{L(R)} + \text{h.c.} \propto t'' \cos\left(\phi_{4}^{R(L)} - \phi_{1'}^{L(R)}\right). \tag{3.1}$$

We switch on the operators in the following way: first, we switch on a small $t \ll t_x$. Since this is a relevant operator, it gaps out the spectrum near $k_x = 0$. Then, we switch on smaller electron-hole couplings $t', t'' < t$. The terms $\psi_2^{R\dagger}\psi_3^{L}$ and $\psi_4^{R\dagger}\psi_{1'}^{L}$ gap out the rest of
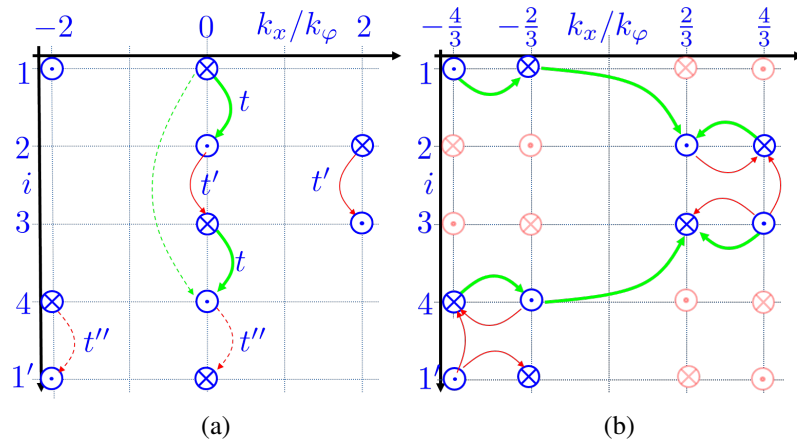
Figure 3.2: (Color Online) (a) A diagrammatic representation of the energy band structure in the case $v \equiv k_F^0/k_\varphi = 1$ (See Fig. 3.1b for definitions of k_φ and k_F^0). The y axis shows the wire index inside the unit cell, and the x axis shows k_x in units of k_φ. The symbol $\odot$ ($\otimes$) represents k_i^L (k_i^R). Colored arrows represent tunneling amplitudes between the wires. (b) The same diagram for a topological insulator with $v = \frac{1}{3}$. Colored arrows now represent the multi-electron processes responsible for the creation of Laughlin-like states. These complex processes in terms of the electrons ($\psi \sim e^{i\phi}$) for $v = 1/3$ are mapped to simple tunneling processes in terms of the fermions $\tilde{\psi} \sim e^{i\eta}$. Thus, $v = 1/3$ for ψ is equivalent to $v = 1$ for $\tilde{\psi}$. In the presence of spin orbit coupling, spin up (blue) and spin down (light red) will experience opposite alternating effective magnetic fields.

the spectrum, leaving a gapless edge mode. As we discussed before, this indicates that there is a non-zero Chern number. Note that the terms $\psi_2^{L\dagger}\psi_3^R$ and $\psi_4^{L\dagger}\psi_{1'}^R$ contain fields which are conjugate to those already pinned by t. Strong quantum fluctuations are therefore expected to suppress these terms.

We now turn to generalize this to Laughlin-like FCI states, with a filling factor $\nu = k_F^0/k_\varphi = 1/m$, where m is an odd integer. For example, the momentum pattern associated with $\nu = 1/3$ is shown in blue in Fig. 3.2b. In this case, multi-electron processes must be considered in order to gap out the bulk. In analogy to the quantum Hall case (described in the previous section), it is enlightening to define new chiral fermion operators

$$\tilde{\psi}_i^{R(L)} = (\psi_i^{R(L)})^{\frac{m+1}{2}}(\psi_i^{\dagger L(R)})^{\frac{m-1}{2}} \propto e^{i\left(q_i^{R(L)}x + \eta_i^{R(L)}\right)}, \qquad (3.2)$$

with $\eta_i^{R(L)} = \frac{m+1}{2}\phi_i^{R(L)} - \frac{m-1}{2}\phi_i^{L(R)}$, and $q_i^{R(L)} = \frac{m+1}{2}k_i^{R(L)} - \frac{m-1}{2}k_i^{L(R)}$. Whereas the original ϕ-fields satisfy $\left[\phi_\rho(x),\phi_\rho(x')\right] = i\pi\rho\,\mathrm{sign}(x - x')$, with $\rho = \pm$ corresponding to R/L, the η-fields satisfy $\left[\eta_\rho(x),\eta_\rho(x')\right] = i\pi m\rho\,\mathrm{sign}(x - x')$. As we saw in the previous section, this ensures that the $\tilde{\psi}$'s are fermionic operators. In addition, it can easily be checked that the resulting structure of the q's is identical to that of the k's in the case of $\nu = 1$ (Fig. 3.2a), so that $\tilde{\psi}$ can be regarded as a fermionic field with $\nu = 1$.

Repeating the analysis of the $\nu = 1$ case, we can now write single $\tilde{\psi}$ tunneling operators, identical to those found in Eq. (3.1) (replacing $\psi \to \tilde{\psi}, \phi \to \eta$, with new tunneling amplitudes $\tilde{t},\tilde{t}'$, and $\tilde{t}''$). In terms of the original electrons, these operators describe the multi-electron processes shown in Fig. 3.2b. Note that when the interactions are strong enough, these operators become relevant [49, 94, 95]. From this point, the process is identical to the construction of the normal CI. The gap due to the $\tilde{\psi}$ tunneling operators ensures that competing processes (for example, single electron tunneling between wires 2 and 3, or 4 and 1') are suppressed, as they contain fields conjugate to the fields pinned by $\tilde{t}$ (which is dominant by our construction).

As we saw in Chapter 2, the fact that the composite η-fields (and not the original ϕ fields) are pinned, leads to the various properties of these Laughlin-like states, like the fractional charge and statistics of the excitations, in analogy to the known FQHE states.

3.4 Non-Abelian Fractional Chern Insulators

As the discussion above shows, the wire-construction provides a path for creating Abelian fractional Chern insulators. It was demonstrated in Ref. [94] that non-Abelian FQHE states can be constructed by enlarging the unit cell, and taking a non-uniform magnetic field inside each unit cell. By our construction, any non-Abelian state constructed in Ref. [94] can be gen-

eralized to non-Abelian CI state. To do so, one can take two unit cells from the construction in Ref. [94], reverse the magnetic field of the second unit cell, and use holes instead of electrons.

In fact, the lack of a total magnetic flux in our system enables simpler constructions of non-Abelian states, which do not have a direct analog in the QHE. We now show that a slight modification of the procedure that enabled the construction of Laughlin-like states may lead to non-Abelian states. We will focus here on a state similar to the $\mathbb{Z}_3$ Read-Rezayi state, but we note that generalizations to other non-Abelian states are possible.

To obtain a $\mathbb{Z}_3$ parafermion state, we take $\nu = 1/3$, and start by writing the $\tilde{\psi}$ (or η) operators. Let us start in the special point where $\tilde{t}, \tilde{t}'$, and the coupling between $\tilde{\psi}_1^R$ and $\tilde{\psi}_4^L$ are tuned to have exactly the same value, denoted by v (at the end, when the topological nature of our construction will be revealed, this strict requirement can be relaxed). As we now demonstrate, this special point in parameter space corresponds to a fixed point described by a non-trivial $\mathbb{Z}_3$ parafermion in each unit cell. In terms of the bosonized η fields, these terms take the form

$$H = v \int dx \left[\cos\left(\eta_2^L - \eta_1^R\right) + \cos\left(\eta_3^R - \eta_4^L\right) + \{2 \leftrightarrow 4\} \right]. \tag{3.3}$$

Defining charge and "spin" degrees of freedom according to $(\phi_c, \theta_c, \phi_s, \theta_s)^T = U\left(\eta_1^R, \eta_2^L, \eta_3^R, \eta_4^L\right)^T$, with

$$U = \frac{1}{\sqrt{24\pi}} \begin{pmatrix} 1 & 1 & 1 & 1 \\ -1 & 1 & -1 & 1 \\ 1 & -1 & -1 & 1 \\ -1 & -1 & 1 & 1 \end{pmatrix},$$

we can write the Hamiltonian in the convenient form

$$H = \int dx \left[\frac{1}{2} \sum_{a=c,s} \left((\partial_x \phi_a)^2 + (\partial_x \theta_a)^2 \right) \right.$$
$$\left. + 2v \cos\left(\sqrt{6\pi}\theta_c\right) \left[\cos\left(\sqrt{6\pi}\theta_s\right) + \cos\left(\sqrt{6\pi}\phi_s\right) \right] \right] dx. \tag{3.4}$$

If we manage to pin the field θ_c, the term $\cos\left(\sqrt{6\pi}\theta_c\right)$ can be regarded as a constant. The simplest way to pin θ_c is to add a multi-electron term of the form

$$v' \int dx \cos\left(\eta_2^L - \eta_1^R - \eta_3^R + \eta_4^L\right) = v' \int dx \cos\left(\sqrt{24\pi}\theta_c\right).$$

While this term is irrelevant, if we increase its bare coupling constant, we can make it flow to strong coupling. Alternatively, one can add density-density interactions that alter the

Luttinger-liquid fixed point in the charge sector, leading to a charge-sector Hamiltonian of the form

$$\int \frac{v^*}{2} \left(K_c \left(\partial_x \phi_c \right)^2 + \frac{1}{K_c} \left(\partial_x \theta_c \right)^2 \right) dx. \tag{3.5}$$

When the repulsive interactions become strong enough (i.e. K_c becomes small enough), the term multiplying v' becomes relevant and θ_c is pinned to the minimum of the cosine. In this case, the term $\cos\left(\sqrt{6\pi}\theta_c \right)$ appearing in Eq. (3.4) is pinned, and can be treated as a constant.

Under these assumptions, the Hamiltonian in Eq. 3.4 describes the $\beta^2 = 6\pi$ critical self-dual Sine-Gordon model, known to realize a $\mathbb{Z}_3$ parafermion CFT [97, 98]. Following the scheme presented in Sec. 2.4, we would like to couple the right moving parafermion sector with the left mover in the next unit (leaving a single chiral parafermion CFT on each edge). However, such coupling requires terms which involve tunneling of quasiparticles [98]. These terms are therefore non-local and cannot be written in terms of the wire degrees of freedom.

To overcome this, we need to effectively create a bulk FQHE state between these modes, in which tunneling of quasiparticles can be generated. This can be done if we slightly modify our construction such that each wire contains two flavors (denoted by a and b). The spectrum as a function of the momenta q (corresponding to the composite fields $\tilde{\psi}$) is shown in Fig. (3.3). We now have effectively 8 wires in each unit cell, out of which we can create an effective bulk FQHE state. Green arrows represent the operators which form the FQHE state, and red arrows represent the operators which create the gapless parafermion modes. The quasiparticle tunneling terms needed to create the $\mathbb{Z}_3$ parafermion state can now be generated through the thin FQHE stripe in each unit cell, and one can construct the desired 2D state with $\mathbb{Z}_3$ parafermion CFT on the edge (in addition to chiral boson modes).
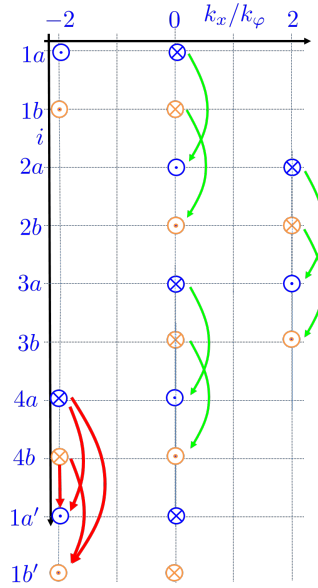
Figure 3.3: The diagrammatic representation of the spectrum of the case where the system is tuned to $\nu = 1/3$ and each wire has two flavors. The momenta shown in the figure are the q's corresponding to the composite fields $\tilde{\psi}$. Blue and orange modes represent the flavors a and b. Green arrows are terms used to effectively create a bulk FQHE state, and red arrows are used to map the problem to the $\beta^2 = 6\pi$ self-dual Sine-Gordon model in each unit cell. The effective bulk supports the quasiparticle tunneling needed to couple the parafermion modes.

The above construction seems to require considerable fine-tuning tuning of the couplings. However, due to the topological nature of the phase we describe, deviations from this specific form are possible, as long as the bulk gap does not close.

3.5 Topological insulators from the wires approach

The entire analysis presented here can also be carried out for spinful electrons if one introduces spin-orbit interactions (in the $\hat{z}$ direction only). This can be done if an alternating electric field is introduced instead of an alternating magnetic field. For example, the electric field can be tuned in such a way that the spin-orbit coupling is positive at wires 1 and 4, and negative at wires 2 and 3. Fig. 3.2b shows the appropriate Fermi-momenta corresponding to $\nu = \frac{1}{3}$ (in blue for spin up and light red for spin down). If one considers only processes which conserve S_z, we get a simple construction for integer, Laughlin-like, and non-Abelian topological insulators [85], which are simply two copies of the FCI states discussed above (with opposite chiral modes for the different spin species). In Chapter 5, we will analyze these models in details. The stability of such states with respect to time-reversal invariant perturbations can be addressed through the arguments described in Ref. [85].

Chapter 4

Imprint of topological degeneracy in quasi-one-dimensional fractional quantum Hall states

This chapter presents the results of our second project, presented in Ref. [63]. In this project, we propose experimental systems which are equivalent to fractional quantum Hall states with a torus topology, known to possess a topological ground state degeneracy. These realizations present measurable imprints of the topological degeneracies, which play a fundamental role in our understanding of fractional phases.

4.1   Introduction

One of the hallmarks of the fractional quantum Hall effect (FQHE) is that if the two-dimensional electron system resides on a manifold with a nontrivial topology, it will have a ground state degeneracy which depends on the topology [99]. For a fractional quantum Hall state on an infinite torus, the degeneracy of the ground state equals the number of topologically distinct fractionalized quasi-particles allowed in that state. Furthermore, no local measurement may distinguish between the degenerate ground states. When the torus is of large but finite size, the degeneracy is split, but the splitting is exponentially small in L, where $L = \min\left\{L_x, L_y\right\}$ and L_x, L_y are the two circumferences of the torus.

In this work we consider two systems that are topologically equivalent to a torus, and - unlike the torus - are within experimental reach. The first is that of an annular shaped electron-hole double-layer in which the electron and hole densities are equal, and are both tuned to the same FQHE state. In the absence of any coupling between the layers, both the

interior edge and the exterior edge of the annulus carry pairs of counter-propagating edge modes of the electrons and the holes. These pairs may be gapped by means of inter-layer back-scattering, resulting in a fully gapped system with the effective topology of the torus. In fact, this system is richer than a seamless torus, since the interior and exterior edges may be gapped in different ways. In particular, gapping the counter-propagating edge modes by coupling them to a superconductor may have interesting consequences. Some of these consequences are central to the current paper.

The second realization we consider is that of a two dimensional time-reversal-invariant fractional topological insulator [85]. To be concrete, we assume that it is constructed of wires subjected to spin-orbit coupling and electron-electron interaction. In this realization, electrons of spin-up form a FQHE state of filling factor ν, and electrons of spin-down form a FQHE of filling factor $-\nu$. Similar to the particle-hole case, the edges carry pairs of counter-propagating edge modes with opposite spins that may be gapped in different ways. Remarkably, when the edge modes are gapped by being coupled to superconductors, the system is invariant under time-reversal, yet topologically equivalent to a FQHE torus.

We use these realizations of a toroidal geometry and their inter-relations to investigate the transition of a fractional quantum Hall system from the thermodynamic two-dimensional to the quasi-one dimensional regime. In particular, we find signatures of the topological ground state degeneracy of the two-dimensional (2D) limit (akin to that of fractional quantum Hall states on a torus) that survive the transition to the quasi one-dimensional (1D) regime and propose experiments in which these signatures may be probed. For example, for an Abelian fractional quantum Hall state, we find a $2\pi d$-periodic Josephson effect, where d is the degeneracy in the 2D thermodynamic limit.

4.2 The main results and the physical picture

4.2.1 The systems considered

The first system we consider - the electron-hole double-layer - is conceptually simple to visualize (see Fig. (4.1a)). We consider an electron-hole double-layer shaped as an annulus with equal densities of electrons and holes, and a magnetic field that forms FQHE states of $\pm\nu$ in the two layers. The system breaks time reversal symmetry, but its low energy physics satisfies a particle-hole symmetry. For most of our discussion we focus on the case $\nu = 1/3$. In that case each edge carries a pair of counter-propagating $\nu = 1/3$ edge modes. The edge modes may be gapped by means of normal back-scattering (possibly involving spin-flip, induced by a magnet) or by means of coupling to a superconductor. In line with common notation, we

D:/Dropbox (Weizmann Institute)/PC/Thesis/Thesis/Paper 2/cont/PC/Thesis
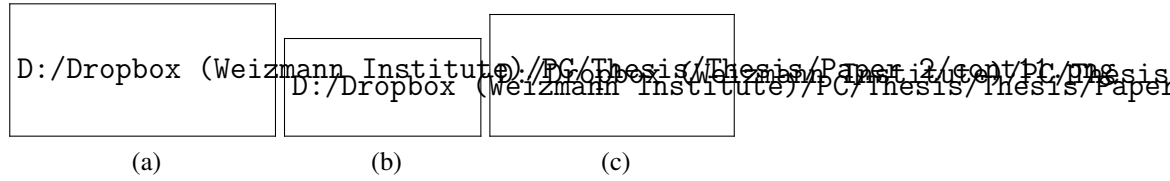
(a)   (b)   (c)

Figure 4.1: (a) The first realization we consider is that of an electron annulus (blue) and a hole annulus (red) under the action of a uniform magnetic field. It is evident that coupling the annuli's edges forms the topology of a torus. The second realization we suggest is that of a fractional topological insulator. Fig. (b) shows a possible model for a fractional topological insulator. We have an array of N wires, with a strong spin-orbit coupling. The spin orbit coupling is linear with the wire index n. The similarity of the resulting spectrum (see Fig. (4.3a) below) to the one corresponding to the wires construction of quantum Hall states suggests an equivalence to two quantum Hall annuli subjected to opposite magnetic fields (each annulus corresponds to a specific spin). (c) The edge modes of the two above models can be gapped out by proximity coupling to superconductors. In the case of a thin (quasi-1D) system, the phase difference between the inner and the outer superconductors leads to a Josephson effect mediated by tunneling across the region of a fractional quantum Hall double layer or a fractional topological insulator. The edge modes can also be gapped using proximity to magnets, in which case one can measure the spin-Josephson effect.

refer to these two ways as F and S respectively.

The second system is a fractional topological insulator. To model the fractional topological insulator we consider an array of N coupled quantum wires of length L_x, each satisfying periodic boundary conditions (Fig. (4.1b)). The wires are subjected to a Rashba spin-orbit coupling, and we consider a case in which the spin-orbit coupling constant in the n'th wire is proportional to $2n-1$ (similar to the model considered by Ref. [100]). Effectively, this form of spin-orbit coupling subjects electrons of opposite spins to opposite magnetic fields. While this particular coupled-wire model of a time reversal invariant topological insulator does not naturally allow for the regime of a large N, other realizations, such as those proposed in the previous chapter, allow for such a regime. These realizations require more wires in a unit cell, and are therefore more complicated that the one considered here. Most of the results of our analysis are independent of the specific realization of the fractional topological insulator, and we present the analysis for the realization that is simplest to consider.

For non-interacting electrons, the spectrum of the array we consider takes the form shown in Fig. (4.3a). Single-electron tunneling processes (which conserve spin) gap out the spectrum in all but the first and last wires, which carry helical modes (Fig. (4.3b)). If the chemical potential is tuned to this gap, then in the limit of large N the system is a topological insulator (TI), and therefore the gapless edge modes are protected by time-reversal symmetry and charge conservation [4].

Both realizations are equivalent to two electron QH annuli with opposite magnetic fields. If the edges are coupled, the two annuli are effectively "stitched" into a torus. The edge modes may be gapped by coupling the two external wires ($n = 1$ and $n = N$) to a superconductor or to a system with appropriate magnetic order. A Zeeman field that is not collinear with the spin-orbit coupling direction is necessary to couple the different spin directions. Moreover, in our coupled-wire model the spin-up and the spin-down electrons at the $n = N$ edge have different Fermi-momenta, so that edge would not be gapped by a simple ferromagnet. In order to conserve momentum one would need to introduce a periodic potential that could modulate the coupling to the ferromagnet at the appropriate wave vector, or one would need to use a spiral magnet with the appropriate pitch. In more sophisticated wire models, such as those discussed in the previous chapter, or in actual realizations of topological insulators, the two edge modes can have the same Fermi momenta, so a simple ferromagnet can be used.

In order to construct a fractional topological insulator, we first tune the chemical potential such that the density is reduced by a factor of three, to $\nu = 1/3$. For an array of wires in a magnetic field and spinless electrons, Kane et al. [49] have introduced an interaction that leads to a ground state of a FQHE $\nu = 1/3$ (as discussed in chapter 2). Here we show that the same interaction, if operative between electrons of the same spin only, leads to a formation of a fractional topological insulator, i.e., to the spin-up electrons forming a $\nu = 1/3$ state and the spin-down electrons forming a $\nu = -1/3$ state.

Both the electron-hole double-layer and spin-orbit wire system have counter propagating edge modes. They are distinct, however, in a few technical details. An electron-hole double layer system has been realized before in several materials, such as GaAs quantum wells and graphene. The requirements we have here - no bulk tunneling, sample quality that is sufficient for the observation of the fractional quantum Hall effect, and a good coupling to a superconductor or a magnet - are not easy to realize, but are not far from experimental reach [101–103]. In addition, we assume that the two layers are far enough such that inter-layer interactions do not play an important role, but close compared to the superconducting coherence length to enable pairing on the edges.

The array of wires we describe can in principle be formed using semi-conducting wires such as InAs and InSb [19, 21, 23], where variable Rashba spin-orbit coupling could be achieved by applying different voltages to gates above the wires. We stress that the wires construction is nothing but a specific example of a fractional topological insulator, and that any fractional topological insulator is expected to present the effects we discuss. Two-dimensional topological insulators were conclusively observed [5, 6, 8, 9, 11, 104, 105], and more recently proximity effects to a superconductor were demonstrated on their edges [10, 106, 107]. However, fractionalization effects due to strong electron-electron interaction were not observed yet

in these systems and are less founded theoretically.

4.2.2 Ground state degeneracy and its fate in the transition to one dimension

In Sec. 4.3 we investigate the topological degeneracy of the ground state in the 2D thermodynamic limit. Using general arguments, we find that the degeneracy depends on the gapping mechanism of the edges: when both edges are gapped by the same mechanism, be it proximity coupling to a superconductor or to a magnet, the topological degeneracy is three, as expected. However, if one edge is gapped using a superconductor and the other is gapped using a magnet the ground state of the system is not degenerate.

Physically, the degeneracy is most simply understood in terms of the charge on the edge modes. For an annular geometry there are two edges, in the interior and the exterior of the annulus, and therefore four edge modes with four charges, q_1, q_2, q_3, and q_4 (here we use the subscript 1,2 to denote the two counter-propagating edge modes on the interior edge, and 3,4 to denote the modes on the exterior edge). Edges 1 and 4 belong to one layer (or one spin direction) and edges 2 and 3 belong to the other layer (other spin direction); see Fig. (4.1a)). It will be useful below to distinguish between the integer part of q_i, which we denote by n_i, and the fractional part denoted by f_i, to which we assign the values $f_i = -1/3, 0, 1/3$, such that $q_i = n_i + f_i$.

When a pair of counter-propagating edge modes, say with charges q_1, q_2, is gapped by normal back-scattering of single electrons, their total charge $q_1 + q_2$ is conserved. Since there is an energy cost associated with the total charge, it assumes a fixed value for all ground states. (The tunneling between the edges gaps the system and makes it incompressible, leading to an energy cost associated with a change of the total charge.) For simplicity, we fix this value to be zero, making $q_1 = -q_2$. A strong back-scattering term makes $n_1 - n_2$ strongly fluctuating *but leaves the fractional part $f_1 = -f_2$ fixed*. As a consequence, there are three topological sectors of states that are not coupled by electron tunneling, characterized by f_1 being 0, 1/3 or -1/3.

Since each of the layers (in the double-layer system) or each spin direction (in the spin-orbit-coupling system) must have an integer number of electrons, the sums $q_1 + q_4$ and $q_2 + q_3$ must both be integers. This condition couples the fractional parts of the charges on all edges. Combining all constraints, we find that when both edges are gapped by a normal backscattering, the following conditions should be fulfilled

$$f_1 = -f_2, \quad f_3 = -f_4, \tag{4.1}$$

$$f_1 = -f_4, \quad f_2 = -f_3. \tag{4.2}$$

There are three solutions for these equations describing three ground states, with $f_l = (-1)^l \frac{p}{3}$, where p may take the values $0, 1, -1$ and $l = 1, 2, 3$, and 4. When both edges are gapped by a superconductor, f_2 and f_4 change sign in Eq. (4.1) and the fractional parts satisfy $f_1 = f_2 = -f_3 = -f_4 = p/3$, Finally, when one edge is gapped by a superconductor and the other by normal back-scattering, only one of the two equations labeled (4.1) change sign and the only possible solution is $f_l = 0$ so that all q's must be integers, and the ground state is unique.

Formally, the degeneracy of the ground state may be shown by an explicit construction of two unitary operators, U_x and U_y, that commute with the low-energy effective Hamiltonian and satisfy the operator relation

$$U_x U_y = U_y U_x e^{\frac{2\pi}{3} i}. \tag{4.3}$$

The existence of a matrix representation of this relation, acting within the ground state manifold, requires a degenerate subspace of minimal dimension 3.

We construct such operators explicitly for both realizations. For both cases, one of these operators, say U_x, measures the f_l's and the other operator, U_y, changes the f_l's by $\pm 1/3$ (the sign depends on l and on the type of gapping mechanism).

Even when L_x is infinite, a finite L_y splits the degeneracy. The source of lifting of the degeneracy is tunneling of quasi-particles between the two edges of the annulus, i.e., tunneling of quasi-particles from the first to the last wire. More precisely, we find that as long as the bulk gap does not close, the only term that may be added to the low-energy Hamiltonian is of the form

$$\lambda U_y + \lambda^* U_y^\dagger \tag{4.4}$$

This term is generated by high orders of perturbation theory that lead to a transfer of quasi-particles between edges. The amplitude λ decays exponentially with the width of the system.

4.2.3 Remnants of the degeneracy in the quasi-one dimensional regime

The topological degeneracy is lifted in the transition from a two-dimensional system to a quasi-one dimensional one, but it leaves behind an imprint which can in principle be measured. This is seen when we add another parameter to the Hamiltonian. For a torus, this parameter may be the flux within the torus. For the systems we consider here, when gapped by one superconductor at the interior edge and one superconductor at the exterior edge, this parameter may be the phase difference φ between the two superconductors. In this case the fractional quantum Hall torus forms the insulator in a superconductor-insulator-superconductor Josephson junction.

The dependence of the spectrum on these parameters is encoded in the amplitude λ of Eq. (4.4). In particular, since the tunneling charge is $2/3$ of an electron charge, which is $1/3$ of a Cooper pair, we find that the tunneling amplitude at the point x along the junction is proportional to the phase factor $e^{i\varphi(x)/3}$, where $\varphi(x)$ is the phase difference between the two superconductors at the point x. For the fractional topological insulator, no magnetic flux is enclosed between the superconductors, and the equilibrium phase difference does not depend on x. In contrast, for the electron-hole quantum Hall realization the magnetic flux threading the electron-hole double layer makes $\varphi(x)$ vary linearly with x, such that the phase of the tunneling amplitude winds as a function of the position of the tunneling. The amplitude λ of Eq. (4.4) is an integral of contributions from all points at which the superconductors are tunnel-coupled,

$$\lambda = \int dx T(x) \tag{4.5}$$

where $T(x)$ is the local tunneling amplitude.

When the superconductors are tunnel-coupled only at a single point (say $x = 0$), such that $T(x) \propto \delta(x)$, the spectrum of the three ground states as a function of φ, which is now the argument of $T(x = 0)$ can be written in the explicit form

$$\Delta E_\alpha = 2t_0 \cos\left(\frac{\varphi - 2\pi\alpha}{3}\right), \tag{4.6}$$

where $\alpha = 0, 1, -1$ enumerates the ground states. This is shown in Fig. (4.2a).

While the amplitude t_0 is exponentially small in the width L_y, or in the number of wires N, we find that the spectrum as a function of the phase difference across the junction has points of avoided crossing in which the scale of the splitting between the two crossing states is proportional to e^{-L_x/ξ_x}, i.e., is exponentially small in L_x (here ξ_x is a characteristic scale which depends on the microscopics). Thus, in the quasi-one-dimensional regime, where L_y or N are small but L_x is infinite, the three states are split, but cross one another at particular values of φ.

Remarkably, this crossing cannot be lifted by any perturbation that does not close the gap between the three degeneracy-split ground states and the rest of the spectrum. This lack of coupling between these states result from the macroscopically different Josephson current (from the inner edge to the outer edge) that they carry. The Josephson junction formed between the two superconductors will show a 6π- periodic DC Josephson effect for as long as the time variation of the phase is slow compared to the bulk energy gap, but fast compared to a time scale that grows as e^{L_x/ξ_x}. The Josephson current distinguishes between the three ground states. This current oscillates as a function of the position of the tunneling point for an electron-hole quantum Hall system and is position-independent for the fractional topological
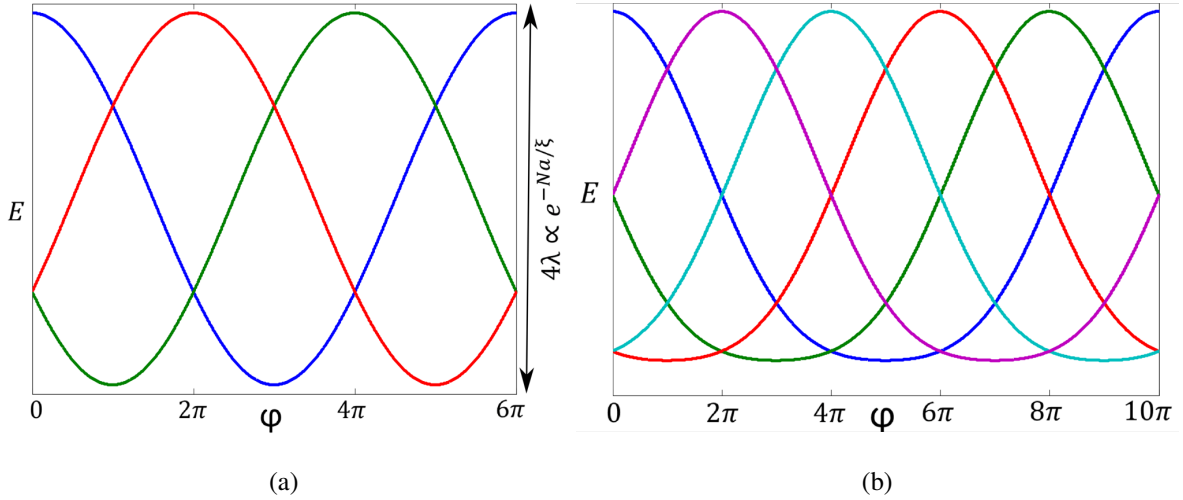
Figure 4.2: (a) The spectrum of the three low energy states as a function of the phase difference φ between the two superconductors (see text for elaboration). The amplitude of oscillations falls exponentially with the number of wires N. For a finite N, each eigenstate has a periodicity of 6π. At the special points $\varphi = \pi n$ the spectrum remains 2-fold degenerate. If the system is of finite length L_x, the degeneracy at these points is lifted by a term that is exponentially small in L_x. (b) The spectrum corresponding to $v = 2/5$ with $\lambda_2/\lambda_1 = 0.2$ as a function of the relative phase difference φ. The periodicity of each eigenstate is 10π and at the points $\varphi = \pi n$, we find two crossing points whose splitting falls exponentially with L_x.

insulator.

When tunneling between edges takes place in more than one point, $T(x)$ in (4.36) is non-zero at all these points, and has to be integrated. A particularly interesting case is that of a uniform junction. In that case $T(x)$ and the Josephson current are constant for the fractional topological insulator, while in the electron-hole double-layer the phase of $T(x)$ winds an integer number of times due to the magnetic flux between the superconductors, and the Josephson current averages to zero.

A magnetic coupling between the electron and hole layers, or between electrons of the two spin directions may lead to a "(fractional) spin Josephson effect", in which spin current takes the place of charge current in the Josephson effect [108–110]. In this case, assuming that the spin up and down electrons are polarized in the z direction, coupling between the edge modes occurs by a magnet that exerts a Zeeman field in the $x - y$ plane. The role of the phase difference in the superconducting case is played here by the relative angle between the magnetization at the interior and exterior edge, but an interesting switch between the two systems we consider takes place. In the electron-hole quantum Hall case the direction of the magnetization is uniform along the edges and a uniform and opposite electric current flows in the two layers.

For the fractional topological insulators the edges are gapped only when for one of the edges the direction of the magnetization in the $x - y$ plane winds as a function of position. As a consequence, in our coupled-wire model the spin current oscillates an integer number of oscillations along the junction, and thus averages to zero.

Our discussion may be extended beyond the case of $\nu = 1/3$. For Abelian states, we find that the periodicity of the Josephson effect is $2\pi/e^*$, where e^* is the smallest fractional charge allowed in the state. In any Abelian state, this is also 2π times the degeneracy of the ground state in the thermodynamic limit.

4.3 Ground state degeneracy in the thermodynamic 2D limit

4.3.1 The coupled wires construction for a Fractional Topological Insulator

In this Section we explain how a fractional topological insulator may be constructed from a set of coupled wires, as a result of a combination of spin-orbit coupling and electron-electron interaction. We start with the case of non-interacting electrons, in which case a 2D topological insulator is formed, and then introduce interactions that lead to the fractionalized phase.

4.3.1.1 The integer case - a non-interacting quantum spin Hall state

We consider an array of N quantum wires, with a Rashba spin-orbit coupling (see Fig. (4.1b)). Each wire is of length L_x and has periodic boundary conditions. We tune the Rashba electric field (which we set to be in the y direction, for simplicity) such that the spin-orbit coupling of wire number n is linear with n. The resulting term in the Hamiltonian takes the form

$$H_{so,n} = (2n-1)uk_x\sigma_z, \tag{4.7}$$

where σ_z is the spin in the z direction, and u is the spin-orbit coupling. The spectrum of wire number n is therefore

$$E_n(k) = \frac{(k_x + (2n-1)k_{so}\sigma_z)^2}{2m}, \tag{4.8}$$

where m is the effective mass, and $k_{so} = \frac{u}{m}$. The energy of the different wires as a function of k_x is shown in Fig. (4.3a).

The similarity of the spectrum to the starting point of the wires construction of the QHE [49, 76, 94] is evident. This system is then analogous to two annuli of electrons of opposite
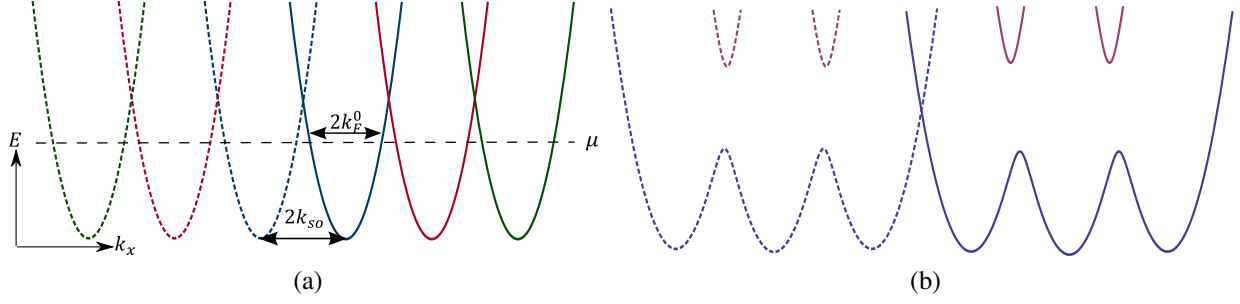
Figure 4.3: (a) The spectrum of a system consisting of three wires (see Fig. (3.1a)) with non-interacting electrons subjected to spin orbit coupling whose magnitude depends on the wire index according to Eq. (4.7), when tunneling between the wires is switched off. The spectra in blue, red, and green correspond to wires number 1,2, and 3. Solid lines correspond to spin-down, and dashed lines correspond to spin-up. (b) The resulting spectrum when a weak spin-conserving tunneling amplitude is switched on between the wires. The bulk is now gapped, with helical modes localized on the edges.

spins subjected to opposite magnetic fields or to the electron-hole double-layer we discussed above (see Fig. (4.1a)).

Following the analogy with the wires construction of the QHE, we define the filling factor as

$$\nu = \frac{k_F^0}{k_{\text{so}}}, \tag{4.9}$$

where k_F^0 is the Fermi momentum without a spin-orbit coupling (see Fig. (4.3a)).

In the "integer" case, $\nu = 1$, the chemical potential is tuned to the crossing points of two adjacent parabolas.

As in the previous chapters, we linearize the spectrum around the Fermi points, and use the usual bosonization technique to define two chiral bosonic fields $\phi_{n,\sigma}^{R/L}$, where n is the wire index, σ is the spin index, and R (L) represents right (left) movers. In terms of these bosonic fields, the fermion operators take the form

$$\psi_{n,\sigma}^{R/L} \propto e^{i\left(\phi_{n,\sigma}^{R/L}+k_{n,\sigma}^{R/L}x\right)}, \tag{4.10}$$

where

$$k_{n,\sigma}^\rho = -\sigma((2n-1)k_{\text{so}}+\rho k_F^0)$$

is the appropriate Fermi-momenta in the absence of interactions and tunneling between the wires, with $\sigma = 1$ (-1) corresponding to spin up (down), and $\rho = 1$ (-1) corresponding to
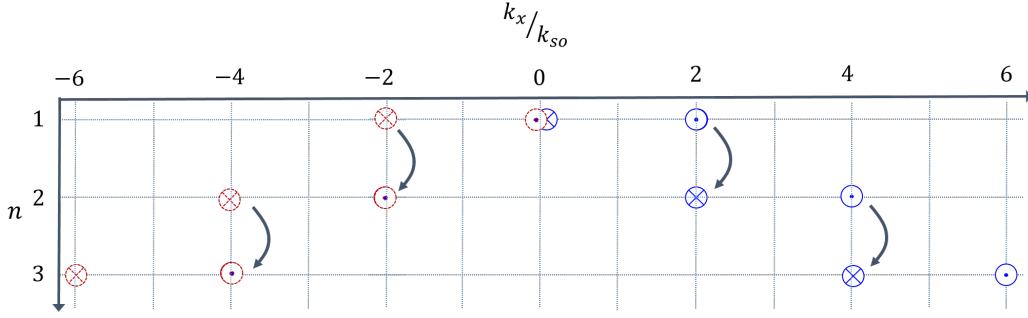
Figure 4.4: A diagrammatic representation of the spectrum in the case $v = 1$, similar to the previous section. One can observe that single electron spin-conserving tunneling operators conserve momentum, and can therefore easily gap out the bulk in this case.

right (left) movers. The chiral fields satisfy the commutation relations

$$\left[\phi^{\sigma}_{n\rho}(x), \phi^{\sigma}_{n\rho}(x')\right] = i\rho\pi\text{sign}(x-x').\tag{4.11}$$

Similar to the previous chapter, once we linearize the spectrum, it becomes convenient to present it diagrammatically by plotting only the Fermi-momenta as a function of the wire index. Fig. (4.4) shows the diagram corresponding to $v = 1$, where a right (left) mover is represented by the symbol $\odot$ ($\otimes$).

One sees that single electron tunneling operators of the type

$$H_{t\downarrow} = t\sum_{n=1}^{N-1}\int dx\left(\psi^{L\dagger}_{n+1,\downarrow}\psi^{R}_{n,\downarrow} + h.c.\right) = t\frac{k^0_F}{\pi}\sum_{n=1}^{N-1}\int dx\cos\left(\phi^L_{n+1,\downarrow} - \phi^R_{n,\downarrow}\right),$$

$$H_{t\uparrow} = t\sum_{n=1}^{N-1}\int dx\left(\psi^{R\dagger}_{n+1,\uparrow}\psi^{L}_{n,\uparrow} + h.c.\right) = t\frac{k^0_F}{\pi}\sum_{n=1}^{N-1}\int dx\cos\left(\phi^R_{n+1,\uparrow} - \phi^L_{n,\uparrow}\right),\tag{4.12}$$

are allowed by momentum conservation (these operators are represented by the arrows in Fig. (4.4)). Noting that these operators commute with one another, the fields within the cosines may be pinned, and therefore the bulk is gapped. These terms, however, leave 4 gapless modes on wires 1 and N: $\phi^R_{1,\uparrow}, \phi^L_{1,\downarrow}, \phi^L_{N,\uparrow}, \phi^R_{N,\downarrow}$. In fact, the above model is a topological insulator, and the gapless helical modes are the corresponding edge modes, protected by time-reversal symmetry and charge conservation. Although our model also has a conservation of S_z, this is not actually necessary to preserve the gapless edge modes.

To completely gap out the spectrum, we have to gap out the two edges separately. This can be done using two mechanisms: proximity coupling of wire 1 and N to a superconductor which breaks charge conservation, or to a magnet which breaks time-reversal symmetry. The terms in the Hamiltonian that correspond to these cases are

$$H_1^S = \Delta_1 \int dx \cos\left(\phi_{1,\uparrow}^R + \phi_{1,\downarrow}^L + \delta_1\right),$$

$$H_1^F = B_1 \int dx \cos\left(\phi_{1,\uparrow}^R - \phi_{1,\downarrow}^L + \beta_1\right),$$

$$H_N^S = \Delta_N \int dx \cos\left(\phi_{N,\uparrow}^L + \phi_{N,\downarrow}^R + \delta_N\right),$$

$$H_N^F = B_N \int dx \cos\left(\phi_{N,\uparrow}^L - \phi_{N,\downarrow}^R + \beta_N + 4k_{so}Nx\right). \tag{4.13}$$

The phases δ_1, δ_N are the phases of the superconducting order parameter of the superconductors that couple to the wires $1, N$ respectively. The phases β_1, β_N are the angles of the Zeeman fields (which lie in the $x-y$ plane) coupling to the wires $1, N$ respectively, with respect to the x-axis. As the last equation shows, for the magnetic field coupled to the n'th wire to allow for a momentum-conserving back-scattering, we must have $\beta_N = -k_{so}Nx$, i.e., the Zeeman field acting on the N'th wire must rotate in the $x-y$ plane at a period of $2\pi/(k_{so}N)$. This field then breaks translational invariance.

4.3.1.2 The fractional case - a Fractional Topological Insulator

We now consider the case $\nu = 1/3$, depicted diagrammatically in Fig. (4.5). Single electron tunneling processes of the type we considered above do not conserve momentum (see Fig. (4.5)) for this filling factor, and one has to consider multi-electron processes in order to gap out the bulk. Motivated by the analysis of the $\nu = 1/3$ FQHE state (see chapter 2), we define new fermion fields

$$\tilde{\psi}_{n,\sigma}^{R/L} = \left(\psi_{n,\sigma}^{R/L}\right)^2 \left(\psi_{n,\sigma}^{L/R}\right)^\dagger \propto e^{i\left(p_{n,\sigma}^{R/L}x + \eta_{n,\sigma}^{R/L}\right)}, \tag{4.14}$$

with

$$\eta_{n,\sigma}^{R/L} = 2\phi_{n,\sigma}^{R/L} - \phi_{n,\sigma}^{L/R},$$

$$p_{n,\sigma}^{R/L} = 2k_{n,\sigma}^{R/L} - k_{n,\sigma}^{L/R}. \tag{4.15}$$

Strictly speaking, the operators in (4.14) should operate at separated yet close points in space, due to the fermionic nature of $\psi_{n,\sigma}^{R/L}$. The commutation relations of the η-fields are given by

$$\left[\eta_{n\rho}^\sigma(x), \eta_{n\rho}^\sigma(x')\right] = 3\pi i \rho \, \text{sign}(x - x'). \tag{4.16}$$

In addition, if one draws the diagram that corresponds to the p's, the effective Fermi-momenta of the $\tilde{\psi}$ fields, one gets the same diagram as in the $\nu = 1$ case (Fig. (4.4)). Single-$\tilde{\psi}$
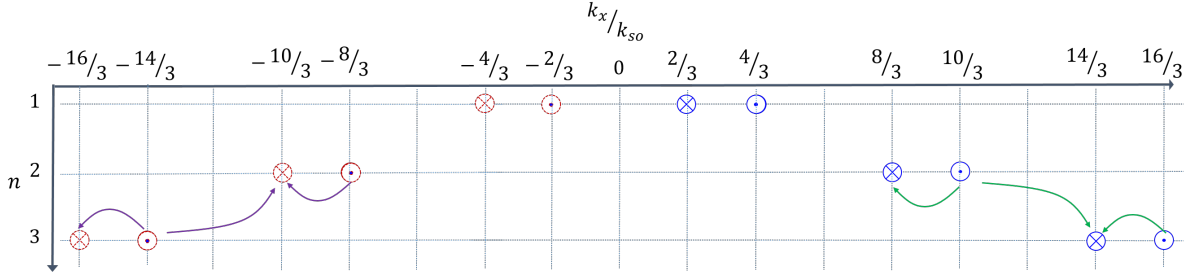
Figure 4.5: A diagrammatic representations of the fractional case $\nu = 1/3$. Now, we find that only multi-electron processes can gap out the bulk. The processes we consider are represented by colored arrows. In terms of the composite $\tilde{\psi}$-fields, however, the diagram corresponding the fractional case is identical to the one corresponding to the integer case $\nu = 1$ (Fig. (4.4)).

tunneling operators conserve momentum, and one can repeat the process that led to a gapped spectrum in the integer case. First, we switch on single-$\tilde{\psi}$ tunneling operators of the form

$$\tilde{H}_{t\downarrow} = \tilde{t} \sum_{n=1}^{N-1} \int dx \left(\tilde{\psi}_{n+1,\downarrow}^{L\dagger} \tilde{\psi}_{n,\downarrow}^{R} + h.c. \right) = \frac{\tilde{t}}{4} \left(\frac{k_F^0}{\pi} \right)^3 \sum_{n=1}^{N-1} \int dx \cos \left(\eta_{n+1,\downarrow}^{L} - \eta_{n,\downarrow}^{R} \right),$$

$$\tilde{H}_{t\uparrow} = \tilde{t} \sum_{n=1}^{N-1} \int dx \left(\tilde{\psi}_{n+1,\uparrow}^{R\dagger} \tilde{\psi}_{n,\uparrow}^{L} + h.c. \right) = \frac{\tilde{t}}{4} \left(\frac{k_F^0}{\pi} \right)^3 \sum_{n=1}^{N-1} \int dx \cos \left(\eta_{n+1,\uparrow}^{R} - \eta_{n,\downarrow}^{L} \right). \quad (4.17)$$

In terms of the $\tilde{\psi}$-fields, it is clear that one cannot write analogous interactions between electrons of opposite spins, and therefore the dominating terms are those that couple electrons with the same spins. Recall that as opposed to the integer case, these operators are irrelevant in the weak coupling limit. However, they may be made relevant if one introduces strong repulsive interactions [49, 94, 95], or a sufficiently strong $\tilde{t}$.

For N wires, Eqs. (4.17) introduces $2N-2$ tunneling terms, which gap out $4N-4$ modes, and leave 4 gapless chiral η-modes on the edges. Two counter-propagating modes are at the $j = 1$ wire, and two are at the $j = N$ wire. Once again, these may be gapped by proximity coupling to a superconductor or a magnet. Operators of the type shown in Eq. (4.13), however, do not commute with the operators defined in Eq. (4.17). The arguments of the cosines in (4.13) cannot then be pinned by Eq. (4.17). The lowest order terms that commute with the

operators in Eq. (4.17) are

$$
\begin{aligned}
\tilde{H}_1^S &= \tilde{\Delta}_1 \int dx \cos\left(\eta_{1,\uparrow}^R + \eta_{1,\downarrow}^L + \tilde{\delta}_1 \right), \\
\tilde{H}_1^F &= \tilde{B}_1 \int dx \cos\left(\eta_{1,\uparrow}^R - \eta_{1,\downarrow}^L + \tilde{\beta}_1 \right), \\
\tilde{H}_N^S &= \tilde{\Delta}_N \int dx \cos\left(\eta_{N,\uparrow}^L + \eta_{N,\downarrow}^R + \tilde{\delta}_N \right), \\
\tilde{H}_N^F &= \tilde{B}_N \int dx \cos\left(\eta_{N,\uparrow}^L - \eta_{N,\downarrow}^R + \tilde{\beta}_N + 4k_{so}Nx \right).
\end{aligned}
\tag{4.18}
$$

Again, for the magnetic coupling to gap the edge modes on the nth wire, it must wind in the $x-y$ plane with a period of $2\pi/(k_{so}N)$. The electronic density is three times smaller than in the previous case, so on average there is $1/3$ of an electron per period. Guided by the analogy between the above construction and the $\nu = 1/3$ FQH state on a torus, we expect the ground state to have a 3-fold degeneracy.

Using the present formalism, we will be able to see how this degeneracy is lifted as one goes from an infinite array to the limiting case of a few wires.

4.3.1.3   Ground state degeneracy in the wire construction

For simplicity, we focus first on the FF case, where the analogy to the FQHE on a torus is explicit. In this case, we define the idealized Hamiltonian as

$$
H_I = \tilde{H}_K + \tilde{H}_{t\uparrow} + \tilde{H}_{t\downarrow} + \tilde{H}_1^F + \tilde{H}_N^F,
\tag{4.19}
$$

where

$$
\tilde{H}_K = \frac{1}{2} \sum_n \sum_{\rho,\rho'} \sum_{\sigma,\sigma'} \int dx \left(\partial_x \eta_{n\rho}^{\sigma} \right) V_{\rho,\rho'}^{\sigma,\sigma'} \left(\partial_x \eta_{n\rho'}^{\sigma'} \right)
\tag{4.20}
$$

is the quadratic term that contains the non-interacting part of the Hamiltonian, and small momentum interactions (for simplicity, we consider only intra-wire small momentum interactions). We assume that all the inter-wire terms become relevant and acquire an expectation value. To investigate the properties of the ground state manifold, we define the two unitary operators

$$
U_y(x) = e^{i\frac{1}{3}\left(\sum_{n=1}^N \left(\eta_{n,\uparrow}^R - \eta_{n,\uparrow}^L + \eta_{n,\downarrow}^R - \eta_{n,\downarrow}^L\right)\right)} = e^{i\upsilon(x)} e^{i\frac{1}{3}\left(\eta_{N,\downarrow}^R - \eta_{N,\uparrow}^L + \eta_{1,\uparrow}^R - \eta_{1,\downarrow}^L\right)},
\tag{4.21}
$$

$$
U_x = e^{i\frac{1}{3}\int_0^L \partial_x \eta_{1,\uparrow}^R dx}.
\tag{4.22}
$$

All the η fields are functions of position x. The phase $\upsilon(x)$ in Eq. (4.21) is given by

$$\upsilon(x) = \frac{1}{3}\left[\sum_{n=1}^{N-1}\left(\eta_{n+1,\uparrow}^{R} - \eta_{n,\uparrow}^{L}\right) - \sum_{n=1}^{N-1}\left(\eta_{n+1,\downarrow}^{L} - \eta_{n,\downarrow}^{R}\right)\right]. \tag{4.23}$$

Since all the operators in the sum are pinned by the bulk Hamiltonian, they may be treated as classical fields, and their value becomes x-independent in any one of the ground states. Similarly, the combination of operators $(\eta_{N,\downarrow}^{R} - \eta_{N,\uparrow}^{L} + \eta_{1,\uparrow}^{R} - \eta_{1,\downarrow}^{L})$ which appears on the right side of Eq. (4.21) is pinned by the coupling to the boundary, and becomes independent of x. Therefore, the operators $U_y(x)$ may be considered to be independent of x within the manifold of ground states.

The form of $U_y(x)$ shown in the first equality of Eq. (4.21) is useful because it allows us to express $U_y(x)$ as a product of electronic operators:

$$U_y = e^{i\left(\sum_{n=1}^{N}\left(\phi_{n,\uparrow}^{R} - \phi_{n,\uparrow}^{L} + \phi_{n,\downarrow}^{R} - \phi_{n,\downarrow}^{L}\right)\right)}. \tag{4.24}$$

where the x-dependence of the operators is omitted for brevity. It can be verified that

$$[U_y(x), U_y(x')] = 0 \tag{4.25}$$

and that

$$[U_x, H_I] = [U_y, H_I] = 0, \tag{4.26}$$

so that operating $U_y(x)$ or U_x on a ground state leaves the system in the ground state manifold. Using the commutation relations of the η-fields, it can also be checked directly that

$$U_x U_y(x) = U_y(x) U_x e^{\frac{2\pi}{3}i}, \tag{4.27}$$

independent of x. The smallest representation of this algebra requires 3×3 matrices [111], which shows that the ground state of the idealized Hamiltonian (4.19) must be at least 3-fold degenerate.

The operators U_y (U_x) can be interpreted as the creation of a quasiparticle-quasihole pair, tunneling of the quasiparticle across the y (x) direction of the torus and annihilating the pair at the end of the process. In fact, if we adopt this interpretation, Eq. (4.27) is a direct consequence of the fractional statistics of the quasiparticles [111].

A similar analysis can be carried out for the SS case. U_x is identical to the operator used
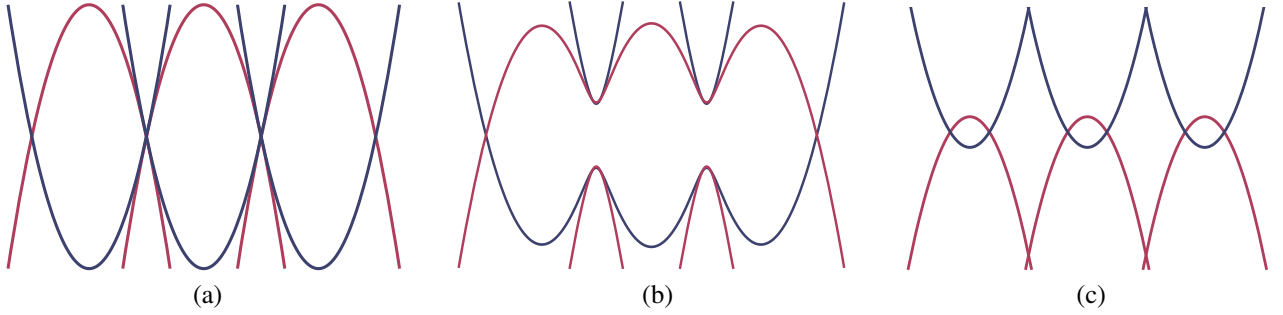
Figure 4.6: (a) The spectrum of the wires model for an electron-hole double layer at filling $v = 1$ when all the inter-wire terms are switched off. The spectra in blue correspond to wires in the electron layer, and the spectra in red correspond wires in the hole layer. (b) The spectrum when tunneling between wires in the same layer is switched on. A gap is formed in the bulk, and we get achiral edge modes. (c) The spectrum in the fractional case $v = 1/3$.

in the FF case, but now U_y takes the form

$$U_y = e^{i\frac{1}{3}\left(\Sigma_{n=1}^{N}\left(\eta_{n,\uparrow}^{R}-\eta_{n,\uparrow}^{L}+\eta_{n,\downarrow}^{L}-\eta_{n,\downarrow}^{R}\right)\right)}, \tag{4.28}$$

and the entire analysis can be repeated.

4.3.2   The coupled wires construction of an electron-hole double layer

In this Section we explain how one can model a quantum Hall electron-hole double layer at a fractional filling factor $v = 1/3$ using a set of coupled wires.

We examine a system with two layers, each containing an array of wires. In one layer, the electron layer, we tune the system such that only states near the bottom of the electronic band are filled. In this case, we can approximate the spectra of the various wires as parabolas. If we add a constant magnetic field B perpendicular to the layers, and use the Landau gauge to write the electromagnetic potential as $\mathbf{A} = -By\hat{x}$, the entire band structure of wire number n will be shifted by an amount $2k_\phi n$, where k_ϕ is defined as $k_\phi = \frac{eBa}{2\hbar}$. The energy of wire number n is therefore written in the form (if we choose the position of wire number 1 to be at $y = a/2$)

$$E_n(k) = \frac{(k_x - (2n-1)k_\phi)^2}{2m} + U_e, \tag{4.29}$$

where U_e is a constant term, and m is the effective mass. In the hole layer the bands of the

various wires are nearly filled, such that we can expand the energy near the maximum as

$$E_n(k) = -\frac{(k_x - (2n-1)k_\phi)^2}{2m} + U_h.$$ (4.30)

In the above, we assumed that the effective masses of the electron and the hole layers have the same magnitude and opposite signs. We assume that $U_h > U_e$, and tune the chemical potential to be $\mu = \frac{U_e + U_h}{2}$. Defining $\delta\varepsilon = \frac{U_h - U_e}{2}$, we get the spectra

$$E_n(k) - \mu = \left[\frac{(k_x - (2n-1)k_\phi)^2}{2m} - \delta\varepsilon\right]\sigma,$$ (4.31)

where $\sigma = 1(-1)$ for the electron (hole) layer. This way the system has a built-in particle-hole symmetry in its low energy Hamiltonian. Notice that as a result of the magnetic field, the spectra of the two layers are shifted in the same direction. This is a consequence of the common origin of the electron and hole spectra from a Bloch band whose shift is determined by the direction of the magnetic field.

We define $k_F^0 = \sqrt{2m\delta\varepsilon}$, and the filling factor is now given by $\nu = \frac{k_F^0}{k_\phi}$. In the case $\nu = 1$, the corresponding spectrum is given by Fig. (4.6a). As before, if we apply tunneling between adjacent wires in the same layer, we get the gapped spectrum in Fig. (4.6b). Furthermore, we see that each edge carries a pair of counter propagating edge modes (one for each layer).

It is straightforward to generalize this to the case of filling $\nu = 1/3$, shown in Fig. (4.6c). To treat this case, we again linearize the spectrum, and write the problem in terms of the chiral bosonic degrees of freedom $\phi_{n,\sigma}^{R/L}$, where now $\sigma = e, h$ represents the layer number, and n represents the wire index. To treat the fractional case, we define new chiral fields $\eta_{n,\sigma}^{R/L} = 2\phi_{n,\sigma}^{R/L} - \phi_{n,\sigma}^{L/R}$. Like before, it can be checked that these modes behave like modes at filling 1, so we can repeat the analysis performed in this case.

This process leaves us with two counter propagating η-modes on each edge: $\eta_{1,e}^L, \eta_{1,h}^R, \eta_{N,e}^R, \eta_{N,h}^L$. These modes can be gapped out by terms analogous to the terms in Eq. (4.18):

$$\tilde{H}_1^S = \tilde{\Delta}_1 \cos\left(\eta_{1,e}^L + \eta_{1,h}^R + \tilde{\delta}_1\right),$$
$$\tilde{H}_1^F = \tilde{B}_1 \cos\left(\eta_{1,e}^L - \eta_{1,h}^R + \tilde{\beta}_1\right),$$
$$\tilde{H}_N^S = \tilde{\Delta}_N \cos\left(\eta_{N,e}^R + \eta_{N,h}^L + \tilde{\delta}_N + 4k_\phi Nx\right),$$
$$\tilde{H}_N^F = \tilde{B}_N \cos\left(\eta_{N,e}^R - \eta_{N,h}^L + \tilde{\beta}_N\right).$$ (4.32)

In contrast to the case of the fractional topological insulator, here the backscattering terms con-

serve momentum, i.e., do not include phases that are linear in x. Rather, the superconducting term $\tilde{H}_N^S$ appears not to conserve momentum. However, the flux between the two superconductors will lead to a winding of the phase difference between them, which can cancel the x-dependent phase of H_N^S.

Let us first consider the situation where the bounding superconductor wires are thin enough that there are no vortices inside them. The energy of a superconducting ring is minimized when $\Delta\phi$, the change in the superconducting phase around the ring is equal to $2e\Phi$, where Φ is the magnetic flux enclosed by a circle embedded at the center of the wire. The value of $\Delta\phi$ is quantized in multiples of 2π, and in practice there may exist a number of metastable states where it differs from $2e\Phi$ by a finite amount and the wire carries a supercurrent around its circumference. Let us consider a model where there is a distance a' between the center of the inner most superconductor and the center of our first electron-hole nanowire and a similar separation between the Nth nanowire and the outer superconductor. If the centers of the nanowires are separated from each other by a distance a, then the flux Φ is equal to $BaL_x(N-1+2(a'/a))$. In this case, if the superconductors are in their ground states, we get $\tilde{\delta}_1 = \left(-2+4\frac{a'}{a}\right)k_\phi x + \tilde{\delta}_1^0$ and $\tilde{\delta}_N = -\left(4N-2+4\frac{a'}{a}\right)k_\phi x + \tilde{\delta}_N^0$, where $\tilde{\delta}_{1(N)}^0$ do not depend on x. If a' is tuned to $a' = a/2$, the oscillating phases are eliminated from Eq. (4.32).

If a' differs from $a/2$, it may be still possible to gap out the edges. If the phase mismatch is small, and if coupling to the superconductor is not too weak, then there can be an adjustment of the electron and hole occupations in the nanowires nearest the two edges, which allows the phase change around the nanowires to match the phase change in the superconductors. The energy gain due to formation of a gap can exceed the energy cost of altering the charge densities in the nanowires.

If the difference between a' and $a/2$ is too large, then carrier densities in the inner and outer nanowires will not change enough to satisfy the phase matching condition. In this case, a variation of the magnetic field of order $1/N$ would eliminate the x-dependence of the phases at the cost of introducing quantum Hall quasiparticles in the bulk of the system. For large N, the density of these quasiparticles will be small. Presumably they will become localized and not take the system out of the quantum Hall plateau.

We note that the separation a' can be engineered, and, in principle can even be made negative. Consider, for example, a situation where the superconducting wire sits above the plane of the nanowires, so that depending on the shape of a cross-section of the wire, its center of gravity may sit inside or outside of the line of contact to the outermost nanowire.

The situation is more complicated if the superconductors are thick enough that they contain vortices in the presence of the applied magnetic field. If the vortices are effectively pinned, however, it should be possible to achieve conditions where the electron-hole system is gapped

and experiments such as Josephson current measurements can be performed.

The degeneracy of the ground states in both the SS and FF cases may be shown by defining the two operators U_x and U_y in exactly in the same form as we did in Sec. 4.3.1.3 (with $\downarrow \rightarrow e$ and $\uparrow \rightarrow h$), and following the same analysis.

4.4 Measurable imprint of the topological degeneracy in quasi-one dimensional systems

We now look at the quantum Hall double-layer system with $\nu = \pm 1/3$. As long as the bulk gap does not close, in the limit of infinite L_x and infinite N (or L_y) we expect deviations from the idealized Hamiltonian not to couple the three ground states. When N and L_y are finite and L_x is still infinite, coupling does occur, and the degeneracy is lifted.

Generally, Hermitian matrices operating within the 3×3 subspace of ground states of the idealized Hamiltonian may all be written as combination of nine unitary matrices $O_{j,k}$

$$\Delta H = \sum_{(j,k)=(-1,-1)}^{(1,1)} \lambda_{j,k} O_{j,k}. \tag{4.33}$$

where

$$O_{jk} = U_x^j U_y^k. \tag{4.34}$$

and $\lambda_{jk} = \lambda^*_{-j,-k} e^{-\frac{i2\pi jk}{3}}$. Note that a direct consequence of Eq. (4.27) is that $U_x^3 = U_y^3 = 1$ (this can most easily be understood by recalling that the operators transport quasiparticles across the torus. Acting three times with each of them is equivalent to transporting an electron around the torus, which cannot take us from one ground state to another). However, in the limit of infinite L_x local operators cannot distinguish between states of different fractional charges, and therefore cannot contain the operator U_x. Thus, up to an unimportant constant originating from λ_{00}, deviations from the idealized Hamiltonian (projected to the ground state manifold) take the form of Eq. (4.4):

$$\Delta H = \lambda U_y + \lambda^* U_y^\dagger, \tag{4.35}$$

The coefficient λ may be expressed as an integral,

$$\lambda = \int dx T(x), \tag{4.36}$$

and we expect that the absolute value of the amplitude $T(x)$ should fall off exponentially with

N. One can see this explicitly in the various models we have constructed from coupled wires. For example, in the case of a fractional topological insulator with magnetic boundaries, the operator U_y, according to (32) and (17) involves a product of factors involving four electronic creation and annihilation operators on each of the N wires. The bare Hamiltonian contains only four-fermion operators on a single wire, and two-fermion operators that connect adjacent wires, with an amplitude t that we consider to be small. The operator U_y can only be generated by higher orders of perturbation theory, in which the microscopic tunneling amplitude t occurs at least $2N$ times. In our analysis, we have assumed that interaction strengths on a single wire are comparable to the Fermi energy E_F, so we expect T to be of order $|t/E_F|^{2N}$ or smaller. Similar arguments apply to the other cases of superconducting boundaries or electron-hole wires. We also note that if the system is time-reversal invariant, we must have $T = T^*$.

The phase of $T(x)$ depends on the realization - electron-hole quantum Hall *vs.* fractional topological insulator - and on the gapping mechanism - two superconductors or two magnets. We start from the case of the fractional topological insulator gapped by two superconductors. Eqs. (4.18) shows that for the edges to be gapped, the superconductors on the two edges should have uniform phases $\tilde{\delta}_1, \tilde{\delta}_N$. We choose a gauge where $\tilde{\delta}_1 = 0$ and denote $\varphi = \tilde{\delta}_N$ to be the phase difference.

In the case of a fractional topological insulator, the proximity gapping terms are

$$\tilde{H}_1^S = \tilde{\Delta}_1 \int dx \cos\left(\eta_{1,\uparrow}^L + \eta_{1,\downarrow}^R + \varphi\right),$$
$$\tilde{H}_N^S = \tilde{\Delta}_N \int dx \cos\left(\eta_{N,\uparrow}^R + \eta_{N,\downarrow}^L\right) \tag{4.37}$$

(note that these terms involve coupling to the superconductor, and we therefore have $\tilde{\Delta}_{1(N)} \propto |\Delta_{1(N)}|$, where $\Delta_{1(N)}$ are the corresponding superconducting order parameters). We define new bosonic fields through the additional transformation

$$\tilde{\eta}_{1,\uparrow}^L = \eta_{1,\uparrow}^L + \frac{\varphi}{2}, \quad \tilde{\eta}_{1,\downarrow}^R = \eta_{1,\downarrow}^R + \frac{\varphi}{2}, \tag{4.38}$$

and $\tilde{\eta}_{n,\sigma}^\rho = \eta_{n,\sigma}^\rho$ for all the other values of n, σ, ρ. If we rewrite the Hamiltonian in terms of the new fields, the phase φ is eliminated from the idealized Hamiltonian. However, this modifies the operator U_y (defined in Eq.(4.21)), which now takes the form

$$U_y = e^{i\frac{1}{3}\left(\sum_{n=1}^N \left(\tilde{\eta}_{n,\uparrow}^R - \tilde{\eta}_{n,\uparrow}^L + \tilde{\eta}_{n,\downarrow}^L - \tilde{\eta}_{n,\downarrow}^R\right)\right)} e^{i\frac{\varphi}{3}}. \tag{4.39}$$

Thus, a non-zero phase difference φ shifts the argument of λ in Eq. (4.35) by $\frac{\varphi}{3}$. In the time

reversal symmetric case λ is real, and we find, by diagonalizing ΔH, that

$$\Delta E_1 = 2\lambda L_x \cos\left(\frac{\varphi}{3}\right),$$

$$\Delta E_2 = 2\lambda L_x \cos\left(\frac{\varphi - 2\pi}{3}\right),$$

$$\Delta E_3 = 2\lambda L_x \cos\left(\frac{\varphi + 2\pi}{3}\right). \tag{4.40}$$

The resulting spectrum as a function of φ is depicted in Fig. (4.2a).

At $\varphi = \pi n$ the degeneracy is not completely lifted, as two states remain 2-fold degenerate. These states are not coupled by the low energy Hamiltonian (4.35) and the lifting of their degeneracy requires terms of $j \neq 0$ in (4.34). Such terms distinguish between states of different edge charges f_i and their amplitude scales as $e^{-(L_x/\xi_x)}$. Neglecting this splitting, Eq. (4.40) shows that all eigenstates have a 6π periodicity. A measurement of the Josephson current, given by the derivative of the energy with respect to φ, can detect the 6π-periodicity. Due to the exponentially small splitting at the crossing points, this property can be observed by changing the flux at a rate that is not slow enough to follow this splitting.

Note that the 6π-periodic component of the spectrum is completely determined by Eq. (4.27). This part of the spectrum is therefore highly insensitive to the microscopic details, and can serve as a directly measurable imprint of the topological degeneracy with only a few wires. There will also be a contribution from ordinary Cooper pair tunneling between the superconductors, which does not distinguish between the ground states and has 2π periodicity. This term will alter the detailed shapes of the three spectra but not their splitting or periodicity. In the case where time reversal symmetry does not hold, λ is not necessarily real. Consequently, the spectrum in Eq. (4.40) is shifted according to $\varphi \to \varphi + \text{Arg}(\lambda)$, and the crossing points are not constrained to be at $\varphi = \pi n$.

Similar results arise in the FF case for a quantum Hall electron-hole double layer. Now, the angle φ is the relative orientation angle of the Zeeman fields (which lies in the $x - y$ plane). To be precise, if we fix the Zeeman field at wire number N to point at the x direction, and the field at wire number 1 to have an angle φ relative to the x direction, we get the proximity terms

$$\tilde{H}_1^F = \tilde{\lambda}_{1F} \int dx \cos\left(\eta_{1,\uparrow}^L - \eta_{1,\downarrow}^R + \varphi\right),$$

$$\tilde{H}_N^F = \tilde{\lambda}_{NF} \int dx \cos\left(\eta_{N,\uparrow}^R - \eta_{N,\downarrow}^L\right). \tag{4.41}$$

Similar to Eq. (4.38), we define new bosonic fields through the transformation

$$\tilde{\eta}_{1,\uparrow}^L = \eta_{1,\uparrow}^L + \frac{\varphi}{2}, \quad \tilde{\eta}_{1,\downarrow}^R = \eta_{1,\downarrow}^R - \frac{\varphi}{2}, \tag{4.42}$$

and $\tilde{\eta}_{n,\sigma}^{\rho} = \eta_{n,\sigma}^{\rho}$ for the other fields. Again, the gapping term acting on the N'th wire returns to its original form (with $\varphi = 0$), but U_y becomes $U_y e^{i\frac{\varphi}{3}}$. Therefore, the spectrum as a function of φ is identical to the spectrum found in the SS case.

In the other two cases, the situation is more complicated, since φ depends on x. For the quantum Hall electron-hole double layer gapped by superconductors φ increases linearly with x, due to the flux penetrating the junction between the two superconductors. For the fractional topological insulator gapped by magnets, Eq. (4.18) requires that β_N increases linearly with x. In both cases, this winding leads to $\lambda = \int dx |t(x)| e^{i2\pi nx/L + i\varphi}$, with n an integer. A uniform tunneling amplitude $|t(x)|$ then leads to a vanishing λ, while non-uniformity allows for a non-vanishing λ.

4.5   Extensions to other Abelian states

We have shown above that it is possible effectively realize experimentally the $\nu = \frac{1}{3}$ FQHE state on a torus, and that by measurement of the Josephson effect in the resulting construction we can directly measure the corresponding topological degeneracy. In this section we extend the above results to other Abelian FQHE states.

For a FQHE state described by a $M \times M$ K-matrix, there is a ground state degeneracy of $d = \det K$ on a torus, and d topologically distinct quasiparticles. Each quasiparticle is a multiple of the minimally charged quasiparticle, whose charge is $e^* = \frac{e}{d}$.

Repeating the analysis we carried out in Sec. 4.3, we consider an electron-hole double layer system or a fractional topological insulator, and couple the counter-propagating edge modes. Since there are now M pairs of counter-propagating modes on each edge, we need m scattering terms. We assume that these terms are all mutually commuting, that they are either all charge-conserving or all superconducting, and that the M edge modes of each layer (spin-direction) are mutually coupled. Under these assumptions, each of the four edges is characterized by a single quantum number - the fractional part of the total charge f_i (with $i = 1, \cdots, 4$), which may take the values $-\frac{d-1}{2d}, -\frac{d-3}{2d}, \cdots, \frac{d-1}{2d}$. The mutual coupling between the M edge modes excludes the possibility of other quantum numbers being constants of motion. Similar to the case where $\nu = 1/3$, the requirements of a total integer charge for each layer or spin direction, together with the mechanism of gapping and the requirement to minimize the energy of the edge Hamiltonians, relate all values of f_i to one another.

We work in a basis $|f\rangle$ where the fractional charges f_i are well defined. We define the unitary operator U_y which transfers a single minimally charged quasiparticle, analogously to the operator defined before, such that $U_y|f\rangle = |(f + e^*/e) \bmod(1)\rangle$. It follows that $U_y^l|f\rangle =

$|(f + le^*/e) \bmod(1)\rangle$, and that $U_y^d = 1$. We therefore have in general

$$\left(U_y^l\right)^\dagger = U_y^{d-l}. \tag{4.43}$$

Again, in the quasi-1D limit where L_x is infinite and N is finite, Hermitian combinations of the operators U_y^l are the only operators capable of lifting the degeneracy. The amplitude of these terms falls exponentially with N. In order to analyze the effects of these perturbations we consider terms of the form

$$\Delta H = \sum_{l=1}^{(d-1)/2} \left(\lambda_l U_y^l e^{i\delta_l} + h.c.\right), \tag{4.44}$$

where $\lambda_l \propto e^{-N/\xi_l}$ is a real coefficient (note that we expect terms with $l > 1$ to result from higher orders in e^{-N}. More specifically, we expect $\xi_l \propto \frac{1}{l}$). The summation was terminated at $(d-1)/2$ because of Eq. (4.43) and the requirement that the Hamiltonian is Hermitian. Again, the resulting spectrum depends on the realization, the gapping mechanism, and the uniformity of the tunneling amplitude. This dependence is similar to the one discussed for $v = 1/3$. For example, for uniform tunneling between two superconductors separated by a fractional topological insulator, a relative phase φ between the two superconductors translates to $\delta_l = \varphi \frac{e^*}{e} l$.

The spectrum of this Hamiltonian for the time reversal symmetric case is then

$$\Delta E_p = 2 \sum_{l=1}^{(d-1)/2} \lambda_l \cos\left(\frac{l}{d}(\varphi + 2p\pi)\right), \tag{4.45}$$

with $p = 1 \ldots d$. Each eigenstate has a $2\pi d$-periodicity, and like the $v = 1/3$ case we find that the overall periodicity is 2π times the degeneracy of the system in the thermodynamic limit. In addition, similar to the $v = 1/3$ case, at the time-reversal invariant points $\varphi = \pi n$, we have degeneracy points protected by the length of the wires. For example, at $\varphi = 0$, we have $\frac{d-1}{2}$ pairs of states $|p\rangle, |d-p\rangle$ $(p = 1, \ldots \frac{d-1}{2})$ which have the same energy. It can easily be checked from Eq. (4.45) that the same number of crossings occurs for any $\varphi = \pi n$. Hence if the spectrum is measured, the degeneracy d can found by simply counting the number of crossing points at $\varphi = \pi n$. Note that due to the terms with $l > 1$, we can have additional crossing points at $\varphi \neq n\pi$. Again, if time reversal symmetry does not hold the crossing points can be shifted. One can still show that in the most general case there must be at least the same number of crossing points as the number of crossing points at $\varphi = \pi n$ in the time reversal invariant case. The smallest number of degeneracy points occurs when the functions ΔE_p

have a single maximum and a single minimum between 0 and $2\pi d$. In that case, the energies that correspond to two different values of p must cross at two points between 0 and $2\pi d$. We therefore have 2 crossing points for each pair p_1, p_2, The total number of degeneracy points, summed over all the pairs p_1, p_2 is therefore $2\binom{d}{2} = d(d-1)$, which is the number of crossing points at all the values $\varphi = \pi n$ in the time reversal invariant case. Depending on the values of λ_l, we may have more than a single minimum and a single maximum, in which case we can get additional crossing points.

As an example we examine the case $\nu = 2/5$, which can be characterized by the K-matrix

$$K = \begin{pmatrix} 3 & 2 \\ 2 & 3 \end{pmatrix}. \tag{4.46}$$

The degeneracy on a torus in this case is $d = 5$ and the spectrum (in the time reversal invariant case) is

$$\Delta E_p = 2\lambda_1 \cos\left(\frac{1}{5}(\varphi + 2p\pi)\right) + 2\lambda_2 \cos\left(\frac{2}{5}(\varphi + 2p\pi)\right), \tag{4.47}$$

with $p = 1\dots 5$. If we take for example $\lambda_2/\lambda_1 = 0.2$, the resulting spectrum is shown in Fig. (4.2b).

Chapter 5

From an array of quantum wires to three-dimensional fractional topological insulators

This chapter presents the results of our third project, presented in Ref. [58]. In previous chapters (and other previous works), it was demonstrated that the coupled-wire approach is an effective tool for constructing tractable models of 2D fractional phases. In this chapter, we extend this approach to 3D and study the resulting time-reversal invariant fractional strong topological insulators.

5.1 Introduction

While topological phases have conclusively been found to exist in three-dimensions (3D), fractional phases are still usually associated with 2D systems. This is a consequence of the well-known theorem stating that anyonic statistics between two point-particles cannot occur in 3D [112, 113].

A possible way to go around this theorem and realize topologically ordered phases in 3D is to consider loop excitations, which can have non-trivial braiding statistics with point-particles, as well as other loops. Indeed, a few recent works [86, 114–121] have used various non-perturbative approaches to discuss fractional topological insulators in 3D. These are the fractional counterparts of the well-studied non-interacting strong topological insulators.

In this work, we extend the coupled-wire approach to 3D, and apply it to the case of fractional topological insulators.

The resulting topologically ordered phase studied here has a novel gapless surface mode,

D:/Dropbox (Weizmann Institute)/PC/Thesis/papers/3D/3d_wires.png

(a)   (b)   (c)
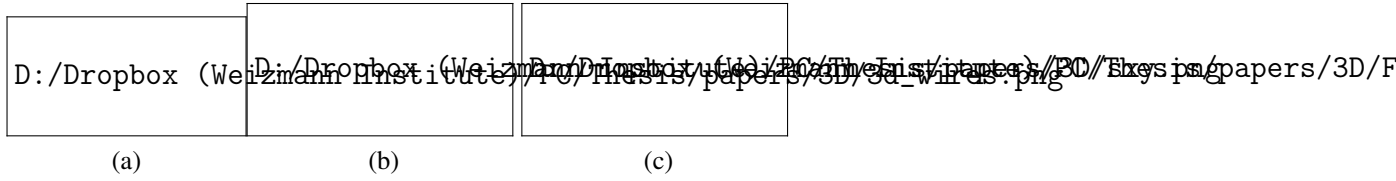
Figure 5.1: (a) A schematic depiction of the array of wires studied in this manuscript. The fractional strong topological insulator phase we construct has an exotic fractional Dirac liquid on the surface. Upon breaking time-reversal symmetry or charge conservation, we end up with a gapped surface displaying unique topological properties. For example, by breaking time-reversal symmetry, we get a halved fractional quantum Hall effect, characterized by a surface Hall conductance of the form $\sigma_{xy} = \frac{1}{2}\frac{e^2}{mh}$, where m is an odd integer (in a state associated with the 2D Laughlin state at filling $\nu = 1/m$). On the magnetic domain wall shown in (b), one therefore finds a chiral Luttinger liquid, similar to the edge mode of the corresponding 2D Laughlin-state. If the system is gapped by proximity to an s-wave superconductor (i.e., by breaking charge conservation), we get an exotic time-reversal invariant topological superconductor. It is interesting to study the boundary between a superconducting region and a magnetic region, as depicted in Fig (c). A fractional Majorana mode, which cannot be described by a free Majorana theory, is found on the interface between the two regions.

which cannot be described by Dirac's theory of free fermions. Throughout this work, we refer to the surface as a fractional Dirac liquid. It is insightful to study what happens to the fractional Dirac theory once it is gapped by breaking time reversal symmetry or charge conservation.

We will see that if a time reversal breaking perturbation is introduced, the surface acquires a Hall conductance of the form $\sigma_{xy} = \frac{1}{2m}\frac{e^2}{h}$ in a state at filling $\nu = 1/m$. This Hall conductance is half that of the associated 2D Laughlin FQH state, and we therefore refer to this effect as a halved fractional quantum Hall effect.

In addition, we will break charge conservation by proximity coupling the surface to an s-wave superconductor. The resulting superconducting state is found to be topologically nontrivial. On the surface of a non-interacting strong topological insulator, for example, one finds a phase that resembles a $p_x + ip_y$ superconductor, but has time reversal symmetry [14]. One way to reveal the topological nature of the surface is to separate the surface into two domains: one with broken time-reversal symmetry, and another with broken charge conservation. It was shown in Ref. [14] that a chiral Majorana mode is localized near the boundary separating the two regions.

Repeating the same thought experiment in the fractional phase, we find a strongly correlated chiral mode on the boundary, which cannot be described by a free Majorana theory. In particular, the tunneling density of states associated with this 1D channel is proportional to ω^{m-1}.

(a) · (b)
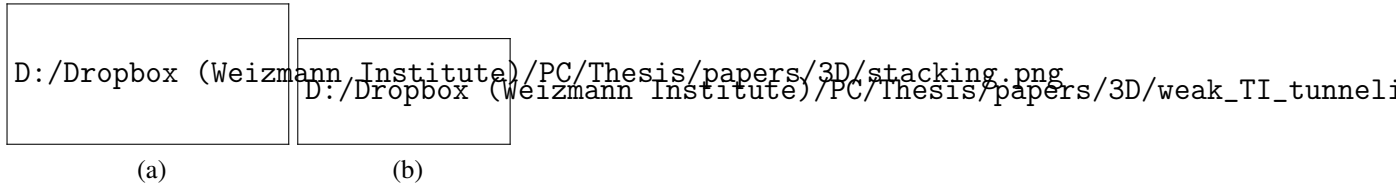
Figure 5.2: (a) The simplified model we use to describe a weak topological insulator. Each plane forms an S_z-conserving 2D topological insulator. The edge of each layer therefore contains counter-propagating spin-up and spin-down modes, represented by red and blue arrows. (b) A diagrammatic depiction of the surface of the simplified model. The vertical direction represents the layer index, and the horizontal direction represents spin. The symbol $\otimes$ ($\odot$) corresponds to a right (left) mover. We introduce nearest-layer coupling terms, represented by arrows connecting different chiral modes. Time reversal symmetry relates the amplitudes of the terms represented by the full arrows to the amplitudes of the terms represented by the dashed arrows. The above model can be decomposed into two decoupled gapless Hamiltonians, represented by the green and purple arrows.

5.2 Fractional weak topological insulators

5.2.1 Weak topological insulators

Before discussing fractional weak topological insulators, we briefly review the physics of non-interacting weak topological insulators.

To construct a simple model for a weak topological insulator, we imagine stacking many 2D topological insulators (see Fig. (5.2a) for illustration).

For simplicity, we assume that the 2D topological insulators in the various layers conserve S_z. We can therefore describe their edge states as counter propagating spin-up and spin-down modes. In the limit where the layers are decoupled, the surface in the xz direction, for example, is composed of these helical modes. The modes are represented diagrammatically in Fig. (5.2b), where the vertical direction represents the layer index, and the horizontal direction represents the spin. The symbol $\otimes$ ($\odot$) corresponds to a right (left) mover.

We now introduce coupling between adjacent layers. In doing so, we consider only the terms represented by the arrows in Fig. (5.2b), as these are the only terms capable of gapping the surface. Time reversal symmetry relates the amplitudes of the terms represented by the full arrows and those represented by the dashed arrows.

To be concrete, if we define the electron annihilation operators $\psi_{n,\uparrow}(x), \psi_{n,\downarrow}(x)$ (where n is the layer index), we can write the low energy surface Hamiltonian in the form

$$H = H_z + H_x, \tag{5.1}$$

where

$$H_x = -iv \sum_n \int dx \left[\psi_{n,\uparrow}^\dagger(x) \partial_x \psi_{n,\uparrow}(x) - \psi_{n,\downarrow}^\dagger(x) \partial_x \psi_{n,\downarrow}(x) \right] \tag{5.2}$$

represents the Hamiltonian of the decoupled helical edge modes, and

$$H_z = t \sum_n \int dx \left[\psi_{n,\uparrow}^\dagger(x) \psi_{n+1,\downarrow}(x) e^{i\alpha} - \psi_{n,\downarrow}^\dagger(x) \psi_{n+1,\uparrow}(x) e^{-i\alpha} + h.c. \right] \tag{5.3}$$

represents their nearest-layer coupling. In the above, α is a fixed phase, which we set to be 0 for simplicity.

If the system has periodic boundary conditions in the x and z directions, k_x and k_z are good quantum numbers. We can therefore write the Hamiltonian in k-space, where it takes the form $H = \sum_{k_z} \int dk_x \psi^\dagger(\vec{k}) \mathcal{H}(\vec{k}) \psi(\vec{k})$, with $\psi(\vec{k}) = (\ \psi_\uparrow(\vec{k}), \quad \psi_\downarrow(\vec{k})\ )^T$ and

$$\mathcal{H} = -2t\sigma_y \sin(k_z a) + vk_x \sigma_z \tag{5.4}$$

(here the σ_i's are Pauli matrices acting on the spin degrees of freedom). We see that we have two Dirac cones on the surface: one around $(k_x = 0, k_z = 0)$, and another around $(k_x = 0, k_z = \pi)$. These are not protected by time-reversal symmetry, as time-reversal invariant terms can couple the two Dirac modes and gap them out. However, such terms necessarily involve a large momentum transfer. Therefore, if lattice translation invariance is also imposed, the two Dirac modes remain protected.

5.2.2 The surface of fractional weak topological insulators

In order to generalize the above simplified model to a fractional weak topological insulator, we imagine stacking layers of 2D fractional topological insulators. Again, we focus on the S_z conserving case, where each 2D fractional topological insulator can be thought of as two decoupled FQHE layers. These two FQH states have equal densities, but opposite fillings $\pm \nu$ and spins.

We focus on the time reversal invariant analog of a Laughlin state with filling $\nu = 1/m$, where m is an odd integer. Before introducing inter-layer coupling terms, the natural way to describe the edge modes of the various layers is in terms of two boson fields $\chi_n^\uparrow$ and $\chi_n^\downarrow$. These modes satisfy the commutation relations

$$\left[\chi_n^\sigma(x), \chi_{n'}^{\sigma'}(x') \right] = \frac{1}{m} i\pi\sigma \delta_{n,n'} \delta_{\sigma,\sigma'} \mathrm{sign}(x-x') + \frac{1}{m^2} i\pi \mathrm{sign}(n-n') + \frac{1}{m^2} \pi \delta_{n,n'} \sigma_y^{\sigma,\sigma'}, \tag{5.5}$$

where in the above $\sigma = 1(-1)$ for spin $\uparrow (\downarrow)$. In terms of these, the chiral fermion operators take the form $\tilde{\psi}_{n,\sigma} \propto e^{im\chi_n^\sigma}$, and the Laughlin quasiparticle operators are given by $\tilde{\psi}_{n,\sigma}^{QP} \propto e^{i\chi_n^\sigma}$. The second and third terms in Eq. 5.5 ensure that fermions associated with different modes anti-commute. If we introduce inter-layer coupling terms, the effective low energy Hamiltonian describing the surface is given by

$$\tilde{H} = \tilde{H}_z + \tilde{H}_x, \tag{5.6}$$

where

$$\tilde{H}_x = \frac{mv}{4\pi} \sum_{n,\sigma} \int dx \, (\partial_x \chi_n^\sigma)^2 \tag{5.7}$$

represents the decoupled chiral Luttinger liquids, and

$$\tilde{H}_z = \tilde{t} \sum_n \int dx \left(\tilde{\psi}_{n,\uparrow}^\dagger \tilde{\psi}_{n+1,\downarrow} - \tilde{\psi}_{n,\downarrow}^\dagger \tilde{\psi}_{n+1,\uparrow} + h.c. \right) \tag{5.8}$$

represents their coupling. In what follows we assume that the amplitude $\tilde{t}$ is large enough such that these operators flow to the strong coupling limit (if they are considered separately). In the integer case, where $m = 1$, $\tilde{H}$ reduces to the Hamiltonian H defined in Eq. (5.1), as can be seen directly by rewriting H using Abelian bosonization. In the fractional case, where $m > 1$, $\tilde{H}$ cannot be mapped to a non-interacting fermionic Hamiltonian. However, the model can still be represented by the diagram shown in Fig. (5.2b). Notice that now the symbols $\otimes$ and $\odot$ represent right and left moving $\tilde{\psi}$ (or χ) fields, respectively.

Each of the two terms in Eq. (5.8), if considered separately, can gap out the spectrum in the thermodynamic limit. However, the two gapped phases that result from these terms are topologically distinct. Noting that the two non-commuting operators have the same amplitude and scaling dimension, it is clear that the system must be in a critical point between the two gapped phases. We emphasize that the criticality of the surface is imposed by time reversal symmetry, and is not a result of fine-tuning the Hamiltonian. It is explicitly assumed that additional interacting terms do not destabilize the critical point. This crucial assumption must be checked for a given microscopic model.

Like in the integer case, this gapless model is represented by two decoupled gapless theories. This can be identified by writing the Hamiltonian in the form $\tilde{H} = \tilde{H}_1 + \tilde{H}_2$, with

$$\tilde{H}_1 = \frac{mv}{4\pi} \sum_{n,\sigma} \int dx \left(\partial_x \chi_{2n}^\uparrow \right)^2 + \left(\partial_x \chi_{2n+1}^\downarrow \right)^2 + \tilde{t} \sum_n \int dx \left(\tilde{\psi}_{2n,\uparrow}^\dagger \tilde{\psi}_{2n+1,\downarrow} - \tilde{\psi}_{2n+2,\uparrow}^\dagger \tilde{\psi}_{2n+1,\downarrow} + h.c. \right),$$
$$\tag{5.9}$$

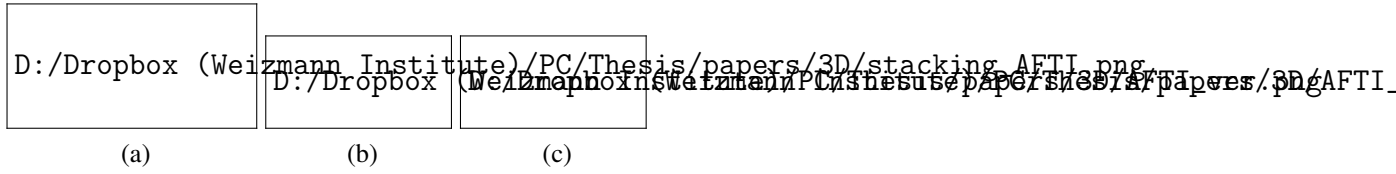(a)   (b)   (c)

Figure 5.3: (a) The simplified model we use to describe an antiferromagnetic topological insulator and its fractional analog. Each layer can be thought of as a single-component QHE system at filling $\pm\nu$ (where $\nu = 1$ in the integer case, and in the fractional case we consider $\nu = 1/m$, where m is an odd integer). Due to the existence of a modified time-reversal symmetry, given by the product of the original time-reversal operator and a translation by a unit cell, the xz surface remains gapless even in the presence of inter-layer coupling terms. The surface can be described in terms of coupled 1D channels, which enables a simple derivation of universal surface properties. We argue that these properties remain true for a strong topological insulator and its fractional analog, where the surface is protected by the local time reversal symmetry. (b) A diagrammatic representation of xz surface of the above model in terms of the coupled 1D chiral edge modes. (c) The diagram that corresponds to the situation where the modified time-reversal symmetry is explicitly broken by introducing a term of the form (5.11) with $\tilde{t}' = \tilde{t}$.

$$\tilde{H}_2 = \frac{m\nu}{4\pi} \sum_{n,\sigma} \int dx \left(\partial_x \chi_{2n+1}^{\uparrow} \right)^2 + \left(\partial_x \chi_{2n}^{\downarrow} \right)^2 + \tilde{t} \sum_{n} \int dx \left(\tilde{\psi}_{2n+2,\downarrow}^{\dagger} \tilde{\psi}_{2n+1,\uparrow} - \tilde{\psi}_{2n,\downarrow}^{\dagger} \tilde{\psi}_{2n+1,\uparrow} + h.c. \right).$$
$$(5.10)$$

The green (purple) arrows in Fig. (5.2b) represent terms belonging to $\tilde{H}_1$ ($\tilde{H}_2$). In the integer case each of these Hamiltonians is described by a low energy Dirac theory, as can be seen by refermionizing the bosonic theories. Importantly, the Hamiltonians $\tilde{H}_1$ and $\tilde{H}_2$ remain gapless in the fractional case as well, as indicated by the argument we have used to show that $\tilde{H}$ is gapless. However, in the fractional case these Hamiltonians cannot be described by a low energy Dirac theory. In the future we refer to their low energy theories as fractional Dirac liquids.

5.3 A simplified model for the surface of fractional strong topological insulators

We have seen above that the simple model for a fractional weak topological insulator can be decomposed into two decoupled gapless theories described by the Hamiltonians $\tilde{H}_1$ and $\tilde{H}_2$. In the integer case, weak topological insulators possess an even number of Dirac cones on the surface, while strong topological insulators necessarily have an odd number of Dirac

cones [13]. By analogy, we naturally expect the low energy theory describing the surface of a fractional strong topological insulator to be related to the surface of a fractional weak topological insulator. We therefore ask whether a single decoupled surface Hamiltonian, say $\tilde{H}_1$, describing left movers on layers with even indices and right movers on layers with odd indices (see Fig. (5.3a)), can faithfully describe the surface of a fractional strong topological insulator.

Strictly speaking, this is clearly impossible since $\tilde{H}_1$ is not independently time reversal invariant. Nevertheless, we follow Ref. [122] in noting that $\tilde{H}_1$ is invariant under a modified time reversal operation, defined as the product of the original time-reversal operator and a translation by a unit cell.

Such a symmetry characterizes antiferromagnetic topological insulators, which can be created, for example, by adding an antiferromagnetic order parameter to a strong topological insulator (without closing the gap). Remarkably, it was shown in Refs. [123, 124] that the introduction of such a time-reversal breaking perturbation does not destroy all the surface Dirac cones. Instead, the remaining Dirac cones are protected by the modified time-reversal operation described above.

This leads us to assume that $\tilde{H}_1$ faithfully describes the surface of the fractional analog of an antiferromagnetic topological insulator. The corresponding gapless surface is expected to be in the same universality class as the surface of a fractional strong topological insulator with a local time-reversal symmetry. We can therefore use $\tilde{H}_1$ to derive some of the universal properties expected to characterize the surface of a fractional strong topological insulator. Notice that the bulk excitations of the fractional antiferromagnetic topological insulator are generally different from the fractional excitations characterizing the 3D fractional strong topological insulator.

As noted in Ref. [122], studying a system with the modified time-reversal symmetry, for which one can write an explicit model of the surface in terms of weakly coupled 1D channels, greatly simplifies the analysis. This is impossible in systems that have a local (unmodified) time-reversal symmetry. To study these using a set of weakly coupled 1D systems, we will be forced to explicitly construct the 3D bulk as well. This will be done in Sec. 5.4.

Again, we depict the surface model using diagrams representing the inter-layer terms coupling the various chiral modes. In particular, the diagram that represents the gapless surface Hamiltonian $\tilde{H}_1$ is shown in Fig. (5.3b).

Until now we have preserved the modified time-reversal symmetry and charge conservation of $\tilde{H}_1$, and thus the surface was found to be gapless. In what follows we focus on the properties of the surface once these protecting symmetries are explicitly broken. We will see below that the resulting gapped fractional Dirac mode has unique properties.

Figure 5.4: A diagrammatic representation, in terms of the $\tilde{\psi}$ (or χ) modes defined at the beginning of Sec. 5.2.2, of the situation where the coefficient $\tilde{t}'$ of the time reversal breaking term changes abruptly from $-\tilde{t}$ to $\tilde{t}$ around $n = 1$. A decoupled chiral $\tilde{\psi}$ mode is seen to be localized near the boundary at $n = 1$, leading to the conclusion that the gapped surface has a halved fractional quantum Hall effect.

To break the modified time reversal symmetry, we add a perturbation of the form

$$\tilde{H}_t = \tilde{t}' \sum_n \int dx \left(\tilde{\psi}^\dagger_{2n,\uparrow} \tilde{\psi}_{2n+1,\downarrow} + \tilde{\psi}^\dagger_{2n+2,\uparrow} \tilde{\psi}_{2n+1,\downarrow} + h.c. \right) \tag{5.11}$$

The physics of the resulting phase becomes transparent at the points $\tilde{t}' = \pm \tilde{t}$, where the Hamiltonian is decomposed into decoupled sine-Gordon models. For example, if $\tilde{t}' = \tilde{t}$ the non-quadratic part of the Hamiltonian takes the form

$$2\tilde{t}' \sum \int dx \left(\tilde{\psi}^\dagger_{2n,\uparrow} \tilde{\psi}_{2n+1,\downarrow} + h.c. \right) = 4\tilde{t}' \sum \int dx \cos \left[m \left(\chi^\uparrow_{2n} - \chi^\downarrow_{2n+1} \right) \right]. \tag{5.12}$$

Thus we end up with a set of mutually commuting cosine terms, which can be pinned in the ground state and fully gap the surface. This configuration is depicted diagrammatically in Fig. (5.3c).

To identify the surface Hall conductance σ_{xy} characterizing this gapped state, we change $\tilde{t}'$ abruptly from $-\tilde{t}$ to $\tilde{t}$ around the point $n = 1$, as demonstrated in Fig. (5.4). It can be seen that a chiral χ-mode, localized on the boundary, remains decoupled. This mode is identical to the mode residing on the edge of a $\nu = 1/m$ Laughlin FQHE state. By invoking the bulk-edge correspondence and noticing that this mode is a result of contributions from the two sides of the boundary, we find that the gapped surface has $\sigma_{xy} = \pm \frac{1}{2m} \frac{e^2}{h}$.

Thus, the gapped surface of the fractional strong topological insulator exhibits a halved fractional quantum Hall effect. We emphasize that the above result is not limited to the special choice of parameters, which were tuned to the so called "sweet point" [52, 125], and is in fact true as long as the gap remains open. Physically, deviations from $\tilde{t}' = \pm \tilde{t}$ in the two regions introduce a non-zero localization length for the boundary mode.

Alternatively, the fractional Dirac liquid can be gapped out by proximity-coupling to an *s*-wave superconductor, i.e., by breaking charge conservation. A superconducting term which

does not violate the modified time-reversal symmetry is given by

$$\tilde{H}_\Delta = \Delta \sum_n \int dx \left(\tilde{\psi}_{2n,\uparrow} \tilde{\psi}_{2n+1,\downarrow} + \tilde{\psi}_{2n,\uparrow} \tilde{\psi}_{2n-1,\downarrow} + h.c. \right). \tag{5.13}$$

Again, the physics becomes simple at a sweet point given by $\Delta = \pm \tilde{t}$. Taking $\Delta = \tilde{t}$, for example, the non-quadratic part of the Hamiltonian can be written as

$$\tilde{H}_\Delta = 2i\tilde{t} \sum_n (-1)^n \int dx \gamma_n^1 \gamma_{n+1}^2, \tag{5.14}$$

with $\tilde{\psi}_{n,\sigma} = \gamma_n^1 + i\gamma_n^2$, and $\left(\gamma_n^i \right)^\dagger = \gamma_n^i$ (notice that we have omitted the spin index, which is fully determined by n). The modes γ_n^i are referred to as fractional Majorana modes. Indeed, in the integer case, these become chiral Majorana modes, described by a free Majorana theory. The structure of this Hamiltonian is depicted diagrammatically in Fig. (5.5b), where the dotted symbols represent the fractional Majorana modes γ_n^1 and γ_n^2. From the form of Eq. (5.14), it is clear that the system is gapped. Notice that Eq. (5.11), describing time-reversal symmetry breaking, can be expressed in terms of the fractional Majorana modes as well. In particular, the non-quadratic part of the Hamiltonian $\tilde{H}_1 + \tilde{H}_t$ with $\tilde{t}' = \tilde{t}$ takes the simple form $2i\tilde{t} \sum_n \int dx \left(\gamma_{2n+1}^1 \gamma_{2n}^2 - \gamma_{2n+1}^2 \gamma_{2n}^1 \right)$, which is depicted in Fig. (5.5a).

Once the surface is gapped by proximity to a superconductor, it forms an exotic time-reversal invariant topological superconductor. A closely related 2D fractional topological superconductor will be studied in details in the next chapter.

However, it is illuminating to examine the boundary between a magnetic region with broken time-reversal symmetry, and a superconducting region. The physics is simplest if we gap the region with $n > 1$ using a time reversal breaking term of the form (5.11) with $\tilde{t}' = \tilde{t}$, and the region with $n < 1$ using a proximity-coupling term of the form (5.13) with $\Delta = \tilde{t}$. This situation is depicted in Fig. (5.5c). We see that a decoupled chiral Majorana mode of the form $\gamma_1^1 = \frac{1}{2} \left(e^{im\chi_1^\downarrow} + e^{-im\chi_1^\downarrow} \right)$ is localized on the boundary. The propagator describing this fractional Majorana field takes the form $\left\langle \gamma_1^1(x,t) \gamma_1^1(0,0) \right\rangle \propto (x+vt)^{-m}$, making it clear that this gapless channel cannot be described by a free Majorana theory. We point out the similarity to the edge mode of the 2D fractional topological superconductor discussed in Refs. [71, 126].

The above analysis relied on a modified time reversal symmetry to directly model the surface using coupled 1D modes. In what follows we treat a 3D model with a local time reversal symmetry. As we will see, the analysis presented in the next sections reproduces the universal results derived here.

D:/Dropbox (Weizma D:/Dropbox (Weizmann Institute)/PC/Thesis/papers/3D/AFI_SC.png

(a)   (b)

D:/Dropbox (Weizmann Institute)/PC/Thesis/papers/3D/AFTI_TR_SC_DOMAIN.png

(c)
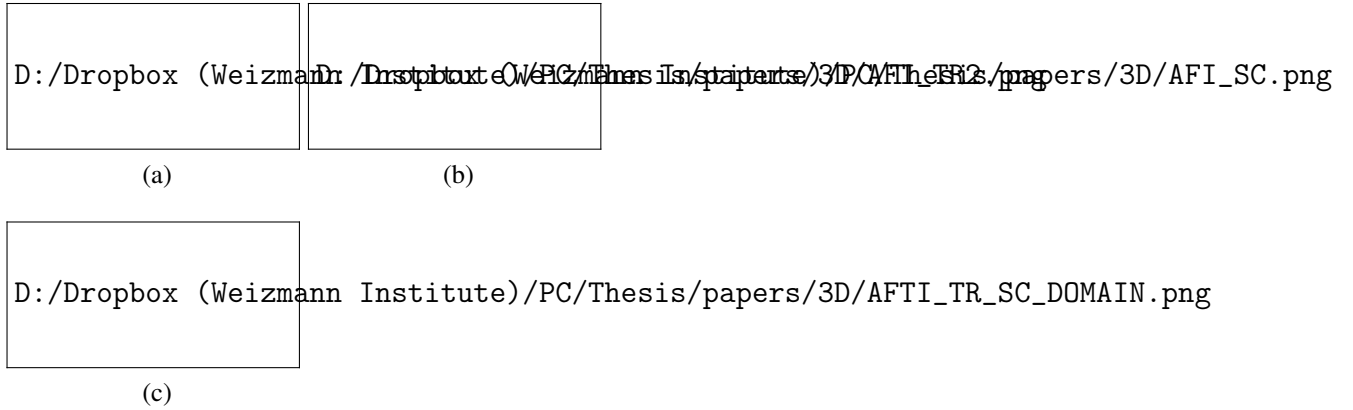
Figure 5.5: A diagrammatic representation of the surface model in terms of the fractional Majorana modes γ_n^i (defined after Eq. (5.14)) in three situations: (a) The modified time reversal symmetry is broken by the perturbation (5.11) with $\tilde{t}' = \tilde{t}$. (b) Charge conservation is broken by a superconducting term of the form (5.13) with $\Delta = \tilde{t}$. (c) The region with $n < 1$ of the surface is gapped by a superconducting term, and the region with $n > 1$ is gapped by a modified time-reversal symmetry breaking term. A chiral fractional Majorana mode is attached to the boundary at $n = 1$. Here the vertical direction represents the index i, and the horizontal direction represents the layer index n. Dotted symbols represent the chiral fractional Majorana modes.

5.4 Fractional Strong topological insulators

5.4.1 Construction of 2D fractional topological insulators

In Sec. 5.4.2-5.4.3 we will construct a 3D model for a fractional strong topological insulator. Our starting point will be the 2D construction of a fractional topological insulator which was introduced in chapter 3. In this section we present this construction in more details, and introduce the general approach used throughout the rest of this work. Unlike the previous section (Sec. 5.3), where we used a simplified model with a modified time-reversal symmetry [see Fig. (5.3a)], here we have a local (unmodified) time reversal symmetry. To avoid confusion, we will use a different set of notations in the analysis that follows.

5.4.1.1 Two-dimensional topological insulator from an array of quantum wires

The 2D model which is the focus of this section is made of $4N$ wires, as depicted in Fig. (5.6a). The j's unit cell is composed of four wires. We note that for convenience the unit cell is shifted by one wire with respect to the unit cell defined in chapter 3.

The first and last wires in each unit cell contain electrons, i.e., their highest occupied states are close to the minimum of the conduction band. In a particle-hole symmetric fashion, the

two other wires contain holes, i.e., their highest occupied states are close to the maximum of the band.

We describe the system in terms of a tight binding model, where each wire is composed of sites at positions $x = a \cdot i$ (see Fig. (5.6a)). Here a is the distance between adjacent sites, and i is an integer enumerating the sites. Adjacent lattice points are coupled with a hopping amplitude t_x $(-t_x)$ in the electron (hole) wires, as depicted by the arrows in Fig. (5.6a). We define the annihilation operator $\psi_{\alpha,s}^{(i,j)}$ for an electron with spin s in wire number α $(\alpha = 1 \dots 4)$ of the unit cell labeled by (i,j). The Hamiltonian that describes the decoupled wires takes the form $H_0 = H_m + H_x$, where

$$H_m = m \sum_{i,j} \left(\sum_{\alpha=1,4} \psi_{\alpha,s}^{(i,j)\dagger} \psi_{\alpha,s}^{(i,j)} - \sum_{\alpha=2,3} \psi_{\alpha,s}^{(i,j)\dagger} \psi_{\alpha,s}^{(i,j)} + h.c. \right), \qquad (5.15)$$

and

$$H_x = -t_x \sum_{i,j} \left(\sum_{\alpha=1,4} \psi_{\alpha,s}^{(i+1,j)\dagger} \psi_{\alpha,s}^{(i,j)} - \sum_{\alpha=2,3} \psi_{\alpha,s}^{(i+1,j)\dagger} \psi_{\alpha,s}^{(i,j)} + h.c. \right). \qquad (5.16)$$

The term H_x describes intra-wire hopping, and the term H_m produces an opposite shift in energy for the electrons and the holes. We note that to have a particle-hole symmetry, the chemical potential is set to be zero. Going to k-space, we write $H = \sum_{\mathbf{k} \in BZ1} \vec{\psi}^\dagger(\mathbf{k}) \mathscr{H}(\mathbf{k}) \vec{\psi}(\mathbf{k})$, with $\vec{\psi} = \begin{pmatrix} \psi_{1\uparrow} & \psi_{2\uparrow} & \psi_{3\uparrow} & \psi_{4\uparrow} & \psi_{1\downarrow} & \psi_{2\downarrow} & \psi_{3\downarrow} & \psi_{4\downarrow} \end{pmatrix}^T$. In addition, we define the matrices τ_i $(i = 1 \dots 3)$ as the Pauli-matrices operating on the wires 1-2 (and 3-4) space. Similarly, the matrices σ_i operate on the (1,2)-(3,4) blocks, and s_i act on the spin degrees of freedom.

In terms of these, the Bloch Hamiltonian corresponding to Eqs. (5.15)-(5.16) takes the form

$$\mathscr{H}_0 = [m - 2t_x \cos(k_x a)] \sigma_z \tau_z. \qquad (5.17)$$

Furthermore, we introduce Rashba spin-orbit interactions with an alternating coupling $\lambda_{\text{so}} (-1)^\alpha$. If the electric field is aligned in the y direction, the resulting term is

$$\mathscr{H}_{\text{so}} = -\lambda_{\text{so}} s_z \tau_z \sin(k_x a). \qquad (5.18)$$

It proves convenient to define new parameters: $\bar{t}_x, k_{\text{so}},$ and k_F^0, satisfying $t_x = \bar{t}_x \cos(k_{\text{so}} a), \lambda_{\text{so}} = 2\bar{t}_x \sin(k_{\text{so}} a), m = 2\bar{t}_x \cos(k_F^0 a)$. In terms of these, it is simple to see that the energy spectra of

the four decoupled wires in each unit cell take the form

$$
\begin{aligned}
E_{1,s} &= 2\bar{t}_x \left[\cos\left(k_F^0 a\right) - \cos\left((k_x - sk_{so})a\right) \right], \\
E_{2,s} &= -2\bar{t}_x \left[\cos\left(k_F^0 a\right) - \cos\left((k_x - sk_{so})a\right) \right], \\
E_{3,s} &= -2\bar{t}_x \left[\cos\left(k_F^0 a\right) - \cos\left((k_x + sk_{so})a\right) \right], \\
E_{4,s} &= 2\bar{t}_x \left[\cos\left(k_F^0 a\right) - \cos\left((k_x + sk_{so})a\right) \right].
\end{aligned}
\tag{5.19}
$$

If we define the filling factor as $\nu = \frac{k_F^0}{k_{so}}$, the spectra corresponding to the spin-up sector are depicted in Fig. (5.6b) for the $\nu = 1$ case, and in Fig. (5.6c) for the $\nu = 1/3$ case. We now introduce small tunneling operators that couple adjacent wires, and write the inter-wire Hamiltonian in the form $H_y + H_y'$, where

$$
H_y = -t_y \sum_{i,j} \left[\psi_{3,s}^{(i,j)\dagger} \psi_{2,s}^{(i,j)} + \psi_{1,s}^{(i,j+1)\dagger} \psi_{4,s}^{(i,j)} + h.c. \right],
\tag{5.20}
$$

$$
H_y' = -t_y' \sum_{i,j} \left[\psi_{2,s}^{(i,j)\dagger} \psi_{1,s}^{(i,j)} + \psi_{4,s}^{(i,j)\dagger} \psi_{3,s}^{(i,j)} + h.c. \right],
\tag{5.21}
$$

with $t_y, t_y' \ll \bar{t}_x$. The parameter t_y describes hopping between two electron-wires or two hole-wires, whereas t_y' couples the electron and hole wires.

The Bloch Hamiltonian can now be written in the form

$$
\begin{aligned}
\mathscr{H} = 2\bar{t}_x &\left[\left(\cos\left(k_F^0 a\right) - \cos\left(k_x a\right) \cos\left(k_{so} a\right) \right) \sigma_z \tau_z - s_z \tau_z \sin\left(k_{so} a\right) \sin\left(k_x a\right) \right] \\
&- t_y' \tau_x - \frac{t_y}{2} \left(\tau_y \sigma_y + \tau_x \sigma_x \right) - \frac{t_y}{2} \left(\tau_x \sigma_x - \tau_y \sigma_y \right) \cos\left(4k_y a\right) - \frac{t_y}{2} \left(\tau_x \sigma_y + \tau_y \sigma_x \right) \sin\left(4k_y a\right).
\end{aligned}
\tag{5.22}
$$

For simplicity, we treat the case where the lattice spacings are identical in the two directions: $a_x = a_y \equiv a$. This requirement can be lifted without affecting any of the topological properties. Notice that in these conventions, the first Brillouin zone is defined as $k_y \in \left(-\frac{\pi}{4a}, \frac{\pi}{4a}\right], k_x \in \left(-\frac{\pi}{a}, \frac{\pi}{a}\right]$.

We first investigate the integer case, $\nu = 1$, where it can be checked from Eq. (5.22) that as long as $t_y \neq t_y'$ and $t_y' \neq 0$, the system is completely gapped when periodic boundary conditions are employed. At $t_y = t_y'$ the gap closes, indicating that there might be a phase transition between two topologically distinct phases. To understand the nature of the insulating phases for different values of t_y and t_y', it is useful to linearize the spectrum around the Fermi-momenta (similar to previous chapters).

Similar to the previous chapters, to keep track of the allowed terms, it is convenient to present the Fermi-momenta as a function of the wire index (i, α), as depicted in Fig. (5.7a) for
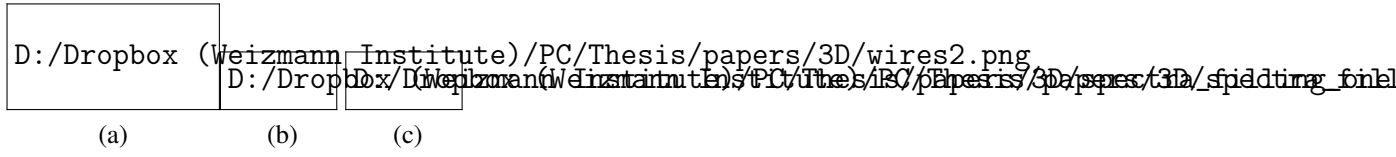
(a)   (b)   (c)

Figure 5.6: (a) The wire construction we use as a realization of a 2D fractional topological insulator. This model is the starting point in our construction of a 3D fractional strong topological insulator (see Sec. 5.4.2-5.4.3). The spectrum of the system depicted in Fig. (5.6a), when the inter-wire terms are switched off for (b) $\nu = 1$, and (c) $\nu = 1/3$. We note that only the spin-up sector is presented here. The energies in blue, cyan, red, and green correspond to wires number 1, 2, 3, and 4, respectively.

the spin-up sector (notice that while the model is equivalent to that depicted in Figs. 3.2a and 3.2b, the unit cell is shifted by one wire). Again, the symbol $\otimes$ ($\odot$) represents a right (left) moving mode, and the arrows represent the coupling between different modes, generated by the terms defined in Eqs. (5.20)-(5.21).

Since the system is fully gapped for $0 < t'_y < t_y$, any such state is adiabatically connected, and therefore topologically equivalent, to the state where t'_y is negligibly small compared to t_y. Therefore, it is simple to see that the terms $\psi_{2,\uparrow}^{i,R\dagger} \psi_{3,\uparrow}^{i,L} + h.c.$ and $\psi_{4\uparrow}^{i,R\dagger} \psi_{1,\uparrow}^{i+1,L} + h.c.$ (and in the same way, $\psi_{2,\downarrow}^{i,L\dagger} \psi_{3,\downarrow}^{i,R} + h.c.$ and $\psi_{4\downarrow}^{i,L\dagger} \psi_{1,\downarrow}^{i+1,R} + h.c.$ for the spin-down sector) dominate, and gap the modes near $k_x = 0$. These terms, however, leave two gapless modes on each edge of the system - one for each spin. For the edge at $i = 1$, these edge modes are $\psi_{1,\uparrow}^{1,L}$, and $\psi_{1,\downarrow}^{1,R}$. The terms $\psi_{1\uparrow}^{i,R\dagger} \psi_{2,\uparrow}^{i,L} + h.c.$ and $\psi_{3\uparrow}^{i,R\dagger} \psi_{4,\uparrow}^{i,L} + h.c.$ (and in the same way $\psi_{1\downarrow}^{i,L\dagger} \psi_{2,\downarrow}^{i,R} + h.c.$ and $\psi_{3\downarrow}^{i,L\dagger} \psi_{4,\downarrow}^{iR} + h.c.$) are responsible for gapping the modes with $k_x \neq 0$. We therefore have a fully gapped bulk with counter-propagating edge modes, protected by time reversal symmetry. Thus, the phase with $t'_y < t_y$ is a topological insulator.

On the other hand, any state with $t'_y > t_y$ is adiabatically connected to the state with $t_y = 0$, where now the terms $\psi_{1,\uparrow}^{i,L\dagger} \psi_{2,\uparrow}^{i,R} + h.c.$ and $\psi_{3,\uparrow}^{i,L\dagger} \psi_{4,\uparrow}^{i,R} + h.c.$ (and in the same way $\psi_{1,\downarrow}^{i,R\dagger} \psi_{2,\downarrow}^{i,L} + h.c.$ and $\psi_{3,\downarrow}^{i,R\dagger} \psi_{4,\downarrow}^{i,L} + h.c$) gap the modes near $k_x = 0$. In this case we have a fully gapped bulk with no edge modes, indicating that the phase we discuss is topologically trivial.

5.4.1.2 Two-dimensional fractional topological insulator from an array of quantum wires

Having found that the above model (defined in Eqs. (5.15)-(5.16) and (5.20)-(5.21)) can be a topological insulator in the $\nu = 1$ case, we now turn to study fractional fillings. We again restrict ourselves here to fillings of the form $\nu = 1/m$, where m is an odd integer.

The diagram that corresponds to the $\nu = 1/3$ case is shown in Fig. (5.7b). We define

the chiral boson fields $\phi_{\alpha,s}^{i,R/L}$, such that $\psi_{\alpha,s}^{i,R/L} \propto \exp\left[i\left(\phi_{\alpha,s}^{i,R/L} + k_{\alpha,s}^{i,R/L}x\right)\right]$, where $k_{\alpha,s}^{i,R/L}$ is the corresponding Fermi-momentum, and the boson fields satisfy the commutation relations

$$\left[\phi_{\alpha,s}^{n,\rho}, \phi_{\alpha',s'}^{n',\rho'}\right] = i\rho\pi\delta_{s,s'}\delta_{\alpha,\alpha'}\delta_{\rho,\rho'}\delta_{n,n'}\text{sign}(x-x') \tag{5.23}$$
$$+ i\pi\left(\text{sign}(n-n') + \delta_{n,n'}\text{sign}(\alpha-\alpha')\right) + \delta_{n,n'}\delta_{\alpha,\alpha'}\pi\left(\sigma_y^{s,s'} + \delta_{s,s'}\sigma_y^{\rho,\rho'}\right),$$

ensuring that the various electron operators anti-commute (notice that as opposed to previous chapters, it now proves important to write the commutation relations between different boson modes explicitly). Motivated by the previous chapters, we define new chiral fermion operators according to

$$\tilde{\psi}_{\alpha,s}^{i,R/L} \propto e^{i\left(\eta_{\alpha,s}^{i,R/L} + q_{\alpha,s}^{i,R/L}x\right)}, \tag{5.24}$$

with

$$\eta_{\alpha,s}^{i,R/L} = \frac{m+1}{2}\phi_{\alpha,s}^{i,R/L} - \frac{m-1}{2}\phi_{\alpha,s}^{i,L/R}, \tag{5.25}$$
$$q_{\alpha,s}^{i,R/L} = \frac{m+1}{2}k_{\alpha,s}^{i,R/L} - \frac{m-1}{2}k_{\alpha,s}^{i,L/R}. \tag{5.26}$$

The commutation relations of the η-fields are

$$\left[\eta_{\alpha,s}^{n,\rho}, \eta_{\alpha',s'}^{n',\rho'}\right] = i\rho m\pi\delta_{s,s'}\delta_{\alpha,\alpha'}\delta_{\rho,\rho'}\delta_{n,n'}\text{sign}(x-x') \tag{5.27}$$
$$+ i\pi\left(\text{sign}(n-n') + \delta_{n,n'}\text{sign}(\alpha-\alpha')\right) + \delta_{n,n'}\delta_{\alpha,\alpha'}\pi\left(\sigma_y^{s,s'} + m\delta_{s,s'}\sigma_y^{\rho,\rho'}\right).$$

As in previous chapters, plotting the diagrams corresponding to the q's, we find that the picture is identical to the one associated with $\nu = 1$ (Fig. (5.7a)). Hence, in terms of the $\tilde{\psi}$-fields, we can repeat the analysis of the $\nu = 1$ case, and write the terms used to obtain a topological
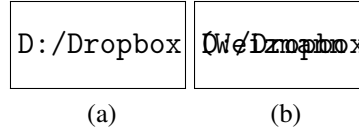
(a)   (b)

Figure 5.7: The diagrams which present the Fermi-momenta of the 2D model as a function of the wire index (labeled by (i,α), where i and α are indices enumerating the unit cells and the position within the unit cell, respectively) for (a) $\nu = 1$, and (b) $\nu = 1/3$. Notice that only the modes with spin-up are presented here.

insulator. Writing these terms using the η bosonic fields, we have:

$$
\begin{aligned}
H_t = \sum_i &\left[\int dx \tilde{t}_y \cos\left(\eta_{4,\uparrow}^{i,R} - \eta_{1,\uparrow}^{i+1,L} \right) + R \longleftrightarrow L, \uparrow \longleftrightarrow \downarrow \right. \\
&+ \int dx \tilde{t}_y \cos\left(\eta_{2,\uparrow}^{i,R} - \eta_{3,\uparrow}^{i,L} \right) + R \longleftrightarrow L, \uparrow \longleftrightarrow \downarrow \\
&+ \sum_s \sum_{\rho = R,L} \int dx \tilde{t}'_y \cos\left(\eta_{1,s}^{i,\rho} - \eta_{2,s}^{i,\overline{\rho}} \right) \\
&\left. + \sum_s \sum_{\rho = R,L} \int dx \tilde{t}'_y \cos\left(\eta_{3,s}^{i,\rho} - \eta_{4,s}^{i,\overline{\rho}} \right) \right].
\end{aligned}
\tag{5.28}
$$

Similar to the integer case, if $\tilde{t}'_y < \tilde{t}_y$ the first two terms in Eq. (5.28) dominate. Assuming they are made relevant, it is evident that the bulk becomes gapped and that the two modes $\eta_{1,\uparrow}^{i,L}$ and $\eta_{1,\downarrow}^{i,R}$ remain decoupled. Each of these modes is similar to the edge mode of a $\nu = 1/m$ Laughlin QHE state.

The above analysis suggests that the fractional analog of a given integer topological phase can be realized if we manage to construct the integer phase from an array of coupled wires. Once this is done, we can obtain a fractional phase by considering an analogous system where the ψ-fields are replaced by the $\tilde{\psi}$-fields (or equivalently, ϕ is replaced by η), as demonstrated above.

This motivates us to use a similar approach in the construction of fractional phases in 3D. Toward this goal, in the next section we will construct a non-interacting strong topological insulator from an array of wires. Then, in Sec. 5.4.3 we will study the fractional phase obtained by reducing the filling to $\nu = 1/m$, and constructing a strong topological insulator in terms of the composite $\tilde{\psi}$-fields.

5.4.2   Strong topological insulators from weakly coupled wires

In order to construct a strong topological insulator we stack 2D layers, each made of the wire construction presented in Sec. 5.4.1, and tune the system such that $\nu = 1$. The resulting 3D system is made of an array of wires, as illustrated in Fig. (5.1a). For simplicity, we assume that the distance between adjacent layers is a as well. The goal of this section is to engineer a time-reversal invariant system with a single Dirac cone near the first and last layers.

To do so, we start by tuning each layer to the critical point between the topological and the trivial phase, such that the 2D bulk contains two Dirac modes. This can be achieved by taking $t_y = t_y'$, in which case the Bloch Hamiltonian describing a single layer is given by

$$
\mathcal{H}_{xy} = 2\bar{t}_x \left[\left(\cos\left(k_{\mathrm{so}}a\right) - \cos\left(k_x a\right) \cos\left(k_{\mathrm{so}}a\right) \right) \sigma_z \tau_z - s_z \tau_z \sin\left(k_{\mathrm{so}}a\right) \sin\left(k_x a\right) \right]
$$
$$
- t_y \tau_x - \frac{t_y}{2} \left(\tau_y \sigma_y + \tau_x \sigma_x \right) - \frac{t_y}{2} \left(\tau_x \sigma_x - \tau_y \sigma_y \right) \cos\left(4k_y a\right) - \frac{t_y}{2} \left(\tau_x \sigma_y + \tau_y \sigma_x \right) \sin\left(4k_y a\right).
$$
$$
(5.29)
$$

To create a topologically non-trivial gapped 3D phase, we perturb the above gapless Hamiltonian by an inter-layer term of the form

$$
\mathcal{H}_z = \frac{1}{2} \left[\left(m' - 2t_z \cos\left(k_z a\right) \right) \tau_x + 2t_z' \sin\left(k_z a\right) s_y \tau_z \right] \left(1 - \sigma_x \right)
\qquad (5.30)
$$

with $m', t_z, t_z' \ll t_y \ll \bar{t}_x$. Unless otherwise noted, we implicitly assume that all the coupling constants are positive.

To see under which circumstances this model forms a strong topological insulator, we now show that if the system is cut at the $z = 0$ plane, a single Dirac mode is localized near the resulting surface. It is clear that as long as the inter-layer coupling terms are small, the important degrees of freedom are those close to the Dirac points in each layer. We therefore project the Hamiltonian onto the low-energy subspace of the intra-layer Hamiltonian (Eq. (5.29)).

The two Dirac cones are located at $k_x = k_y = 0$. Therefore, to identify this low-energy subspace we solve the equation

$$
\mathcal{H}_{xy}(k_x = k_y = 0)\psi_0 = 0
\qquad (5.31)
$$

for the vectors ψ_0. The resulting subspace can be spanned by the four vectors $|\pm 1, s\rangle \equiv |\sigma_x = -1, \tau_x = \pm 1, s\rangle$, defined such that $\sigma_x |\pm 1, s\rangle = -|\pm 1, s\rangle$, $\tau_x |\pm 1, s\rangle = \pm |\pm 1, s\rangle$, $S_z |\pm 1, s\rangle = s |\pm 1, s\rangle$. In what follows, the basis vectors are ordered as $\{|1, \uparrow\rangle, |-1, \downarrow\rangle, |1, \downarrow\rangle |-1, \uparrow\rangle\}$. As

expected, the *xy* Hamiltonian, projected onto the low-energy subspace and expanded to first order in momenta, takes the form of two Dirac cones. To be specific, in the above basis the intra-layer Hamiltonian takes the form

$$\mathscr{H}_{xy} = \begin{pmatrix} 0 & h_{\text{Dirac}} \\ h_{\text{Dirac}}^{\dagger} & 0 \end{pmatrix}, \tag{5.32}$$

where

$$h_{\text{Dirac}} = \begin{pmatrix} 0 & -2\bar{t}_x \sin(k_{\text{so}}a) k_x a + 2it_y k_y a \\ 2\bar{t}_x \sin(k_{\text{so}}a) k_x a - 2it_y k_y a & 0 \end{pmatrix}. \tag{5.33}$$

Once the inter-layer part of the Hamiltonian is projected onto the same low energy subspace, it takes the form

$$\mathscr{H}_z = \begin{pmatrix} h_{1D}(k_z) & 0 \\ 0 & h_{1D}^*(k_z) \end{pmatrix}, \tag{5.34}$$

where $h_{1D}(k_z) = \vec{d} \cdot \vec{\sigma}$, with $\vec{d} = \left(0, 2t_z' \sin(k_z a), m' - 2t_z \cos(k_z a)\right)$, can be thought of as the Hamiltonian of a 1D model.

If $m' < 2t_z$, the planar vector $\vec{d}$ winds once around the origin as k_z winds around the Brillouin zone, indicating that the 1D model is topologically non-trivial. Indeed, in this regime the model can be shown to have zero-energy end modes.

Since the $\hat{z}$ part of our 3D Hamiltonian consists of the two decoupled models h_{1D} and h_{1D}^*, it produces two zero-energy modes on the $z = 0$ surface. It is clear that the full low energy Hamiltonian, projected onto the subspace spanned by these two end modes, must be that of a single Dirac cone.

To see this explicitly, we need an analytic form for the two end modes. This becomes simple if we restrict ourselves to the regime where $2t_z$ is close to m and the gap is small. In this limit, focusing again on the low energy properties, we can expand Eq. (5.34) in small k_z, and get a continuum model. The model h_{1D} then takes the form

$$h_{1D} \approx \begin{pmatrix} m' - 2t_z - t_z\partial_z^2 & -2t_z'a\partial_z \\ 2t_z'a\partial_z & -\left(m' - 2t_z - t_z\partial_z^2\right) \end{pmatrix} \tag{5.35}$$

in the position basis.

Assuming that the system ends at $z = 0$, we look for localized zero-energy eigenstates of this Hamiltonian and its complex conjugate, which vanish at $z = 0$. Plugging in an exponen-

tially decaying function as an ansatz, we find two such solutions

$$|1\rangle = \frac{1}{\sqrt{2}} \begin{pmatrix} 1 \\ 1 \\ 0 \\ 0 \end{pmatrix} f(z), |2\rangle = \frac{1}{\sqrt{2}} \begin{pmatrix} 0 \\ 0 \\ 1 \\ -1 \end{pmatrix} f(z), \tag{5.36}$$

with $f(z) = \frac{\sqrt{2\lambda_+\lambda_-(\lambda_++\lambda_-)}}{\lambda_+-\lambda_-} \left(e^{-\lambda_+z} - e^{-\lambda_-z}\right)$, and $\lambda_\pm = \frac{t_z'\pm\sqrt{t_z'^2+(m'-2t_z)t_z}}{at_z}$.

Projecting the *xy* part of the Hamiltonian (Eq. (5.32)), onto the subspace spanned by the two end modes (Eq. (5.36)), we find a single anisotropic Dirac cone on the surface. The corresponding Hamiltonian takes the form

$$\mathcal{H}_{xy\text{-surface}} = 2a \left[k_y t_y \sigma_y + k_x t_x \sin\left(k_{\text{so}}a\right) \sigma_x\right]. \tag{5.37}$$

Two remarks are in order: first, one can derive the topological nature of the model from the bulk wavefunctions. In fact, recognizing that the system has an inversion symmetry, generated by the operator $\sigma_x \tau_x$, we can implement the procedure introduced in Ref. [13] (relating the $\mathbb{Z}_2$ invariant to the parity of the occupied states at the time-reversal invariant points) and easily evaluate the $\mathbb{Z}_2$ invariant. We have verified that the results of this analysis are consistent with the above derivation, where the surface was studied directly.

Second, we note that since the system is guaranteed to preserve its topological nature as long the gap remains finite, the various parameters are not restricted to the values given above. In particular, the strict requirement $t_y = t_y'$ can be relaxed.

In the next section we study the fractional analog of the model introduced in this section.

5.4.3   Fractional strong topological insulators from weakly coupled wires

In Sec. 5.4.1, when constructing the Laughlin-like $\nu = 1/m$ state in 2D, we saw that one can define the η-fields, in terms of which the problem is mapped to the simple $\nu = 1$ case. Reversing the logic, we see that by taking a topological state with $\nu = 1$, and replacing the ϕ fields by the η fields, we expect to get a fractional state.

In this Section, we follow this approach in generalizing our strong topological insulator to its fractional analog. To do so, we start by writing the Hamiltonian of the $\nu = 1$ case, discussed in the previous section, in terms of the bosonic ϕ-fields. Then we write the same Hamiltonian with the η-fields, and tune the system to filling $\nu = 1/m$, where such terms conserve momentum.

We note that all the fields which are not around $k_x = 0$ are trivially gapped by the intra-layer

terms, as seen most clearly in Fig. (5.7a). Consequently, the topological properties involve only the modes around $k_x = 0$. In what follows, we therefore write only the operators acting on these fields. In addition, we omit the indices R/L, which are fully determined by the spin indices for the $k_x = 0$ modes.

We define the vector

$$\tilde{\Psi}_{i,n} = \left(e^{i\eta_{1,\uparrow}^{i,n}} e^{i\eta_{2,\uparrow}^{i,n}} \quad e^{i\eta_{3,\uparrow}^{i,n}} \quad e^{i\eta_{4,\uparrow}^{i,n}} \quad e^{i\eta_{1,\downarrow}^{i,n}} \quad e^{i\eta_{2,\downarrow}^{i,n}} \quad e^{i\eta_{3,\downarrow}^{i,n}} \quad e^{i\eta_{4,\downarrow}^{i,n}} \right)^T, \qquad (5.38)$$

where i is the index enumerating the unit cells in each layer, and n counts the layers. In these notations, the low energy Hamiltonian takes the form

$$H_x = \sum_{n,i,\alpha,s} \frac{v}{2\pi m} \int dx \left(\partial_x \eta_{\alpha,s}^{i,n} \right)^2, \qquad (5.39)$$

$$H_y = -t_y \sum_{n,i} \int dx \left[\tilde{\Psi}_{i,n}^\dagger \left(\tau_x + \frac{1}{2} \left(\tau_y \sigma_y + \tau_x \sigma_x \right) \right) \tilde{\Psi}_{i,n} + \left(\frac{1}{4} \tilde{\Psi}_{i+1,n}^\dagger \left(\tau_x + i\tau_y \right) \left(\sigma_x + i\sigma_y \right) \tilde{\Psi}_{i,n} + h.c. \right) \right],$$
$$\qquad (5.40)$$

$$H_z = \frac{1}{2} \sum_{n,i} \int dx \left[\left(\tilde{\Psi}_{i,n+1}^\dagger \left(-t_z \tau_x + it_z' s_y \tau_z \right) \left(1 - \sigma_x \right) \tilde{\Psi}_{i,n} + h.c \right) + \tilde{\Psi}_{i,n}^\dagger m' \tau_x \left(1 - \sigma_x \right) \tilde{\Psi}_{i,n} \right].$$
$$\qquad (5.41)$$

For simplicity, we do not consider the effects of density-density interactions between the various modes.

We emphasize that analyzing the problem directly in terms of the bosons is essential in the fractional case. Unfortunately, the bosonic form makes it difficult to see that the above set of non-commuting terms results in a gapped system with a gapless surface. In the $v = 1$ case, we can of course refermionize the above Hamiltonian and repeat the analysis of Sec. 5.4.2 to show this explicitly. In the fractional case, where refermionization does not result in a solvable model, the situation is more subtle as the various inter-wire terms are irrelevant in the weak coupling limit. To avoid additional complications that arise from that, we work in the regime where the bare amplitudes are large and assume that the inter-wire terms flow to the strong coupling limit.

Indeed, in this strong coupling limit, we can neglect the intra-wire terms and the physics becomes practically independent of m because the inter-wire Hamiltonian is quadratic in the fermionic $\tilde{\psi}$-fields. Since we know from the fermionic language that the system is gapped in

```
D:/Dropbox (Weizmann Institute)/PC/Thesis/papers/3D/redu
```

Figure 5.8: A diagrammatic representation of the reduced 2D tight binding model, describing the inter-wire part of the full 3D model. Here, each "lattice point" corresponds to a linearly dispersing mode in the x direction, with a well defined y and z coordinates. The horizontal axis describes the layer and spin indices (n, s), and the vertical axis describes the position within each layer (i, α). Again, the symbol $\otimes$ $(\odot)$ represents a right (left) mover. The green arrows represent the terms in the intra-layer Hamiltonian H_y, and the brown arrows represent inter-layer terms which couple the spin-up modes, and take the form $-2t_z \cos(k_z a)\, \tau_x$ in k-space. We emphasize that the reduced model defined in Eq. (5.40)-(5.41) contains additional terms which are not depicted here. If all the terms are considered, the full 3D model is topologically non-trivial if the reduced model forms a 2D topological insulator. Thus, the analysis of some aspects of the strongly interacting 3D phase is reduced to the analysis of the 2D non-interacting topological phase.

the $m = 1$ case, the same is expected to be true for $m > 1$ in the strong coupling limit. This result is expected to remain true for moderately large bare amplitudes as well.

In what follows, the topological nature of the Hamiltonian is revealed again with the aid of diagrammatic representations. We depict the η modes which are not gapped by intra-layer terms (i.e., the modes near $k_x = 0$) by diagrams of the form shown in Fig. (5.8).

As before, the symbol $\otimes$ $(\odot)$ represents a right (left) mover, and colored arrows connecting two modes represent coupling between them. The horizontal axis represents the layer and spin indices (n, s), and the vertical axis represents the intra-layer position (i, α).

Forgetting for a moment that the symbols represent dispersing 1D modes, if they are treated as states localized on the corresponding lattice points, the diagram presents the 3D problem as a 2D tight-binding model, defined in real space by Eqs. (5.40)-(5.41). The 2D lattice model describing the inter-wire coupling terms is referred to as the reduced 2D model. The usefulness of the reduced tight binding model description is revealed by noting that the full 3D model is topologically non-trivial if the reduced model forms a 2D topological insulator.

If the system is infinite (or periodic) in the $\hat{y}$ and $\hat{z}$ directions, the corresponding momenta are good quantum numbers. We therefore write the problem in terms of its Fourier components k_y and k_z. We note that in order to take advantage of the bosonization description, we do not perform a Fourier transform in the x direction. Consequently, the Hamiltonian takes the form

$$H = H_x + \sum_{\mathbf{k}} \int dx \, \tilde{\Psi}_{\mathbf{k}}^{\dagger}(x) \left(h_y(\mathbf{k}) + h_z(\mathbf{k}) \right) \tilde{\Psi}_{\mathbf{k}}(x), \qquad (5.42)$$

with $\mathbf{k} = (k_y, k_z)$, and

$$\tilde{\Psi}_{\mathbf{k}}(x) = \frac{1}{\sqrt{N_y N_z}} \sum_{j,n} e^{-i(4jk_y a + nk_z a)} \tilde{\Psi}_{j,n}(x), \qquad (5.43)$$

$$h_y(\mathbf{k}) = -t_y \tau_x - \frac{t_y}{2}(\tau_y \sigma_y + \tau_x \sigma_x) - \frac{t_y}{2}(\tau_x \sigma_x - \tau_y \sigma_y)\cos(4k_y a) - \frac{t_y}{2}(\tau_x \sigma_y + \tau_y \sigma_x)\sin(4k_y a),$$
$$(5.44)$$

$$h_z(\mathbf{k}) = \frac{1}{2}\left[\left(m' - 2t_z \cos(k_z a)\right)\tau_x + 2t_z' \sin(k_z a) s_y \tau_z\right](1 - \sigma_x), \qquad (5.45)$$

where N_y is the number of wires in each layer, and N_z is the number of layers (cf. Eqs. (5.29) and (5.30)).

If the 3D model is finite in the $\hat{y}$ or $\hat{z}$ direction, the reduced 2D model has an edge. For $m' < 2t_z$, it can be checked that the reduced model forms a 2D topological insulator, and has counter propagating edge modes. Recalling that each lattice point in the reduced model represents a linearly dispersing η-mode, we argue that these edge states correspond to the gapless surface modes of the original 3D model. Therefore, we can get the surface modes by diagonalizing the reduced tight binding model and finding the corresponding edge states.

In order to get an explicit analytic form, we focus again on the regime where $2t_z$ is close to m', and the gap becomes small. If the system terminates at the $z = 0$ plane, the reduced model has two edge modes which take the form

$$\xi_\beta(x, k_y) = \frac{1}{\sqrt{N_y}} \sum_{j,n} \sqrt{a} f(a \cdot n) e^{-ijk_y a} A_\beta \cdot \tilde{\Psi}_{j,n}(x), \qquad (5.46)$$

where $\beta = 1, 2$ labels the two counter-propagating edge modes, $f(z)$ is the function defined after Eq. (5.36), and the vectors A_β are

$$A_1 = \frac{1}{4}\left(1+i \quad, 1-i \quad, -i-1 \quad, i-1 \quad -i+1 \quad, -i-1 \quad, -1+i \quad, 1+i\right),$$
$$A_2 = A_1^*. \qquad (5.47)$$

In the integer case, where $m = 1$, Eq. (5.46) can be thought of as a bosonic description of the Dirac mode localized near the $z = 0$ surface (we point out the similarity between the fields defined in Eqs. (5.46) and (5.36), up to a different choice of basis). In the fractional case, where $m > 1$, the above gapless modes cannot be described by Dirac's theory of free

fermions. As before, we refer to these more general modes as fractional Dirac modes.

The part of the inter-wire Hamiltonian describing the edge modes of the reduced model (which correspond to the surface mode of the original 3D model) takes the form

$$H_{edge} = 2t_y a \sum_{k_y} \int dk_y \vec{\xi}^{\dagger}(x, k_y) \bar{\tau}_z \vec{\xi}(x, k_y)$$

$$= -2t_y i \int dx dy \vec{\xi}^{\dagger}(x, y) \bar{\tau}_z \partial_y \vec{\xi}(x, y), \tag{5.48}$$

where $\vec{\xi} = \begin{pmatrix} \xi_1 & \xi_2 \end{pmatrix}^T$, and $\bar{\tau}_z$ is a Pauli matrix acting on this basis. To simplify the analysis presented in the next section, the second line of Eq. (5.48) was written in the continuum limit.

In the next section we will use the reduced 2D model formalism to study the properties of the surface once it is gapped by breaking its protecting symmetries. We will see that the resulting gapped fractional Dirac modes have unique properties which distinguish them from massive Dirac fermions.

5.4.4   Gapping the surface

5.4.4.1   Breaking time-reversal symmetry: Halved fractional quantum Hall effect on the surface

Having written a low energy effective surface Hamiltonian using the reduced model, we turn to study what happens when the surface is gapped by breaking time reversal symmetry.

To do so, we introduce a Zeeman field B on the surface. We examine a configuration where B changes sign as we cross the line $y = 0$. By studying the properties of the gapless mode attached to the boundary, we will be able to deduce the surface Hall conductance.

Within the reduced 2D model formalism, the problem of finding the 1D channel attached to a magnetic domain wall on the surface is converted into that of finding the localized zero-energy mode associated with a similar domain wall on the edge of a 2D topological insulator. To be concrete, we use the continuum model described by Eq. (5.48) and add a space dependent perturbation of the form $B(y) \vec{\xi}^{\dagger} \bar{\tau}_x \vec{\xi}$, where $B(y) = B_0 \text{sign}(y)$. This Hamiltonian, and hence the full inter-wire Hamiltonian, has a zero-energy solution of the form

$$\xi_B(x) = \sqrt{\lambda_B} a \sum_{j,n} f(n \cdot a) e^{-\lambda_B |j| a} \beta \cdot \tilde{\Psi}_{j,n}(x), \tag{5.49}$$

with

$$\beta = \frac{1}{2} \begin{pmatrix} 0 & 1 & 0 & -1 & 1 & 0 & -1 & 0 \end{pmatrix}, \tag{5.50}$$

and $\lambda_B = \frac{B_0}{2t_y a}$.

Notice that this mode, being a combination of right movers, is a right moving mode. Furthermore, we argue that it is identical to the chiral mode that resides on the edge of a $\nu = 1/m$ Laughlin QHE state.

To see this, we calculate the electron propagator characterizing this 1D channel, defined as $G_B(x - x', t - t') = \left\langle \tilde{\xi}_B(x',t')\tilde{\xi}_B^{\dagger}(x,t) \right\rangle$. Recall that $\xi_B(x)$ is an exact zero-energy solution of the Inter-wire Hamiltonian for any x. Therefore, we can calculate the expectation value with respect to the quadratic intra-wire Hamiltonian shown in Eq. (5.39) . This results in the propagator

$$G_B(x,t) \propto \frac{1}{(x - vt)^m}. \tag{5.51}$$

This can be derived rigorously by writing the exact equations of motion for $\tilde{\xi}_B$, which indicate that it remains a right mover in the presence of the inter-wire Hamiltonian (i.e., $G_B(x,t) = G_B(x - vt)$). Then, using the known transformation properties of the various fields under the conformal symmetry of the kinetic Hamiltonian, one can rigorously prove Eq. 5.51 without additional assumptions. This procedure is shown explicitly in Appendix A.2 (note that while the system discussed in Appendix A.2 is different, the analysis follows the above line of arguments).

The propagator in Eq. 5.51 is identical to the one characterizing the edge of a $\nu = 1/m$ QHE edge state [77]. Invoking the bulk edge correspondence, we therefore find that $\sigma_{xy} = \pm \frac{1}{2m} \frac{e^2}{h}$, in agreement with Sec. 5.3.

5.4.4.2   Coupling the surface to a superconductor: The emergence of a fractional Majorana mode

Next, we turn to ask what happens when the surface is gapped by breaking charge conservation. This is done by proximity coupling the surface to an s-wave superconductor. It was found in Ref. [14] that when the surface of a strong topological insulator is gapped in this fashion, the resulting phase resembles a spinless $p_x + ip_y$ superconductor, but has time-reversal symmetry.

In our model, this problem corresponds to understanding what happens to the edge of the reduced 2D topological insulator when it is coupled to an s-wave superconductor. This motivates us to write a proximity term of the form $\Delta\left(\xi_1^{\dagger}\xi_2^{\dagger} + h.c.\right)$, coupling the two edge modes of the reduced model. Using the enlarged basis, $\vec{\xi}_N = \left(\begin{array}{cccc} \xi_1(x,y) & \xi_2(x,y) & \xi_2^{\dagger}(x,y) & \xi_1^{\dagger}(x,y) \end{array} \right)^T$, we rewrite the edge Hamiltonian in the form

$$\frac{1}{2}\int dxdy\,\vec{\xi}_N^{\dagger}\left(-2it_y\tau_z\sigma_z\partial_y + \frac{\Delta}{a}\tau_z\sigma_x\right)\vec{\xi}_N. \tag{5.52}$$

In order to reveal the topological nature of the superconducting phase, we consider the boundary between a region with a non-zero B and a region with a non-zero Δ. Studying non-interacting strong topological insulators, the authors in Ref. [14] have found that such a boundary contains a chiral Majorana mode. We now examine what happens in the fractional case.

In the presence of time-reversal breaking and superconducting terms, the edge part of the reduced Hamiltonian takes the form

$$\frac{1}{2}\int dx dy \vec{\xi}_N^\dagger \left[-2it_y \tau_z \sigma_z \partial_y + \frac{B(y)}{a}\tau_x \sigma_z + \frac{\Delta(y)}{a}\tau_z \sigma_x \right] \vec{\xi}_N. \tag{5.53}$$

We consider a simple situation, where $B(y) = B_0 \Theta(y)$ and $\Delta = \Delta_0 \Theta(-y)$ (to be concrete, we assume $\Delta_0 > 0, B_0 > 0$).

The Hamiltonian given by Eq. (5.53) has a zero energy solution of the form

$$\frac{1}{\sqrt{2}}\left(\xi_{B\Delta} + \xi_{B\Delta}^\dagger\right), \tag{5.54}$$

with

$$\xi_{B\Delta} = \sqrt{\frac{2\lambda_B \lambda_\Delta}{\lambda_B + \lambda_\Delta}} a \sum_{j,n} e^{-i\pi/4} f(n\cdot a)\beta \cdot \tilde{\Psi}_{j,n}(x) g(ja), \tag{5.55}$$

$$g(y) = \begin{cases} e^{-\lambda_B y}, y > 0 \\ e^{\lambda_\Delta y}, y < 0 \end{cases}, \tag{5.56}$$

$\lambda_\Delta = \frac{\Delta_0}{2t_y a}$ and $\lambda_B = \frac{B_0}{2t_y a}$. For $m = 1$, we find a self-Hermitian combination of right moving fermions, making it a chiral Majorana mode, in agreement with Ref. [14]. If $m > 1$, we find again a self-Hermitian chiral mode. However, in this case it cannot be described by a free Majorana theory. In particular, the tunneling density of states associated with this mode is proportional to ω^{m-1}, as opposed to the free Majorana case, where the density of states is constant. This is in fact similar to the tunneling density of states characterizing the edge of a $\nu = 1/m$ Laughlin QHE states. To find this result, one can repeat the process that led to Eq. (5.51) and write the propagator of the above fractional Majorana mode. The above results are in agreement with Sec. 5.3, where we have used a modified time-reversal symmetry to directly model the surface.

Chapter 6

Fractional chiral superconductors

This chapter presents the results of our fourth project, presented in Ref. [71]. In previous chapters, we focused on applying the coupled-wire approach for studying fractional insulating phases in 2D and 3D. In this chapter, we extend this approach to superconducting phases, and construct the simplest fractional analog of the chiral $p + ip$ superconductor: a fractional chiral superconductor.

6.1   Introduction

In this work we propose new strongly interacting superconducting phases that are natural fractional counterparts of the non-interacting $p_x + ip_y$ chiral superconductor: *fractional* chiral superconductors (FCSC).

A non-interacting $p_x + ip_y$ superconductor hosts a chiral Majorana mode, or equivalently a $\mathbb{Z}_2$ parafermion theory, at the edge. In contrast, the edge of the FCSC phases we find is described by non-trivial $\mathbb{Z}_{2m}$ parafermion conformal field theories (CFTs), where m can be any odd integer. This makes the FCSC phases close relatives of the well-known $\mathbb{Z}_{2m}$ Read-Rezayi quantum Hall states, whose edge theories have identical non-Abelian components. In addition, while an $h/2e$ vortex in a $p_x + ip_y$ superconductor binds a Majorana zero mode, a vortex in the FCSC phases binds $\mathbb{Z}_{2m}$ parafermion zero modes. Unlike the $p_x + ip_y$ superconductor, however, an FCSC phase generally contains a rich set of deconfined non-Abelian excitations even in the absence of vortices.

Using the coupled-wire approach, we present an analytically tractable model realizing these strongly interacting phases. This allows us to explicitly study their properties and experimental signatures in detail.

By considering a Corbino geometry, we are able to study $h/2e$ vortices in the system. We show that these vortices host non-Abelian parafermion zero-modes by mapping our configu-

ration to domain walls on the edge of a 2D fractional TI [127–129].

6.2 Topological superconductor from an array of coupled wires

We start by reviewing the construction of a $p_x + ip_y$ superconductor, presented in Ref. [52]. In section 6.3, the construction of the fractional phases will proceed in parallel to that of the $p_x + ip_y$ phase, replacing the electron operators in the non-interacting case with the $\tilde{\psi}$-fields, similar to previous sections.

The starting point is an array of decoupled Rashba wires. Similar to Refs. [17, 18], each wire is subjected to a Zeeman field and proximity coupled to an s-wave superconductor,

$$
\begin{aligned}
H = \sum_n \int dx\, \vec{\psi}_n^\dagger(x) \left[-\frac{(\partial_x - iuM\sigma_z)^2}{2M} - \mu + B\sigma_x \right] \vec{\psi}_n(x) \\
+ \int dx \left[\Delta \psi_{n\uparrow}^\dagger(x)\psi_{n\downarrow}^\dagger(x) + \text{h.c.} \right].
\end{aligned}
\tag{6.1}
$$

Here, $\vec{\psi}_n = \begin{bmatrix} \psi_{n\uparrow}(x) & \psi_{n\downarrow}(x) \end{bmatrix}^T$, where $\psi_{ns}(x)$ represents the electron annihilation operator at wire number n with spin s (see Fig. 6.1a). The matrices σ_i are Pauli matrices operating on the spin degrees of freedom. The parameters u, B, and Δ are the Rashba spin-orbit coupling (SOC), the Zeeman field, and the induced superconducting pairing potential, respectively.

Figure 6.1b presents the spectrum of a single wire in the absence of superconductivity and a Zeeman field ($B = \Delta = 0$). We define the Fermi momentum $k_F^0 = \sqrt{2M\mu}$ in the absence of SOC, and the shift $k_{\text{so}} = Mu$ of the parabolas due to SOC. In terms of these, the filling fraction of the system is defined as

$$
v = k_F^0 / k_{\text{so}}.
\tag{6.2}
$$

To study the low energy physics, we linearize the spectrum near the Fermi level, and decompose the fermionic modes into right- and left-moving modes: $\psi_{ns}(x) = \psi_{nsR}(x) + \psi_{nsL}(x)$, with $\psi_{ns\rho}(x) = \psi_{ns\rho}^0(x)e^{ik_{s\rho}x}$. Here, $\psi_{ns\rho}^0$ are the low energy degrees of freedom near the Fermi momenta $k_{s\rho} = \rho k_F^0 - sk_{so}$ (where $\rho = \pm 1$ denotes a right/left moving mode).

The $p_x + ip_y$ superconductor corresponds to $v = 1$. Focusing on the low-energy excitations for $|\Delta - B| \ll B, \Delta$, the Zeeman term $H_B = \int dx \left[B\psi_{n\uparrow R}^\dagger(x)\psi_{n\downarrow L}(x) + \text{h.c.} \right]$ and the pairing term $H_\Delta = \int dx \left\{ \Delta \left[\psi_{n\uparrow R}^\dagger(x)\psi_{n\downarrow L}^\dagger(x) + \psi_{n\uparrow L}^\dagger(x)\psi_{n\downarrow R}^\dagger(x) \right] + \text{h.c.} \right\}$ gap out the wires (see Fig. 6.1b). Indeed, the second term in H_Δ fully gaps the high-momentum degrees of freedom $\psi_{n\uparrow L}$ and $\psi_{n\downarrow R}$, and the low-momentum degrees of freedom, $\psi_{n\uparrow R}$ and $\psi_{n\downarrow L}$, are coupled by the Zeeman
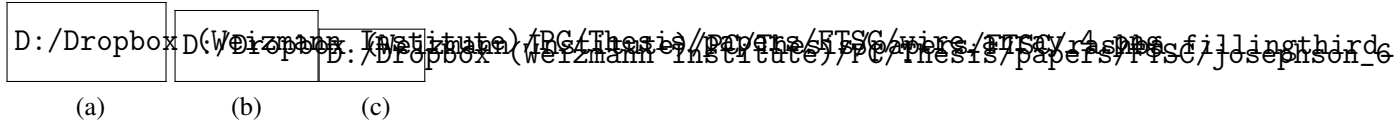
(a)   (b)   (c)

Figure 6.1: (a) A schematic view of the system we use to construct a two-dimensional fractional chiral superconductor (FCSC). The system is composed of an array of N weakly coupled wires with strong Rashba spin-orbit coupling. We demonstrate that the interplay of the Zeeman field, proximity to an s-wave superconductor, and strong interactions can result in FCSC phase with a chiral parafermion CFT at the edges of the sample and parafermionic bound states at the core of vortices. (b) The spectrum of an individual wire in the absence of interactions, Zeeman field, and proximity coupling. The dashed lines specify the chemical potentials corresponding to the situations $\nu = 1$ and $\nu = 1/3$. (c) A Corbino geometry, used in order to study $h/2e$ vortices and the anomalous Josephson effect. By connecting the internal and external parts with a superconducting wire, through which flux can be inserted, the relative phases between the two superconducting regions can be controlled. It is argued that in the quasi-one-dimensional regime this configuration is equivalent to the effective junction shown in Fig. 6.2f, leading to a $4\pi m$-periodic Josephson effect.

term H_B as well as the first term of H_Δ. The fully gapped phases for $\Delta > B$ and $\Delta < B$ are topologically distinct - the first is a 1D trivial phase while the second is a topological superconductor. For $B = \Delta$, the inter-mode part of the Hamiltonian, given by $H_\Delta + H_B$, commutes with the operators

$$\alpha_n(x) = \psi_{n\uparrow R}(x) + \psi_{n\uparrow R}^\dagger(x),$$
$$\beta_n(x) = -i\left[\psi_{n\downarrow L}(x) - \psi_{n\downarrow L}^\dagger(x)\right], \tag{6.3}$$

so the system is gapless.

Tuning to this transition point, we introduce an inter-wire term of the form

$$H_\perp = it_\perp \sum_n \int dx\, \alpha_n(x)\beta_{n+1}(x). \tag{6.4}$$

This term arises naturally in the system of Fig. 6.1a due to a combination of inter-wire hopping, superconductivity, and spin-orbit interaction [52]. It gaps out the bulk degrees of freedom, yet it leaves the Majorana fields $\beta_1(x)$ and $\alpha_N(x)$ decoupled, thus stabilizing a $p_x + ip_y$ phase. This construction can be considered the anisotropic limit of the system studied by Refs. [16, 130]. While it relies on a fine-tuned relation between parameters, the resulting phase is independent of these assumptions, remaining qualitatively identical as long as the bulk gap remains open.

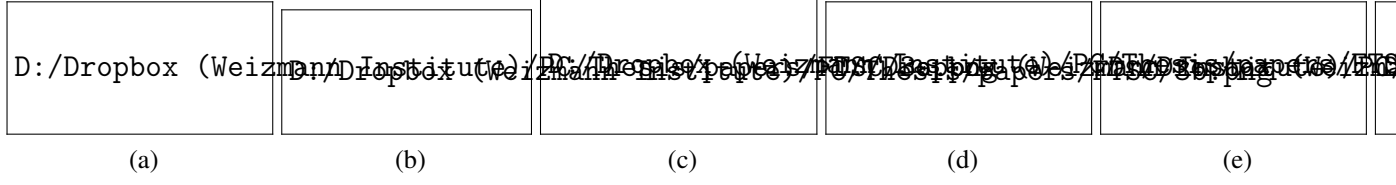|				
D:/Dropbox (Weizmann Institute)	D:/Dropbox (Weizmann Institute)	D:/Dropbox (Weizmann Institute)	D:/Dropbox (Weizmann Institute)	D:/Dropbox (Weizmann
(a)	(b)	(c)	(d)	(e)

Figure 6.2: A schematic depiction of the line of arguments used in order to identify the zero-modes localized at the center of $h/2e$ vortices. (a) We start by placing our FCSC phase in an annular geometry, through which a magnetic flux may be inserted. Without altering the essential characteristics of the system, we cut a thin trench through the annulus. (b) As the presence of zero-modes should not depend on the precise geometry as long as the topological structure is preserved, we focus on the edge theory and fold our system inside-out to a bone shaped geometry. (c) The independence on the precise geometry allows us to shrink the outermost regions. (d) We examine an auxiliary model which has twice as many degrees of freedom, but whose low energy sector coincides with our model. We then show that the auxiliary model in (d) can be adiabatically deformed into a system composed of $\nu = 1/m$ fractional quantum Hall edges coupled by ferromagnetic and superconducting terms. (e) If the flux φ is an even multiple of 2π, we get effective superconducting term throughout the system, meaning there are no zero modes. (f) For odd multiples of 2π, the superconductor in the physical region is replaced by a ferromagnet. The domain walls of the resulting configuration, representing the edges of the original configurations, give rise to parafermionic bound states [127–129].

6.3 Fractional chiral superconductors

To construct a FCSC phase at filling $\nu = 1/m$, where m is an odd integer, we consider the effects of strong interactions, within a bosonized description of the 1D degrees of freedom. Using the standard Abelian bosonization technique, we describe the Hilbert space in terms of bosonic fields $\phi_{ns\rho}$ via $\psi_{ns\rho} \propto e^{i\left(\phi_{ns\rho}+k_{s\rho}x\right)}$.

For $\nu = 1/m$, the analysis of the previous chapter motivates us to define new chiral fermion operators $\tilde{\psi}_{ns\rho} = e^{i\left(\eta_{ns\rho}+q_{s\rho}x\right)}$, with

$$\eta_{ns\rho} = \frac{m+1}{2}\phi_{ns\rho} - \frac{m-1}{2}\phi_{ns\bar{\rho}}. \tag{6.5}$$

The $\tilde{\psi}_{ns\rho}$ fields carry momenta $q_{s\rho} = \frac{m+1}{2}k_{s\rho} - \frac{m-1}{2}k_{s\bar{\rho}}$. Note that the momenta $q_{s\rho}$ carried by the new fields $\tilde{\psi}_{ns\rho}$ match those of a $\nu = 1$ wire. In particular, the operators $\tilde{\psi}_{n\uparrow R}$ and $\tilde{\psi}_{n\downarrow L}$ now have vanishing oscillatory components, allowing us to couple them in various ways without breaking translational symmetry.

Once the Zeeman term is dressed by intra-wire $2k_F$-interactions, it induces a term of the form $\tilde{H}_B = \int \frac{dx}{a^2}\left[\tilde{B}\tilde{\psi}_{n\uparrow R}^{\dagger}(x)\tilde{\psi}_{n\downarrow L}(x)+\text{h.c.}\right]$ (where a is the short distance cutoff). We assume that $\tilde{B}$ is large enough such that this term gaps out the small momentum fields $\tilde{\psi}_{n\uparrow R}$ and $\tilde{\psi}_{n\downarrow L}$.

We may also write dressed pairing terms of the form

$$\tilde{H}_\Delta = \int \frac{dx}{a^2} \left\{ \tilde{\Delta} \left[\tilde{\psi}^\dagger_{n\uparrow R}(x) \tilde{\psi}^\dagger_{n\downarrow L}(x) + \tilde{\psi}^\dagger_{n\uparrow L}(x) \tilde{\psi}^\dagger_{n\downarrow R}(x) \right] + \text{h.c.} \right\}. \tag{6.6}$$

As in the $\nu = 1$ case, the second term in $\tilde{H}_\Delta$ involves high-momentum degrees of freedom and does not compete with the Zeeman term, $\tilde{H}_B$. It fully gaps out the fields $\tilde{\psi}_{n\uparrow L}$ and $\tilde{\psi}_{n\downarrow R}$. The first term in $\tilde{H}_\Delta$ competes with the Zeeman field $\tilde{H}_B$. For $\tilde{\Delta} = \tilde{B} = \lambda$, one obtains a critical theory, similar to the $\nu = 1$ case, which in this case is described by a $\beta^2 = 4\pi m$ self-dual Sine-Gordon model (see Appendix A.1):

$$H = \int dx \left[(\partial_x \theta)^2 + (\partial_x \varphi)^2 + \frac{\lambda}{a^2} \left\{ \cos\left(\sqrt{4\pi m}\varphi\right) + \cos\left(\sqrt{4\pi m}\theta\right) \right\} \right], \tag{6.7}$$

where we have defined $\varphi = \frac{\eta_{n\uparrow R} - \eta_{n\downarrow L}}{2\sqrt{\pi m}}$ and $\theta = \frac{\eta_{n\uparrow R} + \eta_{n\downarrow L}}{2\sqrt{\pi m}}$.

It is, however, a priori unclear whether the critical line $\tilde{B} = \tilde{\Delta}$ is dominated by the $\tilde{B}$ and $\tilde{\Delta}$ terms. In the weak-coupling limit, both $\tilde{B}$ and $\tilde{\Delta}$ flow to zero, giving a trivial Luttinger-liquid fixed point. However, it turns out that when $\tilde{B}$ and $\tilde{\Delta}$ are equal and large enough, a non-trivial multicritical point is encountered.

To show this, we follow the analysis in Ref. [131], and employ an ε-expansion, with $m = 2 + \varepsilon$. In this approach, the scaling dimensions of the $\tilde{B}$ and $\tilde{\Delta}$ terms are small, thus pushing the competition between the first and higher order terms of the RG equations to the region in which the perturbative RG analysis applies. As we show in Appendix A.1, the RG equation describing the flow of $\lambda = \tilde{B} = \tilde{\Delta}$ takes the form

$$\frac{d\lambda}{dl} = -\varepsilon\lambda + \pi^2 \lambda^3. \tag{6.8}$$

When $\lambda > \sqrt{\varepsilon}/\pi$, a flow to large coupling ensues and the low energy theory is no longer capable of describing the model. The point $\lambda = \sqrt{\varepsilon}/\pi$ is a multicritical point separating the $\tilde{B}$-dominated phase, the $\tilde{\Delta}$-dominated phase, and the gapless phase. Extrapolating to ε of order unity, we assume that such a critical point persists. For completeness, we study the full phase diagram of the system in Appendix A.1.

To uncover the nature of the CFT describing the multicritical point, it is useful to review the physics of classical 2D $\mathbb{Z}_k$ (clock or Potts) models. As discussed in detail in Refs. [132–134], such models possess self-dual lines. For $k \leq 4$, there is a self-dual critical point that separates the disordered and ordered ($\mathbb{Z}_k$ symmetry broken) phases. For $k > 4$, some regions of the self-dual line are contained in gapless phases, while others consist of first order transitions. The different regions of the self-dual line are separated by multicritical points [132, 134]. It

was argued in Ref. [135] that these are described by a $\mathbb{Z}_k$ parafermion CFT. In addition, it is well known that the low energy physics of self-dual $\mathbb{Z}_k$ models is described by $\beta^2 = 2\pi k$ self-dual Sine-Gordon models [97, 136]. The above prompts us to identify the finite-coupling multicritical point in our self-dual Sine-Gordon models with those of the $\mathbb{Z}_k$ models. This indicates that our model at the multicritical point is described by a $\mathbb{Z}_{2m}$ parafermion CFT.

In what follows, we assume that each wire is tuned to the multicritical point, and is therefore described by a $\mathbb{Z}_{2m}$ parafermion theory. At this critical point, the fields

$$\tilde{\alpha}_n(x) = e^{i\eta_{n\uparrow R}(x)} + e^{-i\eta_{n\uparrow R}(x)}$$
$$\tilde{\beta}_n(x) = -i\left[e^{i\eta_{n\downarrow L}(x)} - e^{-i\eta_{n\downarrow L}(x)}\right] \tag{6.9}$$

commute with the inter-mode Hamiltonian $\tilde{H}_B + \tilde{H}_\Delta$. As we demonstrate in Appendix A.2, the propagators describing this low energy theory take the form $\langle \tilde{\alpha}_n(z)\tilde{\alpha}_n(z')\rangle \propto (z - z')^{-m}$ and $\left\langle \tilde{\beta}_n(\bar{z})\tilde{\beta}_n(\bar{z}')\right\rangle \propto (\bar{z} - \bar{z}')^{-m}$, with $z = x + i\tau$. We identify these fields with the ψ_m and $\bar{\psi}_m$ primary fields of the $\mathbb{Z}_{2m}$ theory, which indeed have conformal dimension $m/2$ [135].

Similar to the non-interacting case [see Eq. (6.4)], we introduce the inter-wire term

$$\tilde{H}_\perp = i\tilde{t}_\perp \sum_n \int \frac{dx}{a^2} \tilde{\alpha}_n(x)\tilde{\beta}_{n+1}(x). \tag{6.10}$$

Since the inter-wire Hamiltonian in Eq. (6.10) has the same form as the self-dual intra-wire Hamiltonian and is composed of fields which commute with the intra-wire coupling terms, $\tilde{t}_\perp$ flows according to the RG equation (6.8). Therefore, if $\tilde{t}_\perp$ is large enough, a flow to large coupling ensues and this Hamiltonian leaves the fields $\tilde{\beta}_1$ and $\tilde{\alpha}_N$ gapless. These fields represent the local electron operators on the edges. In fact, a full chiral $\mathbb{Z}_{2m}$ parafermion CFT is expected to reside on each edge. Using the propagator of the $\tilde{\alpha}$ and $\tilde{\beta}$ fields, we find that the electrons' tunneling density of states $N(\omega)$, associated with the edge, scales with an anomalous exponent: $N(\omega) \propto \omega^{m-1}$.

Similar to the non-interacting case, the strict constraints on the various parameters may be lifted as long as the bulk gap does not close.

6.4 Non-Abelian defects and $4\pi m$-periodic Josephson effect

To study the non-Abelian defects residing at the core of vortices, we examine the configuration presented in Fig. 6.2a. The FCSC is shaped like an annulus, and the flux threading the annulus is given by an odd multiple of $h/2e$. In analogy to the non-interacting case [137], we expect to find zero modes on the two edges of the system. It will prove useful to cut a thin trench in

the annulus. In this case, the flux through the center of the annulus can be chosen to enter in the coupling across the trench, and we can deform our system in such a way that connects it with the configuration studied in Refs. [127–129] (see Fig. 6.2f).

Given that we are only interested in finding zero energy modes, we have a large amount of freedom in deforming the geometry of the problem while preserving its topology. We first fold the edge "inside-out" leading to the bone-shaped configuration depicted in Fig. 6.2b. We may then shrink the outermost regions without introducing inter-edge coupling. This leads to the simple 1D geometry presented in Fig. 6.2c, in which the counter-propagating edge modes $\tilde{\alpha}_R$ and $\tilde{\beta}_L$ (defined in the region $0 < x < l$) are connected at $x = 0, l$.

The zero-mode properties are solely encoded in the low energy edge theory. We therefore have the additional freedom of changing the Hamiltonian governing the gapped degrees of freedom. One must only ensure that the modes $\tilde{\alpha}_R$ and $\tilde{\beta}_L$, and the other primary fields of the parafermion CFT, remain gapless, while the other microscopic degrees of freedom, such as $\tilde{\alpha}_L$ and $\tilde{\beta}_R$, remain gapped.

An auxiliary model, in which the latter fields are coupled directly, while bulk degrees of freedom are projected out, satisfies this condition. The corresponding Hamiltonian is given by

$$
\begin{aligned}
H_{\text{auxiliary}} &= i\tilde{t}_a \int_0^l dx \tilde{\beta}_R(x)\tilde{\alpha}_L(x) \\
&= \tilde{t}_a \int_0^l dx \left[\tilde{\psi}_R(x)\tilde{\psi}_L(x) - \tilde{\psi}_R^\dagger(x)\tilde{\psi}_L(x) + h.c. \right],
\end{aligned}
\tag{6.11}
$$

where we have used $\tilde{\alpha}_\rho = \tilde{\psi}_\rho + \tilde{\psi}_\rho^\dagger$ and $\tilde{\beta}_\rho = \left(\tilde{\psi}_\rho - \tilde{\psi}_\rho^\dagger \right)/i$. While it gaps $\tilde{\alpha}_L$ and $\tilde{\beta}_R$, this Hamiltonian leaves the fields $\tilde{\alpha}_R, \tilde{\beta}_L$ gapless. Notice that strictly speaking, $\tilde{t}_a$ must be tuned to a multicritical point for the low-energy theory to remain identical. However, since we will soon break the self duality of the problem, this will not be important.

The auxiliary model simplifies our analysis, as it allows us to formulate the problem in terms of the chiral bosonic modes η_R and η_L, such that $\tilde{\psi}_\rho = e^{i\eta_\rho}$. Mathematically, the Hamiltonian in Eq. (6.11) describes two edge modes of a $\nu = 1/m$ fractional quantum Hall state, coupled by a specific combination of ferromagnetic and superconducting terms.

Next, we include the physical coupling between the edge modes across the trench,

$$
\begin{aligned}
H_{\text{trench}} &= i\tilde{t}(\varphi) \int_0^l dx \tilde{\alpha}_R(x)\tilde{\beta}_L(x) \\
&= \tilde{t}(\varphi) \int_0^l dx \left[\tilde{\psi}_R(x)\tilde{\psi}_L(x) + \tilde{\psi}_R^\dagger(x)\tilde{\psi}_L(x) + h.c. \right],
\end{aligned}
\tag{6.12}
$$

where $\varphi = 2\pi\frac{\Phi}{h/2e}$, and $\Phi = nh/2e$ is the flux through the center of the annulus. In the gauge

in which the flux only enters into $\tilde{t}(\varphi)$, we have $\tilde{t}(\varphi) = \tilde{t}_0 \cos\left(\frac{\varphi}{2}\right)$.

Finally, it is necessary to introduce the correct boundary conditions, such that $\tilde{\alpha}_R \to \tilde{\beta}_L$ at $x = 0$ and $\tilde{\beta}_L \to \tilde{\alpha}_R$ at $x = l$ (see Fig. 6.2c). This can be implemented by extending the model to $-\infty < x < \infty$, and strongly coupling α_R and β_L beyond the ends of the physical system, such that they acquire a large gap in these regions. Within the auxiliary model, formulated in terms of the two η fields, we can do this by introducing strong superconducting terms for $x < 0$ and $x > l$:

$$H_{\text{bc}} = \Delta_{\text{bc}} \int_{x<0, x>l} dx \left[\tilde{\psi}_R(x) \tilde{\psi}_L(x) + \text{h.c.} \right]. \tag{6.13}$$

The full auxiliary model is depicted in Fig. 6.2d. Alternatively, note that one can also use a ferromagnetic term. This would not change our conclusions regarding the existence of zero modes.

While the choice of coupling constants $\tilde{t}_a$ and (Δ_{bc}) seems arbitrary, unphysical zero energy degrees of freedom may appear if these are not properly chosen. In order to avoid these, we first choose the auxiliary coupling constant such that $\text{sign}(\tilde{t}_a) = \text{sign}(\Delta_{\text{bc}})$ (otherwise the coefficient of the term $i\tilde{\beta}_R \tilde{\alpha}_L$ changes sign at $x = 0, l$).

An additional consistency condition is obtained by noting that no physical zero-energy modes should appear in the absence of flux. This leads to the constraint $\text{sign}(\Delta_{\text{bc}}) = \text{sign}[\tilde{t}(\varphi = 0)]$.

To be consistent with these constraints, the coefficients of our auxiliary model must satisfy

$$\text{sign}(\tilde{t}_a) = \text{sign}(\Delta_{\text{bc}}) = \text{sign}(\tilde{t}_0). \tag{6.14}$$

Clearly, the gap does not close as long as the various coupling constants do not change sign. In particular, the presence (or absence) of zero-modes in not affected by varying the various parameters without altering their signs. We may therefore choose $\tilde{t}_0 = \tilde{t}_a \left| \cos\left(\frac{\varphi}{2}\right) \right|^{-1}$, in which case the Hamiltonian in the region $0 < x < l$ takes the form

$$H_{\text{trench}} + H_{\text{auxiliary}} =$$
$$\tilde{t}_a \int_0^l dx \left\{ \tilde{\psi}_R(x) \tilde{\psi}_L(x) \left[1 + \text{sign}\left(\cos\frac{\varphi}{2} \right) \right] \right.$$
$$\left. - \tilde{\psi}_R^\dagger(x) \tilde{\psi}_L(x) \left[1 - \text{sign}\left(\cos\frac{\varphi}{2} \right) \right] + \text{h.c.} \right\} \tag{6.15}$$

While the trench allows us to continuously vary φ, we take the discrete values $\varphi = 2\pi n$, where n counts the number of $h/2e$ vortices. As Eq. (6.15) implies, if φ is an even multiple of 2π, the Hamiltonian reduces to superconducting terms throughout space, thus preventing the existence of zero energy modes (see Fig. 6.2e). On the other hand, if φ is an odd multiple of 2π it is clear that the superconductor in the region $0 < x < l$ is replaced by a ferromagnet, and we

end up with the S-F-S configuration studied in Refs. [127–129] (see Fig. 6.2f). Notice that if we had chosen to implement the boundary conditions in Eq. (6.13) using ferromagnetic terms, we would end up with an F-S-F configuration for odd multiples of 2π, and ferromagnetic terms throughout space for even multiple of 2π.

Following the results of Refs. [127–129], we conclude that the S-F-S and F-S-F configurations found above give rise to parafermion zero-modes ξ_i, with $i = 1, 2$, located at the interfaces $x = 0, l$. These operators satisfy

$$\xi_1 \xi_2 = \xi_2 \xi_1 e^{i \frac{\pi}{m}}, \tag{6.16}$$

and $\xi_i^{2m} = 1$. Eq. (6.15) implies that the spectrum is 4π-periodic as a function of φ.

We note that the interfaces correspond to the circular edges of the original annulus, so that this line of arguments indicates that $h/2e$ vortices in the FCSC system bind protected parafermionic zero-modes.

Once our annular system is transformed into the setup presented in Fig. 6.2f for an odd number of vortices, it is natural to ask whether we can control the relative phase between the two effective superconducting order-parameters and measure the Josephson effect, which was previously shown to be $4\pi m$-periodic [128, 129].

Recall that the superconductors shown in Fig. 6.2f were introduced to impose the boundary conditions, and in particular, do not correspond to the physical superconductor in proximity to our system. Nevertheless, we argue that such an effective Josephson junction can be generated by creating a physical Josephson junction in our system. This is done by considering a physical weak link cutting the physical s-wave superconductor at a fixed radial coordinate into two concentric annuli (see Fig. 6.1c). This allows us to control the relative superconducting phases between the external and the internal parts of our system by connecting the two edges with an external superconducting wire, through which flux is inserted. Notice that coupling between electrons across the cut can effectively stitch the two parts of system, leading to a gapped FCSC phase throughout the system (including the area above the cut).

Since the edges of our annular system correspond to the interfaces in the auxiliary configuration, we effectively control the relative phases between the two auxiliary superconductors shown in Fig. 6.2f [1]. Examining the quasi one dimensional regime, in which coupling between the two edge modes of our annular system is induced, the arguments above indicate that the junction shown in Fig. 6.1c gives rise to a $4\pi m$-periodic Josephson effect. Notice that the radial width of the junction must be comparable to the correlation length in the bulk, allowing

---

[1]Notice that the phase differences in the effective and the physical Josephson junctions play a similar role in changing the wave function of the low energy electron operators. This indicates that changing the phase difference in the physical junction results in a phase difference in the effective junction as well.

anyons to tunnel between the inner and the outer edges.

6.5 Bulk excitations

Clearly, the FCSC phase we construct is topologically ordered. While we leave the detailed study of the bulk excitations to future studies, we anticipate that the topologically distinct bulk excitations will be associated with the various low-energy sectors of the parafermionic edge theory through the bulk-edge correspondence. The low energy sectors are generated by the primary fields of the parafermion CFT, which can be labeled by $\Phi_{[k,\bar{k}]}$ [135], where the integers k and $\bar{k}$ are defined mod $4m$, and $k + \bar{k}$ is even. In terms of these, the parafermion fields are given by $\psi_n = \Phi_{[2n,0]}$ and $\bar{\psi}_n = \Phi_{[0,2n]}$ (with $n = 1, \cdots, 2m - 1$), and the spin operators σ_n are given by $\sigma_n = \Phi_{[n,n]}$.

However, in identifying the deconfined bulk excitations with the primary fields of the edge CFT, we must exclude the operators which acquire a non-trivial phase as they wind around the electron, which in our case is identified with the field ψ_m (or $\bar{\psi}_m$). In particular, since the electron acquires a phase of π as it winds around a vortex, the corresponding field must be associated with a confined excitation (i.e., the energy of two such excitations diverges as we separate them [2]). More generally, the phase associated with winding $\Phi_{[k,\bar{k}]}$ around the electron ψ_m ($\bar{\psi}_m$) is given by $\gamma_{[k,\bar{k}]} = \pi k$ ($\bar{\gamma}_{[k,\bar{k}]} = \pi \bar{k}$) [135]. This shows, for example, that while the parafermion fields ψ_n are all deconfined in the bulk, the spin operators σ_n, with odd n, must be confined.

---

[2]Notice that such confined excitation can be introduced to the system externally. For example, a vortex in a $p_x + ip_y$ superfluid is confined, but it can be induced by applying an external effective magnetic field.

Chapter 7

Composite Weyl semimetal as a parent state for three dimensional topologically ordered phases

This chapter presents the results of our fifth project, presented in Ref. [73]. In this project, we leverage the recently discovered duality between the $2+1$-dimensional Dirac theory and the theory of quantum electrodynamics (QED_3) to propose strongly correlated fractional states in 3+1 dimensions.

7.1 Introduction

It has recently been discovered that a single (2+1) dimensional Dirac cone of weakly interacting electrons is dual to the strongly interacting gauge theory QED_3 for a single flavor of dual fermions [138–142]. Subsequently, this fermionic duality was realized to be part of a larger 'web of dualities' [143–150]. A natural application of the fermionic duality is the study of possible surface phases of 3D TIs, which feature a single electronic Dirac cone and can thus equivalently be described as QED_3 for dual fermions. This dual description is a natural 'parent state' of various topologically ordered phases, such as the 'T-Pfaffian' which arises when dual fermion form a BCS superconductor [151–154].

In this work, we leverage these insights to develop a strongly correlated parent state in (3+1) dimensions, where emergent fermions couple to a dynamical gauge field, similar to the (3+1) dimensional theory of quantum electrodynamics—QED_4. This is achieved by combining the (2+1) dimensional duality with the mechanism of *spontaneous interlayer coherence* of the emergent fermions[155, 156], which deconfines them in the third dimension. Conse-
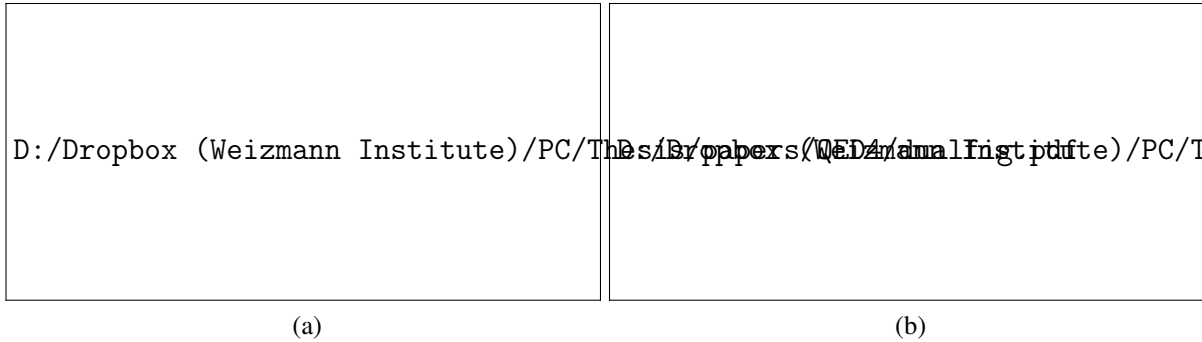
D:/Dropbox (Weizmann Institute)/PC/Thesis/papers/QED4/analfig.puf

D:/Dropbox (Weizmann Institute)/PC/Thesis/papers

(a)   (b)

Figure 7.1: (a)A schematic depiction of the superlattice we study. The system is composed of alternating topological and normal insulators. Each interface contains a single Dirac cone, known to be dual to a QED_3 theory describing neutral fermions coupled to an emergent gauge field. We demonstrate that interactions can deconfine the neutral fermions, leading to a QED_4 theory, from which non-trivial three-dimensional phases descend. (b) The phase diagram describing the properties of the system as a function of the mass m and the amplitude Δ of the dual pairing terms. We show that the QED_4 theory serves as a parent state for the dual Weyl semimetal state and topologically ordered gapped phases. If the mass is large enough, the system is in a Weak topological phase, with the dual fermions forming a band insulator which is adiabatically connectable to a stack of Chern insulators.

quently, this emergent QED_4 only arises as a consequence of strong interactions, unlike the QED_3 that constitutes an equivalent (dual) description of free Dirac fermions.

Despite this difference, pairing of emergent fermions has an analogous effect to that occurring in $(2+1)$ dimensions. In both cases, the emergent gauge field acquires a gap, leading to various fractionalized phases. Specifically, we will discuss gapless composite Weyl semimetals, gapped topologically ordered phases, and symmetry-enriched topological phases (SETs). The first of these—the 'composite' Weyl semimetal—is an electric insulator that features Majorana-Weyl nodes of emergent fermions in the bulk. The composite Weyl semimetal phase should be contrasted with the fractional chiral metal proposed in Ref. [64], which is not insulating. Merging the Majorana-Weyl nodes results in a fully gapped phase with fractional point-like and line-like excitations. In fact, the resulting phase is the 3D analog of the toric code [157]. Finally, by carefully tracing the action of electronic symmetries onto these degrees of freedom, we can use the understanding of *free fermion* topological superconductors to distinguish SETs, which may carry symmetry protected fractional surface states.

7.2   The model

Our model consists of alternating thin layers of topological and normal insulators, as shown in Fig. 7.1a. Such a configuration was previously used in Ref. [158] to construct a Weyl semimetal phase [35–45]. The interfaces between adjacent layers are enumerated by the integer index z. In the simplest case, each interface contains a single Dirac cone, described by the continuum action

$$S = i \sum_z \int d^2x dt \, \bar{\Psi}_z \gamma_{\mu z} (\partial^\mu - iA^\mu) \Psi_z \, , \tag{7.1}$$

where $\Psi_z = \begin{pmatrix} \psi_{z\uparrow} & \psi_{z\downarrow} \end{pmatrix}^T$ are Dirac electrons; A^μ are components of electromagnetic potential with space-time index $\mu = 0, 1, 2$; γ-matrices are represented as $\gamma_{0z} = \sigma_1$, $\gamma_{1z} = -i(-1)^z \sigma_2, \gamma_{2z} = i(-1)^z \sigma_3$; and $\bar{\Psi} = \Psi^\dagger \gamma_{0z}$. The theory possesses anti-unitary time reversal and particle-hole symmetries of the form $\mathscr{T}\Psi\mathscr{T}^{-1} = i\sigma_2\Psi$ and $\mathscr{C}\Psi\mathscr{C}^{-1} = \sigma_1\Psi^\dagger$, which are broken by non-zero magnetic flux $\vec{\nabla} \times \vec{A}$ and chemical potential A^0, respectively.

Each (2+1) dimensional Dirac theory can be equivalently described by a dual QED$_3$ [138–142], with dual Dirac fermions $\widetilde{\Psi}_z = \begin{pmatrix} \tilde{\psi}_{z\uparrow} & \tilde{\psi}_{z\downarrow} \end{pmatrix}^T$ coupled to an *emergent* $U(1)$ gauge field a^μ. The dual action for our multi-layer system is given by $S_{\text{dual}} = \sum_z \int d^3x \mathscr{L}_{\text{dual},z}$

$$\mathscr{L}_{\text{dual},z} = i\bar{\widetilde{\Psi}}_z \gamma_{\mu z} \left(\partial^\mu - ia_z^\mu \right) \widetilde{\Psi}_z + \frac{a_{\mu,z}\varepsilon_{\mu\nu\kappa}\partial_\nu A_{\kappa,z}}{4\pi} + \dots \, , \tag{7.2}$$

where the ellipsis denotes 'generic' terms such as a Maxwell action for a and short-range interactions between the dual fermions. Importantly, the roles of particle-hole and time reversal symmetries are interchanged in the dual formulation: $\mathscr{T}\widetilde{\Psi}\mathscr{T}^{-1} = \sigma_1\bar{\widetilde{\Psi}}^\dagger$ and $\mathscr{C}\widetilde{\Psi}\mathscr{C}^{-1} = i\sigma_2\widetilde{\Psi}$. The single electron of the original theory corresponds to a 4π monopole in the gauge field, which in turn binds two fermionic zero modes [143], one of which is occupied. In the continuum, the 4π monopole therefore binds a dual fermion, in analogy to the familiar attachment of two flux quanta in the conventional composite-fermion approaches.

Next, we couple the layers to form 3D phases, similar to the layer construction presented in Ref. [121]. The simplest such coupling, direct inter-layer tunneling of electrons, involves the insertion of 4π monopoles in the various layers, and therefore confines the gauge field, leading to free fermion phases. We initially tune such couplings to zero and will allow them back at a later stage. Non-trivial phases could easily arise if dual fermions (instead of electrons) were able to tunnel between different layers. However, these are not local excitations and there is no microscopic process that allows them to transfer between layers, i.e., dual fermions are confined in the z direction. They may, however, become liberated when interactions between

different layers generate strong inter-layer correlations.

7.3   Inter-layer coherence

To illustrate this mechanism we follow Ref. [155] and consider a simple density-density inter-action term of the form $S_{\text{int}} = \sum_z \int d^2x dt \, \mathscr{L}_{\text{int},z}$ with $\mathscr{L}_{\text{int},z} = u \sum_{\alpha=\uparrow,\downarrow} \widetilde{\Psi}^\dagger_{z,\alpha} \widetilde{\Psi}_{z,\alpha} \widetilde{\Psi}^\dagger_{z+1,\alpha} \widetilde{\Psi}_{z+1,\alpha}$.
Next, we use (dynamical) Hubbard-Stratonovich fields χ_α to decouple the interaction as

$$\mathscr{L}_{\text{int},z} = \sum_{\alpha=\uparrow,\downarrow} \left(\chi_{z,\alpha} \widetilde{\Psi}^\dagger_{z,\alpha} \widetilde{\Psi}_{z+1,\alpha} + \text{H.c.} \right) + \frac{|\chi_{z,\alpha}|^2}{u} . \tag{7.3}$$

Notice that under a gauge transformation $\widetilde{\Psi}_z \to \widetilde{\Psi}_z e^{i\phi_z}$ and $a^\mu_j \to a^\mu_z + \partial_\mu \phi_z$. Imposing gauge invariance then requires that $\chi_{z,\alpha}$ transforms as $\chi_{z,\alpha} \to \chi_{z,\alpha} e^{i(\phi_z - \phi_{z+1})}$. It is convenient to write $\chi_{z,\alpha} = \chi^0_{z,\alpha} e^{-ia^3_z}$ such that $a^3_z \to a^3_z + \phi_{z+1} - \phi_z$ under gauge transformations and the magnitude $\chi^0_{z,\alpha} = |\chi_{z,\alpha}|$ is gauge invariant. For sufficiently strong interactions the system may enter a phase with $\langle \chi^0_{z,\alpha} \rangle = \chi_0 \neq 0$ where fluctuations of the magnitude $|\chi^0_{z,\alpha}|$ are massive while phase fluctuations remain gapless. The effective Lagrangian of Eq. (7.3) then becomes

$$\mathscr{L}_{\text{int},z} = \chi_0 \left(e^{-ia^3_z} \widetilde{\Psi}^\dagger_z \widetilde{\Psi}_{z+1} + \text{H.c.} \right) + \frac{1}{\kappa} (\partial_\mu a^3_z)^2 , \tag{7.4}$$

where the precise value of the coupling κ depends on details and is unimportant here. The density-density interaction term thus induces coherence between the layers and generates dual fermion tunneling. In Appendix B.1, we demonstrate this explicitly in a tractable coupled-wire model. We note that since we no longer have independent gauge symmetries for each layer, the gauge-field should be thought of as a 3D gauge field, with a^3 defined above acting as its z-component.

It is instructive to first analyze the system in a mean-field approximation where all four components of a vanish. In this case, the model is non-interacting and the problem is reduced to studying the band structure of the dual fermions. Since the band structure is equivalent to the one studied in Ref. [158] (at the time-reversal and inversion symmetric point), we expect to have a $(3+1)$-dimensional Dirac theory at low energies. Therefore, reintroducing the gauge degrees of freedom, we expect to obtain the $(3+1)$-dimensional theory of Dirac fermions coupled to a $U(1)$ gauge field—QED$_4$—described by the action

$$S_{\text{QED}_4} = i \int d^3x dt \, \bar{\Psi}' \Gamma_\mu (\partial^\mu - ia^\mu) \widetilde{\Psi}' + \dots , \tag{7.5}$$

where $\mu = 0, \dots, 3$ is the spacetime index, $\widetilde{\Psi}'$ is a 4-dimensional Dirac spinor, and Γ_μ are

4×4 matrices satisfying the Clifford algebra. Notice that despite the isotropic appearance of Eq. (7.5) the physical properties of this system are highly anisotropic. The coupling of the physical electromagnetic field A^μ is the same as in Eq. (7.2) and A^3 completely decouples from S_{QED_4}. A detailed derivation of this low-energy description is provided in Appendix B.2. In what follows we turn to investigate the properties of this non-trivial fixed point and its instabilities.

7.4   Inter-layer tunneling of electrons

While the QED_4 state is not expected to describe a stable state, it is nevertheless natural to ask about its fate upon including tunneling of *electrons* between neighboring layers. On general grounds, we expect that building up the correlations required for inter-layer tunneling of dual fermions will simultaneously suppress the electronic Green function. On the other hand, QED_4 is weakly coupled at long distances and the Green function of dual fermions is essentially free. Following this reasoning, the dual fermion has a smaller scaling dimension than the electron and we expect that the inter-layer coherent state is unstable against weak electron tunneling, at least in some parameter range.

To support this expectation, recall that an operator that creates physical charge ne corresponds to a $4\pi n$ monopole insertion M_n in the gauge theory [139–141, 143, 144]. Making use of the fact that QED_4 is free in the infrared, we find the monopole propagator

$$\left\langle M_n(x) M_n^\dagger(0) \right\rangle \sim |x|^{-q^2 n^2 / 4\pi^2}. \tag{7.6}$$

(See Ref. [159] and the Appendix B.4 for an alternative derivation.) The value of the non-universal number q is set by the short-range interactions of the microscopic electrons. We take this result to indicate that the scaling dimension of the physical electron in the emergent QED_4 varies continuously, analogous to the case of Luttinger liquids in $1 + 1$ dimensions. Hence, we expect to find a range of parameters for which inter-layer tunneling of electrons is irrelevant.

The electronic conductivity of the QED_4 state can easily be computed. In the absence of electronic tunneling between layers, charge in each layer is conserved and the action is independent of A_3. Again assuming that dual fermions decouple from the gauge field, we integrate out a to obtain the effective action $\propto \sum_{\alpha=0}^2 (A_\alpha)^2$ for the electromagnetic vector potential. It follows that the QED_4 state is superconducting in each plane and insulating in the z direction. Including irrelevant electron tunneling allows inter-layer currents and thus reintroduces A_3. The conductivity in the z direction then vanishes as $\omega \to 0$ with a non-universal power law that is again related to the coupling q.

7.5 Composite Weyl semimetal

The QED$_4$ fixed point described above holds only at a fine-tuned point in parameter space. We now turn to study the phases resulting from perturbing this theory. First, we introduce the perturbation

$$S_m = m \sum_z \int d^2x dt \, \bar{\widetilde{\Psi}}'_z \widetilde{\Psi}_z = m \sum_z \int d^2x dt \, \bar{\Psi}_z \Psi_z \, , \qquad (7.7)$$

which acts as a mass term in the decoupled layer limit $\chi_0 = 0$. This term matches the time-reversal breaking terms introduced in Ref. [158], which was shown to stabilize a Weyl semimetal phase as long as m/χ_0 is small enough. We therefore expect to obtain a low-energy theory consisting of two Weyl fermions coupled to a gauge field. As we demonstrate in Appendix B.3, this is indeed the case, and the low energy action is given by

$$S_{\text{Weyl}} = i \sum_{\beta=1}^{2} \int d^3x dt \, \widetilde{\Psi}^\dagger_\beta \sigma^\beta_\mu \left(\partial^\mu - i a^\mu_j \right) \widetilde{\Psi}_\beta \, , \qquad (7.8)$$

where β enumerates the two Weyl cones, the Ψ_β-fields are Weyl spinors, $\sigma^\beta_\mu = \sigma_\mu$ for $\mu = 0, \dots, 2$ and $\sigma^\beta_3 = (-1)^\beta \sigma_3$. Notice that while the two Weyl theories are technically equivalent to a single Dirac theory, they are associated with degrees of freedom located at different momenta $k_z = \pm \cos^{-1} \left(\frac{|m|}{2\chi_0} \right)$, prompting us to regard them as separate theories.

Furthermore, notice that the dual fermion number is not a microscopically conserved quantity, meaning that pairing terms are naturally generated. The simplest of these takes the form

$$S_\Delta = \Delta \sum_z \int d^2x dt \left(\widetilde{\Psi}_z i \sigma_2 \widetilde{\Psi}_z + \text{H.c.} \right) \, . \qquad (7.9)$$

Such a term has two important effects: First, it provides a Higgs mass to the gauge field. In addition, the low energy Weyl fermions are shifted to $k_z = \pm \cos^{-1} \left(\frac{\sqrt{m^2 - \Delta^2}}{2\chi_0} \right)$. This means that the composite Weyl semimetal phase survives as long as $|\Delta| \leq |m|$ and $m^2 \leq 4\chi_0^2 + \Delta^2$ (see Fig. 7.1b for the phase diagram). We note that in the more generic case, where Δ is not the same in all layers, each Weyl cone splits into two Majorana-Weyl cones [160]. In such cases, one can access an additional Majorana-Weyl semimetal phase, where two of the four cones couple and become massive, resulting in only two gapless Majorana-Weyl cones.

Once the dynamical gauge field $\vec{a}$ is gapped, the electric current $\vec{J} \propto \vec{\nabla} \times \vec{a}$ is suppressed, and the system becomes electrically insulating. However, there are still gapless neutral excitations in the bulk whose contribution to the thermal transport is the same as for the original electrons. We would like to compare this composite Weyl semimetal phase to the 'composite Dirac liquid' (CDL), proposed to arise on the surface of a 3D topological insulator [61]. The

CDL state arises from QED_3 when the gauge degrees of freedom are gapped by the formation of a dual-fermion superconductor, leaving behind a Dirac cone of neutral fermions. The Dirac point is not protected by any symmetries and the CDL thus requires a certain amount of fine tuning. In contrast, the composite Weyl semimetal represents a stable phase of matter.

7.6 Topologically ordered and symmetry enriched phases

Starting with the composite Weyl semimetal, one can readily access two distinct fully gapped phases. The first phase, represented by the blue regions in Fig. 7.1b, is obtained when the two Weyl nodes meet on the edge of the Brillouin zone and annihilate. The second phase, depicted by the green regions in Fig. 7.1b, is obtained when the two Weyl points coincide at the origin. As we demonstrate in Appendix B.5, the above indicates that the two phases are distinguished by their topological properties, with one of them having a completely trivial band structure and the other forming a 3D stacked quantum Hall state of dual fermions, referred to as a thermal Hall insulator.

Regardless of the properties of band structure, when the system exhibits a pairing gap, the gapped excitations consist of the dual fermions and vortex lines. As usual, when a dual fermion encircles a vortex line, it acquires a phase of π. Therefore, our system hosts deconfined point- and line-like excitations, with non-trivial mutual statistics, i.e., it exhibits topological order. In fact, it realizes the three-dimensional incarnation of the toric code [157], where the two types of point-particles exhibit the same mutual statistics.

The topological order is correct for any gapped superconducting state. It is therefore natural to ask whether we can also stabilize phases associated with strong topological band indices and non-trivial surface states. We note that the only topological class in 3D allowing for topologically non-trivial superconducting phases is class DIII [47, 48], with time reversal symmetry satisfying $\mathscr{T}^2 = -1$. In the non-interacting limit, this class exhibits infinitely many distinct topological phases, each of which is described by an integer valued topological invariant. Interactions reduce the number of topologically distinct phases, leading to a $\mathbb{Z}_{16}$ classification [161–164]. The topologically ordered state discussed above has a ground state degeneracy of eight on a three-dimensional torus. This degeneracy is consistent with time-reversal symmetry, hinting that it might indeed be possible to enrich it with a DIII topological band index.

In our case, the original time-reversal symmetry acts as an effective anti-unitary particle-hole (or chirality) symmetry in the dual formulation. The presence of pairing terms leads to an additional unitary particle-hole symmetry. Multiplying the two symmetries, we obtain an anti-unitary time-reversal symmetry $\widetilde{\mathscr{T}}$ satisfying $\widetilde{\mathscr{T}}^2 = -1$. Thus, as long as the physical time-

reversal symmetry is preserved, the dual action indeed belongs to class DIII, and symmetry enriched phases can arise.

If the system is in a phase with a non-zero strong invariant, the surface hosts an integer number of symmetry protected Majorana cones, comprised of dual fermions.

7.7   QED$_4$ at finite density

Finally, we want to briefly mention the possibility of 'doping' the emergent fermions to a non-zero density by applying a magnetic field along the stacking direction. The (2+1)d duality maps physical magnetic flux onto dual-fermion density and thus each layer features a Fermi surface of dual fermions—essentially the composite Fermi liquid (CFL) that arises in the half-filled Landau level. Upon forming inter-layer coherence, these two-dimensional CFLs turn into a single three dimensional Fermi surface which may be more stable against various instabilities than the Dirac theory. A closely related three-dimensional state of composite Fermions (but without a Dirac dispersion) was envisaged in Ref. [155] as a possible description of layered semimetals such as graphite under a strong magnetic field. Within our model, such a state corresponds to introducing a gap to the emergent Dirac fermions that is smaller than their chemical potential.

Chapter 8

Spin liquids from Majorana Zero Modes in a Cooper Box

This chapter presents the results of our last project, presented in Ref. [74]. In this project, we propose a path for realizing interacting spin models with semiconductor nanowires. We show that these ideas can be used to realize systems with non-trivial criticality, as well as spin-liquid phases.

8.1   Introduction

Quantum spin models are of paramount importance in condensed matter physics. While spin-models were traditionally devised to study magnetically ordered materials, they are nowadays known to exhibit highly non-trivial behavior, such as diverse critical phenomena and topological order.

An important mathematical tool used to uncover these non-trivial properties is the fermionization of the spins to Majorana degrees of freedom, which in a few notable cases leads to exact solutions. Important examples are the Jordan-Wigner transformation [165], which allows for exact solutions of spin-1/2 models, such as the XXZ and Ising models [166–168], as well as the two-dimensional Yao-Kivelson (YK) model [169]. A more recent example is the Kitaev transformation [170], originally used to solve the Kitaev honeycomb model and demonstrate the emergence of non-Abelian spin-liquid behavior.

Recent strong evidence indicate the emergence of Majorana zero modes (MZMs) on the edges of semiconductor nanowires with spin-orbit coupling, which are in proximity to an *s*-wave superconductor [16–25]. When a few such MZMs are placed in a quantum dot with strong Coulomb interactions, a so called Majorana-Cooper-Box or MZM island, is formed.
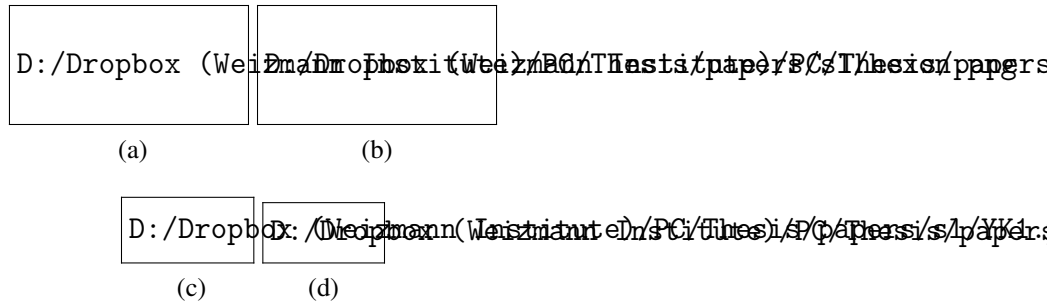
```
D:/Dropbox (Weizmann Institute)/PhD/Thesis/paper/hexon/papers
```
(a)

```
D:/Dropbox (Weizmann Institute)/PhD/Thesis/paper/hexon/papers
```
(b)

```
D:/Dropbox (Weizmann Institute)/PhD/Thesis/paper/hexon/papers
```
(c)

```
D:/Dropbox (Weizmann Institute)/PhD/Thesis/paper/hexon/papers
```
(d)

Figure 8.1: (a) The basic hexon building block, consisting of three semiconductor nanowires. The wires are assumed to the in the topological regime, in which each edge has a protected Majorana zero mode. In the presence of strong charging energy, we demonstrate that each hexon is equivalent to two spin-1/2 degrees of freedom. (b) By forming an array of hexons, we effectively model spin chains. (c) The hexons can also be arranged in a 2D structure, giving rise to the Yao-Kivelson model shown in Fig. (d).

The MZMs in the island can be mapped onto spin degrees of freedom. For example, considering four MZMs in an islands, each pair forms a fermion, thus generating four degenerate states. Including the constraint on the total number of particles in the box due to the strong Coulomb interactions, an effective two-level system–or a spin $1/2$–is formed. Indeed, similar ideas have been used to study the so-called "topological Kondo effect" [171–176], and realize spin-liquid models [177–179]. Such models are of interest due to their promise as platforms for fault tolerant quantum computing.

This approach is reciprocal to the common fermionization of spin models: instead of starting with physical spins and mapping them to Majorana degrees of freedom through mathematical transformations, we begin with physical MZMs and map them onto spins.

In this work we propose a different setup, where each box is made of three semiconducting wires, and demonstrate that in the presence of a strong charging energy, two effective spin degrees of freedom emerge at low energies. Due to the presence of six MZMs, we refer to our building block as an "hexon" [180]. The hexon building blocks are shown to be highly tunable, and in fact, controlling the coupling between different MZMs (e.g., by tuning local chemical potential) allows us to fully determine the coupling between different spins and the effective magnetic field they experience. If many such building blocks are arranged in a one-dimensional (1D) line, or cover the two-dimensional (2D) plane, this allows us to simulate a plethora of spin models in 1D and 2D.

To demonstrate the above, we present explicit realizations of 1D $SU(2)$-invariant models, the XXZ model, the transverse field Ising model, and the 2D Yao-Kivelson spin-liquid model. By modulating the distance between a specific pair of MZMs as a function of time and mea-

suring the induced charge at a distance, we propose measurable imprints of gapless points in these systems.

8.2   The hexon

The basic building block in our construction is the so-called hexon [180], illustrated in Fig. 8.1a. Each hexon is composed of three semiconductor nanowires with strong spin-orbit coupling. The wires are proximity coupled to an *s*-wave superconductor. Applying a strong Zeeman field drives the wires into the topological regime, in which protected MZMs reside near the ends of each wire [16–25]. The Majorana zero modes are conveniently denoted by the operators a_α, b_α, with the indices $\alpha = x, y, z$, as illustrated in Fig. 8.1a. The presence of six Majorana zero modes leads to a degeneracy of 8.

Taking Coulomb blockade into account, and assuming that the charging energy E_C is the largest energy scale in play, we fix the charge, and therefore the parity, of the entire hexon by controlling a back-gate voltage. At low energies, the parity of the entire hexon can be written in terms of the MZMs as

$$\mathcal{P} = ia_1 a_2 a_3 b_1 b_2 b_3. \tag{8.1}$$

Thus, by controlling the back-gate voltage, we can effectively apply the constraint $\mathcal{P} = 1$ (or similarly, $\mathcal{P} = -1$), thus reducing the ground state degeneracy to 4.

To find a useful parametrization of the remaining 4-dimensional low energy subspace, we define spin-1/2 operators according to [181]

$$S_a^x = ia_y a_z, \quad S_a^y = ia_x a_z, \quad S_a^z = ia_x a_y \tag{8.2}$$

$$S_b^x = ib_y b_z, \quad S_b^y = ib_x b_z, \quad S_b^z = ib_x b_y. \tag{8.3}$$

It can easily be checked that these are in fact spin-1/2 operators (i.e., they satisfy the relation $S^l S^m = i\varepsilon_{klm} S^k + \delta_{lm}$), which commute with the total parity [Eq. (8.1)], and therefore do not violate the parity-fixing constraint. The number of states indeed coincides with the degeneracy of a two-spin system, and we find that at low energies the six MZMs are reduced to *two* effective spin-1/2 degrees of freedom. In what follows, the effective spin degrees of freedom will be used to design non-trivial spin models by engineering the coupling between different MZMs.

8.3   Coupling the spins

We start by studying the terms that arise from coupling the MZMs within the hexon. The first of these arises when the lengths l_α of the wires (see Fig. 8.1b) are made short enough such that the Majorana wavefunctions at the two ends overlap. In this case we get terms of the form

$$H_1 = i \sum_{\alpha=x,y,z} J_\alpha a_\alpha b_\alpha, \tag{8.4}$$

where the coupling constants J_α are controlled by the lengths l_α. Notice that the sign of J_α can also be tuned as the overlap between the MZM wave-functions generically changes sign as a function of l_α. Alternatively, by tuning the chemical potential in the wire, one controls the localization length of the MZMs and therefore their coupling. Taking the constraint $\mathscr{P} = 1$ into account, and using Eqs. (8.2) and (8.3), we can write these as

$$H_1 = \sum_{\alpha=x,y,z} J_\alpha S_a^\alpha S_b^\alpha. \tag{8.5}$$

One can also generate a different set of terms by coupling MZMs of the same type (a with a and b with b), e.g., by changing the distance between wires. This generates coupling terms of the form

$$H_2 = i \sum_{\alpha\alpha'} \tilde{t}_{\alpha\alpha'} \left(a_\alpha a_{\alpha'} + b_\alpha b_{\alpha'} \right). \tag{8.6}$$

In terms of the spin operators, H_2 can be written as

$$H_2 = \sum_\alpha B_\alpha \left(S_a^\alpha + S_b^\alpha \right), \tag{8.7}$$

with $B_\alpha \propto \varepsilon_{\alpha\beta\gamma} \tilde{t}_{\beta\gamma}$.

   To recapitulate, we find that each hexon is equivalent to two spins degrees of freedom, and that the effective coupling between the two spins, as well as coupling to an external magnetic field, can be controlled by tuning the coupling between the MZMs (for example, with gate potentials). In what follows we use these hexon building blocks to form 1D and 2D interacting spin models.

8.4 Realizing $SU(2)$-invariant spin chains

Consider the array of hexons depicted in Fig. 8.1b. As we discussed above, these are equivalent to an array of spins, labeled by $\vec{S}_{j,\gamma}$, where j enumerates the different hexon unit cells and $\gamma = a, b$ differentiates between the two spins in each unit cell.

We start by assuming that the distance between different wires is large such that the effective Zeeman field [B_α in Eq. (8.7)] vanishes, yet the lengths l_α are small enough to generate H_1-type terms of the form

$$H_1 = \sum_j \sum_{\alpha=x,y,z} J_\alpha S_{j,a}^\alpha S_{j,b}^\alpha, \tag{8.8}$$

Coupling terms of the form $S_{j,b}^\alpha S_{j+1,a}^\alpha$ can additionally be generated by bringing different hexons close to each other. This generates tunneling terms of the form

$$H_{\text{tunneling}} = i \sum_{\alpha=x,y,z} \tilde{t}'_\alpha \sum_j b_{\alpha j} a_{\alpha j+1}. \tag{8.9}$$

These terms, however, alter the parity of the hexons and therefore do not commute with the constraint. Under our assumption that the charging energy E_C is the largest energy scale, the tunneling terms in Eq. (8.9) thus scale down to zero. Nevertheless, we can form combinations of these terms that commute with the constraint. The lowest order terms generated in perturbation theory take the form

$$H_1' = \sum_{\alpha=x,y,z} J_\alpha' \sum_j S_{j,b}^\alpha S_{j+1,a}^\alpha \tag{8.10}$$

where $J_\alpha' \propto \frac{\Pi_{\alpha' \neq \alpha} \tilde{t}'_{\alpha'}}{E_C}$.

At low energies, our model is therefore given by a combination of Eqs. (8.8) and (8.10). For simplicity, we start by assuming that the system was tuned to be $SU(2)$-invariant, i.e., $J_\alpha = J$, and $J_\alpha' = J'$. We further assume that $J, J' > 0$.

Clearly, if $J > J'$, we get a fully gapped dimerized phase, in which the two spins corresponding to each hexon form a singlet state. In the opposite regime where $J' > J$, the system is again in a dimerized phase, now with adjacent spins originating from different hexons forming singlet states.

The two above phases are topologically distinct, with the second state giving rise to a protected decoupled spin on each edge. As such, we expect to find a critical point if we tune $J = J'$. Indeed, at this point our model becomes the spin-$\frac{1}{2}$ Heisenberg model, known to be dual to a 1D model of interacting fermions. The latter is described by the Luttinger-liquid

fixed point Hamiltonian

$$H_{LL} = \frac{v}{2\pi} \int dx \left[K \left(\partial_x \theta \right)^2 + \frac{1}{K} \left(\partial_x \varphi \right)^2 \right], \tag{8.11}$$

with the Luttinger parameter $K = \frac{1}{2}$ [182], the spin operator $S_z(x) = \frac{1}{\pi} \partial_x \varphi$, and $[\theta(x), \varphi(x')] = i\pi\Theta(x - x')$. The Luttinger parameter can be varied if the $SU(2)$ symmetry is broken to $U(1)$, i.e., if one of the components J_α is not the same as the other two. Indeed, mutual capacitance terms generically renormalize the Luttinger parameter [183]. Notice that we neglected higher order tunneling terms as a renormalization group analysis indicates they are irrelevant.

8.5   Experimental signature

The above constitutes an example of realizing a critical spin model from the physical MZMs. It is natural to ask whether one can measure imprints of the gapless spin model in the current realization. Such an imprint is required to distinguish between gapless and gapped states, as well as between gapless states described by different conformal field theories (CFTs).

Clearly, given that the charge degrees of freedom are gapped, one cannot use electronic transport measurements. A possible route is then to use thermal conductance measurements instead. While such measurements are possible, and were in fact used recently to detect imprints of the non-Abelian nature of the quantum Hall plateau at filling $5/2$ [148, 184, 185], they are difficult in practice.

Instead, we propose an alternative experiment in which a time-dependent gate modulating the coupling between two specific MZMs is applied. If we choose these to be a_{xj_0} and a_{yj_0} (or similarly b_{xj_0} and b_{yj_0}) in a specific unit cell, we obtain a time-dependent Hamiltonian of the form $H_{\text{pert}} = f(t)S^z(x_0)$, where for simplicity we assume that $f(t) = V_0 \cos(\omega t + \phi_0)$.

To find imprints of the gapless nature of the underlying state, we propose to measure the expectation value of $S^z_{j,a} = ia_{xj}a_{yj}$ (or similarly $S^z_{j,b} = ib_{xj}b_{yj}$) in a distant unit cell j, at later times. We refer to this quantity as the *induced parity* of these MZMs. Performing linear response, the value of $S^z(x, t)$, i.e., the induced parity of the appropriate pair of MZMs at point x and time t, is given by

$$\langle S^z(x,t) \rangle = \int dt' f(t') \chi(t - t', x - x_0), \tag{8.12}$$

with χ being the dynamic susceptibility: $\chi(t - t', x - x') = i \langle [S^z(x,t), S^z(x',t')] \rangle \Theta(t - t')$. As we demonstrate in Appendix C, in a *non-chiral* critical point, where the (time-ordered) correlation function takes the form $G \sim \alpha^{4h}/(x^2 - v^2 t^2)^{2h}$ (with α being the short distance cutoff,

and h the conformal dimension), we obtain

$$\langle S^z(x,t) \rangle = \frac{V_0 \alpha^{4h}}{v^{2h+\frac{1}{2}}} \left(\frac{\omega}{|\Delta x|} \right)^{2h-\frac{1}{2}} \times \Re \left\{ B e^{i(\omega t + \phi_0)} K_{\frac{1}{2}-2h} \left(i \frac{\omega |\Delta x|}{v} \right) \right\} \qquad (8.13)$$

where $\Delta x = x - x_0$, B is a complex dimensionless constant, and $K_n(z)$ is the modified Bessel function of the second kind. Using the asymptotic form $K_n(z) \sim \sqrt{\frac{\pi}{2z}} e^{-z}$, we obtain $\langle S^z(x,t) \rangle \propto \frac{V_0 \alpha^{4h}}{v^{2h}} \frac{\omega^{2h-1}}{|\Delta x|^{2h}} \cos \left[\omega \left(t - \frac{|\Delta x|}{v} \right) + \varphi_0 \right]$ at large distances, where φ_0 is a constant phase. By measuring the induced parity at a distance from the perturbation, we can thus get an imprint of the critical nature of the transition, and in particular, directly measure the critical exponent h. Moving away from the critical point, Eq. (8.13) becomes an exponential decay.

In our case, the Luttinger-liquid description in Eq. (8.11) implies that the $S_z - S_z$ time ordered correlation function is described by $h = 1/2$, leading to $\langle S^z(x,t) \rangle \propto \frac{V_0 \alpha^2}{v|\Delta x|} \cos \left[\omega \left(t - \frac{|\Delta x|}{v} \right) + \phi_0 \right]$ (see Appendix C for details).

8.6   The transverse field Ising model

The flexibility of altering the various length scale in our setup allows us to realize a large set of spin models which goes beyond the above $SU(2)$ invariant chains. In what follows we provide an explicit construction of another prominent spin chain - the transverse field Ising model - defined by the Hamiltonian

$$H_{\text{Ising}} = \sum_j \left[-J S_j^z S_{j+1}^z + h S_j^x \right]. \qquad (8.14)$$

The first term can be generated similarly to the above: by making the length l_z of the z-type wires short enough and simultaneously bringing x and y type wires coming from adjacent hexons closer to each other. If these terms are taken to have identical amplitudes, they generate the first term in Eq. (8.14). In addition, assuming the distance between the y- and z-wires in each hexon is made short, we generate H_2-type terms, giving rise to the second term in Eq. (8.14).

As is well known, the transverse field Ising model possesses two different phases. For $J > h$, the ground state of the system spontaneously breaks the $S^z \to -S^z$ symmetry and the spins collectively point in the $\pm z$ direction. In the opposite regime, where $h > J$, the state is not in a symmetry broken phase, and is connectable to the state in which all the spins form an eigenstate of S_x with eigenvalue -1. The above two phases are separated by a gapless critical point at $h = J$, in which case the effective spin chain is described by an Ising fixed point with

central charge $c = \frac{1}{2}$ [186].

To probe this critical point, we can repeat the above experiment where a local time dependent gate modulates the z component of the magnetic field at point x_0, and a charge probe at point x effectively measures the induced $S_z(x,t)$. Since S_z can be identified with the σ primary field of the Ising CFT at low energies, its correlation function scales with $h = 1/16$. We can find the induced parity by plugging this into Eq. (8.13). The dependence of the parity on the distance and frequency provides a direct imprint of the non-trivial CFT.

8.7 The 2D Yao-Kivelson spin liquid

In the above analysis, we have demonstrated that the hexon building blocks provide a fruitful playground for realizing 1D spin chains. As we argue now, the same ideas can be applied to 2D spin models. To demonstrate this, we explicitly construct the so-called Yao-Kivelson model [169], which realizes a non-Abelian spin-liquid state.

To do that, we sort the hexons in structures similar to Fig. 8.1c. Notice that the labels x, y, z of the MZMs are now alternating. In each hexon, we assume that the colored wire is made short and therefore induces $S_a^\alpha S_b^\alpha$-type terms. Correlated tunneling terms between different hexons also generate $S_a^\alpha S_b^\alpha$-type terms, with α determined by geometry - i.e., α is chosen such that $\Pi_{\alpha' \neq \alpha} \tilde{t}'_{\alpha'}$ is maximized. The resulting dominating terms are shown in Fig. 8.1c in terms of the MZMs and in terms of the spin degrees of freedom in the inset.

If many such building blocks are connected in a way that covers the 2D plane, we obtain the decorated honeycomb lattice geometry, shown in Fig 8.1d, where each link is given a label α, stating the dominating $S^\alpha S^\alpha$ term. The resulting spin Hamiltonian is identical to the YK Hamiltonian, known to generate a non-Abelian spin liquid state in the so-called B-phase (as long as the coupling at the $x', y',$ and z' links is not too large), which in addition spontaneously breaks time reversal symmetry. The Abelian A-phase of the Kitaev honeycomb model can also be realized, for example, if we take the z' coupling to be much larger than x', y'. Other proposals for realizing this phase were given in Refs. [178, 179]. The advantage of the current proposal is the ability to control all the coupling terms with gate potentials.

Within the B-phase, the edge of the sample gives rise to a chiral Ising CFT, similar to the edge of a $p + ip$ superconducting state, which can be constructed from arrays of Majorana wires as well [52, 71]. As opposed to the $p + ip$ superconducting state, however, the resulting state is topologically ordered, with the σ-particle being deconfined. We note that one can obtain the above spin-liquid from the $p + ip$ superconducting state by condensing h/e vortices [152].

In order to measure imprints of the gapless edge, we again repeat the experiment above on

the edge. As shown in Appendix C, the induced S_z is given by

$$\langle S^z(x,t)\rangle = V_0 \frac{\omega^{2h-1}\alpha^{2h}}{v^{2h}} \cos\left[\omega\left(t - \frac{\Delta x}{v}\right) + \varphi_0\right], \tag{8.15}$$

with h being the smallest dimension among the operators excited by S^z. In contrast to the 1D case, here the perturbation operates on a chiral edge, and therefore cannot act as the σ primary field on that edge alone.

Chapter 9

Discussion

Throughout this thesis, we have studied topologically ordered phases of matter. The inherent role played by interactions makes these phases extremely difficult to analyze theoretically. In particular, a complete classification of topologically ordered phases does not exist.

A central part of my PhD focused on the coupled-wire approach, which is an efficient machinery allowing us to write tractable models for topologically ordered phases. As we have demonstrated throughout this thesis, it can be used to write tractable models for a variety of topologically ordered and symmetry enriched phases in two- and three-dimensions.

It would be interesting to ask whether the same approach can be used to more generally *classify* topological orders in two-dimensions. This can be done if we start with an array of electronic wires, and tune each unit cell to a critical point described by a general CFT, denoted by $\mathscr{C}$, with the set of primary fields $\mathscr{O}_{R/L}^i$ (where i enumerates the primary fields associated with $\mathscr{C}$).

To construct a topologically ordered state, we couple different wires such that a chiral version of $\mathscr{C}$ resides on the edge. Such a coupling takes the form $\mathscr{O}_{R,j}^{*\dagger}\mathscr{O}_{L,j+1}^{*}$, for some primary field $\mathscr{O}^*$ (see the lower section of Fig. 2.1 for a schematic depiction of these terms). An important subtlety arises when we note that these terms must be made from local electronic terms, which in most known cases means that the fields $\mathscr{O}_{R/L}$ themselves represent local electron fields. In such a case, to satisfy the fermionic anti-commutation relations, the chiral field $\mathscr{O}_{R/L}$ coupled between different unit cells must have a dimension of the form $n/2$, with n being an odd integer.

Once the phase has been constructed, the bulk excitations can be studied through the bulk-edge correspondence, whereby the primary fields of the edge CFT can be associated with bulk excitations. In addition, the statistics of these excitations can be deduced directly from the edge CFT. Notice, however, that primary fields which have a non-trivial statistics with the electron field must represent confined bulk excitations, otherwise the many-body wavefunction

would be multi-valued.

As an example of this scheme, let us discuss the construction of two closely related, yet very different, states of matter: the $p + ip$ superconductor and the Moore-Read quantum Hall state. The first of these is not topologically ordered, and has a chiral Ising CFT on the edge. The latter is a non-Abelian topologically ordered state, and also possesses an Ising edge theory (in addition to a bosonic charge mode). One can then ask how two states with such similar edge theories can have such diametrically different bulk properties, given the bulk-edge correspondence.

The answer lies in the identification of the electron field. In the $p + ip$ superconductor, the electron field is simply given by the ψ-operator of the Ising CFT. Noting that the other non-trivial primary field of the Ising CFT - the σ operator - has a non-trivial statistics with ψ, it must then be confined in the bulk. In this case, the spectrum of deconfined excitations is clearly not rich enough to result in topological order.

The Moore-Read state is different in that the ψ field does not represent the local electron. Instead, the local electron can be written as $\Psi_{\text{el}} = \psi e^{i\phi}$, where ϕ is the bosonic charge mode satisfying $[\phi(x), \phi(x')] = 2\pi i \text{sgn}(x - x')$. While the σ operator again has a non-trivial statistics with the electron, we can construct a primary operator of the form $\xi_{\text{qh}} = \sigma e^{i\frac{\phi}{4}}$ (describing a quasihole excitation), whose statistics with the electron can be verified to be trivial. Such operators are therefore associated with deconfined excitations which have a non-trivial statistics and give rise to topological order. This demonstrates that very similar edge CFTs can be associated with vastly different bulk properties, given different identifications of the electron field.

The above discussion suggests that a classification of a large set of topological orders can be reduced to classifying all CFTs containing candidate electronic fields (having the appropriate conformal dimensions). In CFTs that contain more than one such candidate field, distinct topological phases generally arise. Within the approach described above, the considerable amount of knowledge on conformal field theories in 1D can be used to (partially) classify topological orders.

Note that the above approach fails to describe topologically ordered phases which do not have an electron operator, such as spin liquid states. For example, the Kitaev honeycomb model, again gives rise to an Ising CFT on the edge, but now the electron does not appear in the low energy edge theory. In this case, there are no limitations on the spectrum of deconfined excitations, and the state is topologically ordered.

References

[1] K. Klitzing, G. Dorda, and M. Pepper, Physical Review Letters **45**, 494 (1980).

[2] D. C. Tsui, H. L. Stormer, and A. C. Gossard, Physical Review Letters **48**, 1559 (1982).

[3] O. Pankratov, S. Pakhomov, and B. Volkov, Solid State Communications **61**, 93 (1987).

[4] C. L. Kane and E. J. Mele, Physical Review Letters **95**, 226801 (2005).

[5] B. A. Bernevig, T. L. Hughes, and S.-C. Zhang, Science (New York, N.Y.) **314**, 1757 (2006).

[6] M. König, S. Wiedmann, C. Brüne, A. Roth, H. Buhmann, L. W. Molenkamp, X.-L. Qi, and S.-C. Zhang, Science **318**, 766 (2007).

[7] C.-X. Liu, X.-L. Qi, and S.-C. Zhang, Physica E: Low-dimensional Systems and Nanostructures **44**, 906 (2012).

[8] A. Roth, C. Brüne, H. Buhmann, L. W. Molenkamp, J. Maciejko, X.-L. Qi, and S.-C. Zhang, Science **325**, 294 (2009).

[9] K. C. Nowack, E. M. Spanton, M. Baenninger, M. König, J. R. Kirtley, B. Kalisky, C. Ames, P. Leubner, C. Brüne, H. Buhmann, L. W. Molenkamp, D. Goldhaber-Gordon, and K. A. Moler, Nat. Mater. **12**, 787 (2013).

[10] I. Knez, R.-R. Du, and G. Sullivan, Phys. Rev. Lett. **109**, 186603 (2012).

[11] E. M. Spanton, K. C. Nowack, L. Du, G. Sullivan, R.-R. Du, and K. A. Moler, Phys. Rev. Lett. **113**, 026804 (2014).

[12] L. Fu, C. Kane, and E. Mele, Physical Review Letters **98**, 106803 (2007).

[13] L. Fu and C. Kane, Physical Review B **76**, 045302 (2007).

[14] L. Fu and C. Kane, Physical Review Letters **100**, 096407 (2008).

[15] D. Hsieh, D. Qian, L. Wray, Y. Xia, Y. S. Hor, R. J. Cava, and M. Z. Hasan, Nature **452**, 970 (2008).

[16] J. D. Sau, R. M. Lutchyn, S. Tewari, and S. Das Sarma, Phys. Rev. Lett. **104**, 040502 (2010).

[17] R. M. Lutchyn, J. D. Sau, and S. Das Sarma, Physical Review Letters **105**, 077001 (2010).

[18] Y. Oreg, G. Refael, and F. von Oppen, Physical Review Letters **105**, 177002 (2010).

[19] V. Mourik, K. Zuo, S. M. Frolov, S. R. Plissard, E. P. A. M. Bakkers, and L. P. Kouwenhoven, Science **336**, 1003 (2012).

[20] L. P. Rokhinson, X. Liu, and J. K. Furdyna, Nature Physics **8**, 795 (2012).

[21] M. T. Deng, C. L. Yu, G. Y. Huang, M. Larsson, P. Caroff, and H. Q. Xu, Nano lett. **12**, 6414 (2012).

[22] H. O. H. Churchill, V. Fatemi, K. Grove-Rasmussen, M. T. Deng, P. Caroff, H. Q. Xu, and C. M. Marcus, Physical Review B **87**, 241401 (2013).

[23] A. Das, Y. Ronen, Y. Most, Y. Oreg, M. Heiblum, and H. Shtrikman, Nat. Phys. **8**, 887 (2012).

[24] A. D. K. Finck, D. J. Van Harlingen, P. K. Mohseni, K. Jung, and X. Li, Physical Review Letters **110**, 126406 (2013).

[25] S. M. Albrecht, A. P. Higginbotham, M. Madsen, F. Kuemmeth, T. S. Jespersen, J. Nygård, P. Krogstrup, and C. M. Marcus, Nature **531**, 206 (2016).

[26] L. Fu, Physical Review Letters **106**, 106802 (2011).

[27] T. H. Hsieh, H. Lin, J. Liu, W. Duan, A. Bansil, and L. Fu, Nat. Commun. **3**, 982 (2012).

[28] Y. Tanaka, Z. Ren, T. Sato, K. Nakayama, S. Souma, T. Takahashi, K. Segawa, and Y. Ando, Nat. Phys. **8**, 800 (2012).

[29] P. Dziawa, B. Kowalski, K. Dybko, R. Buczko, A. Szczerbakow, M. Szot, E. Łusakowska, T. Balasubramanian, B. M. Wojek, M. Berntsen, *et al.*, Nat. Mater. **11**, 1023 (2012).

[30] S.-Y. Xu, C. Liu, N. Alidoust, M. Neupane, D. Qian, I. Belopolski, J. Denlinger, Y. Wang, H. Lin, L. Wray, *et al.*, Nat. Commun. **3**, 1192 (2012).

[31] C.-X. Liu, R.-X. Zhang, and B. K. VanLeeuwen, Phys. Rev. B **90**, 085304 (2014).

[32] C. Fang and L. Fu, Phys. Rev. B **91**, 161105 (2015).

[33] K. Shiozaki, M. Sato, and K. Gomi, Phys. Rev. B **91**, 155120 (2015).

[34] Z. Wang, A. Alexandradinata, R. J. Cava, and B. A. Bernevig, Nature **532**, 189 (2016).

[35] S. Shuichi Murakami, New Journal of Physics **9**, 356 (2007).

[36] X. Wan, A. M. Turner, A. Vishwanath, and S. Y. Savrasov, Physical Review B **83**, 205101 (2011).

[37] M. Z. Hasan, S.-Y. Xu, I. Belopolski, and S.-M. Huang, Annual Review of Condensed Matter Physics **8**, 289 (2017).

[38] P. Hosur and X. Qi, (2013), 10.1016/j.crhy.2013.10.010, arXiv:1309.4464 .

[39] S.-Y. Xu, I. Belopolski, N. Alidoust, M. Neupane, G. Bian, C. Zhang, R. Sankar, G. Chang, Z. Yuan, C.-C. Lee, S.-M. Huang, H. Zheng, J. Ma, D. S. Sanchez, B. Wang, A. Bansil, F. Chou, P. P. Shibayev, H. Lin, S. Jia, and M. Z. Hasan, Science (New York, N.Y.) **349**, 613 (2015).

[40] B. Q. Lv, H. M. Weng, B. B. Fu, X. P. Wang, H. Miao, J. Ma, P. Richard, X. C. Huang, L. X. Zhao, G. F. Chen, Z. Fang, X. Dai, T. Qian, and H. Ding, Physical Review X **5**, 031013 (2015).

[41] S.-M. Huang, S.-Y. Xu, I. Belopolski, C.-C. Lee, G. Chang, B. Wang, N. Alidoust, G. Bian, M. Neupane, C. Zhang, S. Jia, A. Bansil, H. Lin, and M. Z. Hasan, Nature Communications **6**, 7373 (2015).

[42] H. Weng, C. Fang, Z. Fang, B. A. Bernevig, and X. Dai, Physical Review X **5**, 011029 (2015).

[43] S.-Y. Xu, N. Alidoust, I. Belopolski, Z. Yuan, G. Bian, T.-R. Chang, H. Zheng, V. N. Strocov, D. S. Sanchez, G. Chang, C. Zhang, D. Mou, Y. Wu, L. Huang, C.-C. Lee, S.-M. Huang, B. Wang, A. Bansil, H.-T. Jeng, T. Neupert, A. Kaminski, H. Lin, S. Jia, and M. Zahid Hasan, Nature Physics **11**, 748 (2015).

[44] H. Zheng, S.-Y. Xu, G. Bian, C. Guo, G. Chang, D. S. Sanchez, I. Belopolski, C.-C. Lee, S.-M. Huang, X. Zhang, R. Sankar, N. Alidoust, T.-R. Chang, F. Wu, T. Neupert, F. Chou, H.-T. Jeng, N. Yao, A. Bansil, S. Jia, H. Lin, and M. Z. Hasan, ACS Nano 10, 1378 (2016).

[45] L. X. Yang, Z. K. Liu, Y. Sun, H. Peng, H. F. Yang, T. Zhang, B. Zhou, Y. Zhang, Y. F. Guo, M. Rahn, D. Prabhakaran, Z. Hussain, S.-K. Mo, C. Felser, B. Yan, and Y. L. Chen, Nature Physics 11, 728 (2015).

[46] Y. Zhou, K. Kanoda, and T.-K. Ng, Rev. Mod. Phys. 89, 025003 (2017).

[47] A. Schnyder, S. Ryu, A. Furusaki, and A. Ludwig, Physical Review B 78, 195125 (2008).

[48] A. Kitaev, in AIP Conference Proceedings, Vol. 1134 (AIP, 2009) pp. 22–30.

[49] C. Kane, R. Mukhopadhyay, and T. Lubensky, Physical Review Letters 88, 036401 (2002).

[50] J. C. Y. Teo and C. L. Kane, Phy. Rev. B 89, 085101 (2014).

[51] J. Klinovaja and D. Loss, Physical Review Letters 111, 196401 (2013), arXiv:1302.6132 .

[52] I. Seroussi, E. Berg, and Y. Oreg, Physical Review B 89, 104523 (2014).

[53] T. Neupert, C. Chamon, C. Mudry, and R. Thomale, (2014), arXiv:1403.0953 .

[54] E. Sagi and Y. Oreg, Phy. Rev. B 90, 201102(R) (2014).

[55] J. Klinovaja and D. Loss, Phy. Rev. B 90, 045118 (2014).

[56] T. Meng and E. Sela, Phys. Rev. B 90, 235425 (2014).

[57] R. A. Santos, C.-W. Huang, Y. Gefen, and D. B. Gutman, Phys. Rev. B 91, 205141 (2015).

[58] E. Sagi and Y. Oreg, Phys. Rev. B 92, 195137 (2015).

[59] G. Gorohovsky, R. G. Pereira, and E. Sela, Physical Review B 91, 245139 (2015).

[60] T. Meng, T. Neupert, M. Greiter, and R. Thomale, Phys. Rev. B 91, 241106 (2015).

[61] D. F. Mross, A. Essin, and J. Alicea, Phys. Rev. X 5, 011011 (2015).

[62] T. Meng, Phys. Rev. B **92**, 115152 (2015).

[63] E. Sagi, Y. Oreg, A. Stern, and B. I. Halperin, Physical Review B **91** (2015), 10.1103/PhysRevB.91.245144.

[64] T. Meng, A. G. Grushin, K. Shtengel, and J. H. Bardarson, Phys. Rev. B **94**, 155136 (2016).

[65] H. Isobe and L. Fu, Phys. Rev. B **92**, 081304 (2015).

[66] S. Sahoo, Z. Zhang, and J. C. Y. Teo, Physical Review B **94**, 165142 (2016), arXiv:1509.07133 .

[67] T. Iadecola, T. Neupert, C. Chamon, and C. Mudry, Phys. Rev. B **93**, 195136 (2016).

[68] Y. Fuji, Y.-C. He, S. Bhattacharjee, and F. Pollmann, Phys. Rev. B **93**, 195143 (2016).

[69] P.-H. Huang, J.-H. Chen, P. R. S. Gomes, T. Neupert, C. Chamon, and C. Mudry, Phys. Rev. B **93**, 205123 (2016).

[70] C. L. Kane, A. Stern, and B. I. Halperin, Phys. Rev. X **7**, 031009 (2017).

[71] E. Sagi, A. Haim, E. Berg, F. von Oppen, and Y. Oreg, Physical Review B **96**, 235144 (2017).

[72] C. L. Kane and A. Stern, (2018), arXiv:1804.02177 [cond-mat.str-el] .

[73] E. Sagi, A. Stern, and D. F. Mross, (2018), arXiv:1806.01860 .

[74] E. Sagi, H. Ebisu, Y. Tanaka, A. Stern, and Y. Oreg, (2018), arXiv:1806.03304 .

[75] V. Yakovenko, Physical Review B **43**, 11353 (1991).

[76] S. Sondhi and K. Yang, Physical Review B **63**, 054430 (2001).

[77] X.-G. Wen, *Quantum Field Theory of Many-body Systems: From the Origin of Sound to an Origin of Light and Electrons (Oxford Graduate Texts)* (Oxford University Press, USA, 2007) p. 512.

[78] S. A. Parameswaran, R. Roy, and S. L. Sondhi, Comptes Rendus Physique **14**, 816 (2013).

[79] E. Tang, J.-W. Mei, and X.-G. Wen, Physical Review Letters **106**, 236802 (2011).

[80] K. Sun, Z. Gu, H. Katsura, and S. Das Sarma, Physical Review Letters **106**, 236803 (2011).

[81] T. Neupert, L. Santos, C. Chamon, and C. Mudry, Physical Review Letters **106**, 236804 (2011).

[82] D. N. Sheng, Z.-C. Gu, K. Sun, and L. Sheng, Nature communications **2**, 389 (2011).

[83] Y.-F. Wang, H. Yao, Z.-C. Gu, C.-D. Gong, and D. N. Sheng, Physical Review Letters **108**, 126805 (2012).

[84] N. Regnault and B. A. Bernevig, Physical Review X **1**, 021014 (2011).

[85] M. Levin and A. Stern, Physical Review Letters **103**, 196803 (2009).

[86] M. Levin, F. J. Burnell, M. Koch-Janusz, and A. Stern, Physical Review B **84**, 235145 (2011).

[87] M. Levin and A. Stern, Phys. Rev. B **86**, 115131 (2012).

[88] H. Chen and K. Yang, Phys. Rev. B **85**, 195113 (2012).

[89] S. Furukawa and M. Ueda, Phys. Rev. A **90**, 033602 (2014).

[90] P. Ghaemi, J. Cayssol, D. N. Sheng, and A. Vishwanath, Phys. Rev. Lett. **108**, 266801 (2012).

[91] T. Neupert, L. Santos, S. Ryu, C. Chamon, and C. Mudry, Phys. Rev. B **84**, 165107 (2011).

[92] C. Repellin, B. A. Bernevig, and N. Regnault, Phys. Rev. B **90**, 245401 (2014).

[93] B. Halperin, Physical Review B **25**, 2185 (1982).

[94] J. C. Y. Teo and C. L. Kane, (2011), arXiv:1111.2617 .

[95] Y. Oreg, E. Sela, and A. Stern, (2013), arXiv:1301.7335 .

[96] J. Klinovaja and D. Loss, (2013), arXiv:1311.3259 .

[97] P. Lecheminant, A. O. Gogolin, and A. A. Nersesyan, Nuclear Physics B **639**, 502 (2002).

[98] R. S. K. Mong, D. J. Clarke, J. Alicea, N. H. Lindner, P. Fendley, C. Nayak, Y. Oreg, A. Stern, E. Berg, K. Shtengel, and M. P. A. Fisher, Phys. Rev. X **4**, 011036 (2014).

[99] X. Wen and Q. Niu, Phys. Rev. B **41**, 9377 (1990).

[100] J. Klinovaja and D. Loss, Phy. Rev. Lett. **112**, 246403 (2014).

[101] R. V. Gorbachev, A. K. Geim, M. I. Katsnelson, K. S. Novoselov, T. Tudorovskiy, I. V. Grigorieva, A. H. MacDonald, S. V. Morozov, K. Watanabe, T. Taniguchi, and L. A. Ponomarenko, Nat. Phys. **8**, 896 (2012).

[102] A. Kou, B. E. Feldman, A. J. Levin, B. I. Halperin, K. Watanabe, T. Taniguchi, and A. Yacoby, Science (New York, N.Y.) **345**, 55 (2014).

[103] J. Eisenstein, Annu. Rev. Condens. Matter Phys. **5**, 159 (2014).

[104] C. Liu, T. Hughes, X.-L. Qi, K. Wang, and S.-C. Zhang, Phys. Rev. Lett. **100**, 236601 (2008).

[105] L. Du, I. Knez, G. Sullivan, and R.-R. Du, (2013), arXiv:1306.1925 .

[106] S. Hart, H. Ren, T. Wagner, P. Leubner, M. Mühlbauer, C. Brüne, H. Buhmann, L. W. Molenkamp, and A. Yacoby, , 20 (2013), arXiv:1312.2559 .

[107] V. S. Pribiag, A. J. A. Beukman, F. Qu, M. C. Cassidy, C. Charpentier, W. Wegscheider, and L. P. Kouwenhoven, (2014), arXiv:1408.1701 .

[108] J. Nilsson, A. R. Akhmerov, and C. W. J. Beenakker, Phys. Rev. Lett. **101**, 120403 (2008).

[109] L. Jiang, D. Pekker, J. Alicea, G. Refael, Y. Oreg, A. Brataas, and F. von Oppen, Phys. Rev. B **87**, 075438 (2013).

[110] F. Pientka, L. Jiang, D. Pekker, J. Alicea, G. Refael, Y. Oreg, and F. von Oppen, New J. Phys. **15**, 115001 (2013).

[111] C. Nayak, A. Stern, M. Freedman, and S. Das Sarma, Rev. Mod. Phys. **80**, 1083 (2008).

[112] S. Doplicher, R. Haag, and J. E. Roberts, Communications in Mathematical Physics **23**, 199 (1971).

[113] S. Doplicher, R. Haag, and J. E. Roberts, Communications in Mathematical Physics **35**, 49 (1974).

[114] J. Maciejko, X.-L. Qi, A. Karch, and S.-C. Zhang, Physical Review Letters **105**, 246809 (2010).

[115] C. Hoyos, K. Jensen, and A. Karch, Physical Review D **82**, 086001 (2010).

[116] B. Swingle, M. Barkeshli, J. McGreevy, and T. Senthil, Physical Review B **83**, 195139 (2011).

[117] J. Maciejko, X.-L. Qi, A. Karch, and S.-C. Zhang, Physical Review B **86**, 235128 (2012).

[118] B. Swingle, Physical Review B **86**, 245111 (2012).

[119] A. Chan, T. Hughes, S. Ryu, and E. Fradkin, Physical Review B **87**, 085132 (2013).

[120] J. Maciejko, V. Chua, and G. Fiete, Physical Review Letters **112**, 016404 (2014).

[121] C.-M. Jian and X.-L. Qi, Physical Review X **4**, 041043 (2014).

[122] D. F. Mross, A. Essin, and J. Alicea, (2014), arXiv:1410.4201 .

[123] R. S. K. Mong, A. M. Essin, and J. E. Moore, Physical Review B **81**, 245209 (2010).

[124] C. Fang, M. J. Gilbert, and B. A. Bernevig, Physical Review B **88**, 085406 (2013).

[125] A. Y. Kitaev, Physics-Uspekhi **44**, 131 (2001).

[126] A. Vaezi, (2013), arXiv:1307.8069 .

[127] N. H. Lindner, E. Berg, G. Refael, and A. Stern, Physical Review X **2**, 041002 (2012).

[128] D. J. Clarke, J. Alicea, and K. Shtengel, Nat. Commun. **4**, 1348 (2013).

[129] M. Cheng, Phys. Rev. B **86**, 195126 (2012).

[130] J. Alicea, Phys. Rev. B **81**, 125318 (2010).

[131] D. Boyanovsky, J. Phys. A: Math. Gen. **22**, 2601 (1989).

[132] E. Domany and E. K. Riedel, Phys. Rev. B **19**, 5817 (1979).

[133] F. C. Alcaraz and R. Koberle, J. Phys. A **13**, L153 (1980).

[134] P. Dorey, R. Tateo, and K. E. Thompson, Nucl. Phys. B **470**, 317 (1996).

[135] A. B. Zamolodchikov and V. A. Fateev, Zh. Eksp. Teor. Fiz. **89**, 380 (1985).

[136] P. B. Wiegmann, J. Phys. C: Solid State Phys. **11**, 1583 (1978).

[137] N. Read and D. Green, Phys. Rev. B **61**, 10267 (2000).

[138] D. T. Son, Phys. Rev. X **5**, 031027 (2015).

[139] C. Wang and T. Senthil, Phys. Rev. X **5**, 041031 (2015).

[140] M. A. Metlitski and A. Vishwanath, Phys.Rev. B **93**, 245151 (2016).

[141] M. A. Metlitski, (2015), arXiv:1510.05663 [hep-th] .

[142] D. F. Mross, J. Alicea, and O. I. Motrunich, Phys. Rev. Lett. **117**, 016802 (2016).

[143] N. Seiberg, T. Senthil, C. Wang, and E. Witten, Annals of Physics **374**, 395 (2016).

[144] A. Karch and D. Tong, Phys. Rev. X **6**, 031043 (2016).

[145] J. Murugan and H. Nastase, Journal of High Energy Physics **2017**, 1 (2017).

[146] S. Kachru, M. Mulligan, G. Torroba, and H. Wang, Phys. Rev. D **94**, 085009 (2016).

[147] S. Kachru, M. Mulligan, G. Torroba, and H. Wang, Phys. Rev. Lett. **118**, 011602 (2017).

[148] D. F. Mross, J. Alicea, and O. I. Motrunich, Phys. Rev. X **7**, 041016 (2017).

[149] J.-Y. Chen, J. H. Son, C. Wang, and S. Raghu, Phys. Rev. Lett. **120**, 016602 (2018).

[150] H. Goldman and E. Fradkin, (2018), arXiv:1801.04936 [cond-mat.str-el] .

[151] P. Bonderson, C. Nayak, and X.-L. Qi, J. Stat. Mech. Theor. Exp. **2013**, P09016 (2013).

[152] C. Wang, A. C. Potter, and T. Senthil, Phys. Rev. B **88**, 115137 (2013).

[153] X. Chen, L. Fidkowski, and A. Vishwanath, Phys. Rev. B **89**, 165132 (2014).

[154] M. A. Metlitski, C. L. Kane, and M. P. A. Fisher, Phys. Rev. B **92**, 125111 (2015).

[155] J. Alicea, O. I. Motrunich, G. Refael, and M. P. A. Fisher, Phys. Rev. Lett. **103**, 256403 (2009).

[156] Y. You, (2017), arXiv:1704.03463 [cond-mat.str-el] .

[157] A. Kitaev, Annals of Physics **303**, 2 (2003).

[158] A. A. Burkov and L. Balents, Phys. Rev. Lett. **107**, 127205 (2011).

[159] E. C. Marino, International Journal of Modern Physics A **09**, 4009 (1994).

[160] T. Meng and L. Balents, Phys. Rev. B **86**, 054504 (2012).

[161] L. Fidkowski, X. Chen, and A. Vishwanath, Phys. Rev. X **3**, 041016 (2013).

[162] X. C. M. A. Metlitski, L. Fidkowski and A. Vishwanath,   (2014), arXiv:1406.3032 [cond-mat.str-el] .

[163] T. Senthil, Annual Review of Condensed Matter Physics **6**, 299 (2015).

[164] C. Wang and T. Senthil, Phys. Rev. B **89**, 195124 (2014).

[165] P. Jordan and E. Wigner, Zeitschrift fï¿œr Physik **47**, 631 (1928).

[166] E. Lieb, T. Schultz, and D. Mattis, Annals of Physics **16**, 407 (1961).

[167] B. S. Shastry and D. Sen, Physical Review B **55**, 2988 (1997).

[168] Y. R. Wang, Physical Review B **46**, 151 (1992).

[169] H. Yao and S. A. Kivelson, Physical Review Letters **99**, 247203 (2007).

[170] A. Kitaev, Annals of Physics **321**, 2 (2006).

[171] B. Béri and N. R. Cooper, Physical Review Letters **109**, 156803 (2012).

[172] A. Altland and R. Egger, Physical Review Letters **110**, 196401 (2013).

[173] B. Béri, Physical Review Letters **110**, 216803 (2013).

[174] A. Zazunov, A. Altland, and R. Egger, New Journal of Physics **16**, 015010 (2014).

[175] A. Altland, B. Béri, R. Egger, and A. Tsvelik, Physical Review Letters **113**, 076401 (2014).

[176] S. Plugge, L. A. Landau, E. Sela, A. Altland, K. Flensberg, and R. Egger, Physical Review B **94**, 174514 (2016).

[177] M. Barkeshli and J. D. Sau, (2015), arXiv:1509.07135 .

[178] L. Landau, S. Plugge, E. Sela, A. Altland, S. Albrecht, and R. Egger, Physical Review Letters **116**, 050501 (2016).

[179] S. Plugge, A. Zazunov, E. Eriksson, A. M. Tsvelik, and R. Egger, Physical Review B **93**, 104524 (2016).

[180] T. Karzig, C. Knapp, R. M. Lutchyn, P. Bonderson, M. B. Hastings, C. Nayak, J. Alicea, K. Flensberg, S. Plugge, Y. Oreg, C. M. Marcus, and M. H. Freedman, Physical Review B **95**, 235305 (2017).

[181] A. Romito and Y. Gefen, Physical Review Letters **119**, 157702 (2017).

[182] T. Giamarchi, *Quantum Physics in One Dimension* (Clarendon Press, 2004).

[183] L. I. Glazman and A. I. Larkin, Phys. Rev. Lett. **79**, 3736 (1997).

[184] M. Banerjee, M. Heiblum, V. Umansky, D. E. Feldman, Y. Oreg, and A. Stern, (2017), arXiv:1710.00492 .

[185] C. Wang, A. Vishwanath, and B. I. Halperin, (2017), arXiv:1711.11557 .

[186] A. Belavin, A. Polyakov, and A. Zamolodchikov, Nuclear Physics B **241**, 333 (1984).

Appendix A

Appendix: Fractional chiral superconductors

A.1 The renormalization group equations of the self-dual Sine-Gordon model

A.1.1 The ε expansion

The Hamiltonians describing either the inter- and intra- wire coupling terms, discussed in chapter 6, can be written as

$$H = \int dx \left[\frac{1}{2\pi m} (\partial_x \eta_1)^2 + \frac{1}{2\pi m} (\partial_x \eta_2)^2 + \frac{\tilde{B}}{a^2} \cos(\eta_1 - \eta_2) + \frac{\tilde{\Delta}}{a^2} \cos(\eta_1 + \eta_2) \right],$$

where η_1 (η_2) is a right (left) moving mode satisfying

$$\left[\eta_j(x), \eta_j(x') \right] = m\pi i (-1)^j \operatorname{sign}(x - x'),$$

and the units were chosen such that the Fermi-velocity is $v = 1$. Specifically, in chapter 6, the coefficients were tuned to the self dual line, such that $\tilde{B} = \tilde{\Delta}$.

To write the Hamiltonian in a more convenient form, we define

$$\varphi = \frac{\eta_1 - \eta_2}{2\sqrt{\pi m}}$$
$$\theta = \frac{\eta_1 + \eta_2}{2\sqrt{\pi m}}.$$

The commutation relations of these fields are given by

$$\left[\varphi(x), \theta(x')\right] = i\Theta(x - x').$$

In terms of these, the Hamiltonian takes the form

$$H = \int dx \left[(\partial_x \theta)^2 + (\partial_x \varphi)^2 + \frac{\tilde{B}}{a^2} \cos\left(2\sqrt{\pi m}\varphi\right) + \frac{\tilde{\Delta}}{a^2} \cos\left(2\sqrt{\pi m}\theta\right)\right].$$

We next wish to isolate the explicit cutoff dependence by writing the cosines in terms of their normal-ordered versions:

$$\cos\left(2\sqrt{\pi m}\varphi\right) =: \cos\left(2\sqrt{\pi m}\varphi\right) : e^{-2m\pi\langle\varphi^2\rangle}$$

$$\cos\left(2\sqrt{\pi m}\theta\right) =: \cos\left(2\sqrt{\pi m}\theta\right) : e^{-2m\pi\langle\theta^2\rangle},$$

where the averages are taken with respect to the quadratic part of the Hamiltonian.

Denoting the small distance cutoff by a and the large distance cutoff by L, we find that

$$e^{-2m\pi\langle\varphi^2\rangle} = e^{-2m\pi\langle\theta^2\rangle} = \left(\frac{a}{L}\right)^m.$$

Therefore, the Hamiltonian can be written in the form

$$\begin{aligned} H &= \int dx \left[(\partial_x \theta)^2 + (\partial_x \varphi)^2 \right. \\ &\quad \left. + \frac{\tilde{B}}{L^2} \left(\frac{a}{L}\right)^{m-2} : \cos\left(2\sqrt{\pi m}\varphi\right) : + \frac{\tilde{\Delta}}{L^2} \left(\frac{a}{L}\right)^{m-2} : \cos\left(2\sqrt{\pi m}\theta\right) : \right] \end{aligned}$$

In performing the renormalization group, we quantify the dependence of the coefficients on $l = \log\frac{L}{a}$.

At tree level, we simply use the explicit cutoff dependence of the coefficients to calculate $\frac{d\bar{B}}{dl}, \frac{d\bar{\Delta}}{dl}$, with $\bar{B} = \tilde{B}\left(\frac{a}{L}\right)^{m-2}, \bar{\Delta} = \tilde{\Delta}\left(\frac{a}{L}\right)^{m-2}$. The resulting tree level RG equations are given by

$$\begin{aligned} \frac{d\bar{B}}{dl} &= (2 - m)\bar{B} \\ \frac{d\bar{\Delta}}{dl} &= (2 - m)\bar{\Delta}, \end{aligned}$$

giving a flow to weak coupling for $m > 2$. This is true in particular at the self-dual point $\tilde{B} = \tilde{\Delta} = \tilde{\lambda}$ we wish to focus on.

Clearly, if a flow to large coupling is to occur for large λ, it must result from higher order terms. The next possible non-vanishing correction to the RG equation of λ is of order λ^3,

as the second order correction vanishes at the self-dual line. Indeed, if the λ^3 term has a positive coefficient, it induces a flow to large couplings for large λ. However, for such a term to overcome the negative contribution of the first order term, λ should be of order 1 (assuming the coefficients are of order 1 and recalling that in our model $m = 3, 5$, etc.). Such a situation steps beyond the range of validity of the perturbative RG analysis.

To overcome the above technical difficulty, we study the situation in which m is slightly above its marginal value: $m = 2 + \varepsilon$, with $\varepsilon \ll 1$. In this case, the negative first order contribution is proportional to ε:

$$\frac{d\bar{B}}{dl} = -\varepsilon B$$
$$\frac{d\bar{\Delta}}{dl} = -\varepsilon \Delta,$$

and therefore, if the third order contribution is positive, the critical point between the two regimes is controlled by the small parameter ε and is therefore expected to be within the range of validity of the perturbative RG analysis. Indeed, we will find such a critical point satisfying $\lambda_c \propto \sqrt{\varepsilon}$.

The critical point found for small ε indicates that a similar critical point exists for $\varepsilon = 1$ as well, above which the coupling constants flows to large coupling (assuming no additional critical points are induced as ε is increased from $0 < \varepsilon \ll 1$ to $\varepsilon = 1$).

We next turn to explicitly derive the form of the third order RG equations. The analysis presented below closely parallels the analysis presented in Ref. [131].

A.1.2   Third order RG equations and the phase diagram

To calculate the higher orders of the renormalization group equations, we generally write the partition function as

$$Z = \int D\varphi e^{-S_0 - S_1},$$

with

$$S_0 = \tfrac{1}{2} \int d\tau dx \left[(\partial_\tau \varphi)^2 + (\partial_x \varphi)^2 \right].$$

$$S_1 = \int \frac{d\tau dx}{L^2} \left[\bar{B} : \cos\left(\sqrt{8\pi (1 + \delta_B)} \varphi \right) : + \bar{\Delta} : \cos\left(\sqrt{8\pi (+\delta_\Delta)} \theta \right) : \right],$$

where θ is related to φ according to the condition:

$$i\partial_\mu \varphi = \varepsilon^{\mu\nu}\partial_\nu \theta. \tag{A.1}$$

In addition, we have defined $\bar{B} = \tilde{B}\left(\frac{a}{L}\right)^{2\delta_B}, \bar{\Delta} = \tilde{\Delta}\left(\frac{a}{L}\right)^{2\delta_\Delta}$.

In order to follow the strategy outlined above, we assume δ_B and δ_Δ are small. As these parameters flow as well, we will write the third order RG equations for $\bar{B}, \bar{\Delta}, \delta_B, \delta_\Delta$. Once these are derived, we will focus on the self-dual line defined according to $\bar{B} = \bar{\Delta} = \bar{\lambda}$ and $\delta_B = \delta_\Delta = \frac{\varepsilon}{2}$.

To derive the RG equations, we expand the partition function in orders of S_1:

$$Z = \int D\varphi D\theta e^{-S_0}\left(1 - S_I + \frac{1}{2}S_I^2 - \frac{1}{6}S_I^3 + \cdots\right). \tag{A.2}$$

Next, we will use the Operator Product Expansions (OPEs) of the resulting high orders to get corrections to the original action.

Taking only the first order into account, we get the contribution

$$\frac{d\bar{B}}{dl} = -2\delta_B \bar{B}$$
$$\frac{d\bar{\Delta}}{dl} = -2\delta_\Delta \bar{\Delta}.$$

To second order, terms of the form $\bar{B}^2$ and $\bar{\Delta}^2$ renormalize the Kinetic term. Notice that we discard the non-singular term of order $\bar{B}\bar{\Delta}$, which results in an irrelevant term.

We first calculate the $\bar{B}^2$ component of $S_2 = -\frac{1}{2}S_I^2$:

$$-\frac{\bar{B}^2}{2}\int d^2x_1 d^2x_2 L^{-4} : \cos\left(\sqrt{8\pi(1+\delta_B)}\varphi(\vec{x}_1)\right) :: \cos\left(\sqrt{8\pi(1+\delta_B)}\varphi(\vec{x}_2)\right) : .\tag{A.3}$$

In order to calculate the OPE [131], we use the definition of normal ordering to write

$$: \cos\left(\sqrt{8\pi(1+\delta_B)}\varphi(\vec{x}_1)\right) :: \cos\left(\sqrt{8\pi(1+\delta_B)}\varphi(\vec{x}_2)\right) :$$
$$= e^{8\pi(1+\delta_B)\langle\varphi^2\rangle}\cos\left(\sqrt{8\pi(1+\delta_B)}\varphi(\vec{x}_1)\right)\cos\left(\sqrt{8\pi(1+\delta_B)}\varphi(\vec{x}_2)\right).$$

This can be rewritten as

$$\frac{1}{2}e^{8\pi(1+\delta_B)\langle\varphi^2\rangle}\left[\cos\left(\sqrt{8\pi(1+\delta_B)}\{\varphi(\vec{x}_1)+\varphi(\vec{x}_2)\}\right) + \cos\left(\sqrt{8\pi(1+\delta_B)}\{\varphi(\vec{x}_1)-\varphi(\vec{x}_2)\}\right)\right].$$

Writing the two cosines in terms of their normal ordered versions, we get

$$\frac{1}{2}\left[: \cos\left(\sqrt{8\pi(1+\delta_B)}\{\varphi(\vec{x}_1)+\varphi(\vec{x}_2)\}\right) : \frac{1}{c(\vec{x}_1-\vec{x}_2)}\right.$$
$$\left.+ : \cos\left(\sqrt{8\pi(1+\delta_B)}\{\varphi(\vec{x}_1)-\varphi(\vec{x}_2)\}\right) : c(\vec{x}_1-\vec{x}_2)\right]$$

with

$$c(\vec{x}_1-\vec{x}_2) = e^{8\pi(1+\delta_B)\langle\varphi(\vec{x}_1)\varphi(\vec{x}_2)\rangle} = \left(\frac{|\vec{x}_1-\vec{x}_2|}{L}\right)^{-4(1+\delta_B)}.$$

The first term results in irrelevant terms, and is therefore ignored. The second term is dominated by the region in which the two points $\vec{x}_1$ and $\vec{x}_2$ are close to each other. This allows us to approximate

$$\cos\left(\sqrt{8\pi(1+\delta_B)}\{\varphi(\vec{x}_1)-\varphi(\vec{x}_2)\}\right) \approx 1 - 4\pi(1+\delta_B)\left(\varphi(\vec{x}_1)-\varphi(\vec{x}_2)\right)^2$$
$$= 1 - 4\pi(1+\delta_B)\left((\vec{x}_1-\vec{x}_2)\cdot\nabla\varphi(\vec{x})\right)^2,$$

where $\vec{x}$ is the center of mass coordinate. Plugging this back into Eq. (A.3), and performing the integral over the relative coordinate $\vec{x}_1-\vec{x}_2$, we get a correction of the form

$$2\pi^2\log\frac{L}{a}\bar{B}^2(1+\delta_B)\left[\frac{1}{2}\int\left((\partial_x\varphi)^2+(\partial_\tau\varphi)^2\right)d^2x\right].$$

Similarly, the $\bar{\Delta}^2$ terms

$$: \cos\left(\sqrt{8\pi(1+\delta_\Delta)}\theta(\vec{x}_1)\right) :: \cos\left(\sqrt{8\pi(1+\delta_\Delta)}\theta(\vec{x}_2)\right) := \tag{A.4}$$

$$\frac{1}{4\left(\frac{|\vec{x}_1-\vec{x}_2|}{L}\right)^{4(1+\delta_\Delta)}}\left(2 - 4\pi(1+\delta_\Delta)|\vec{x}_1-\vec{x}_2|^2\left[(\partial_x\theta(\vec{x}))^2+(\partial_\tau\theta(\vec{x}))^2\right]\right). \tag{A.5}$$

Using Eq. (A.1) and integrating over the relative coordinate, we obtain the correction

$$-2\pi^2\log\frac{L}{a}\bar{\Delta}^2(1+\delta_\Delta)\left[\frac{1}{2}\int\left((\partial_x\varphi)^2+(\partial_\tau\varphi)^2\right)d^2x\right].$$

Taken together, the second order corrections are given by

$$S_2 = 2\pi^2\log\frac{L}{a}\left\{\bar{B}^2(1+\delta_B)-\bar{\Delta}^2(1+\delta_\Delta)\right\}\left[\frac{1}{2}\int\left((\partial_x\varphi)^2+(\partial_\tau\varphi)^2\right)d^2x\right].$$

The second order term clearly renormalizes the kinetic part of the action.

The third order contributions are given by a combination of $S_3^a = \frac{1}{6}S_1^3$ and $S_3^b = S_1S_2$ (the

latter contribution arises when one re-exponentiates the partition function in Eq. A.2).

We first look at the S_3^a-term. The corrections of the type $\bar{B}^3$ and $\bar{B}\bar{\Delta}^2$ renormalize the B-term while terms of the form $\bar{\Delta}^3$ and $\bar{\Delta}\bar{B}^2$ renormalize the Δ-term. Let us first look at the $\bar{B}^3$ order term:

$$\frac{1}{6}\bar{B}^3 \int \Pi_{n=1}^3 \left[\frac{d^2 x_n}{L^2} : \cos\left(\sqrt{8\pi(1+\delta_B)}\varphi(\vec{x}_n) \right) : \right].$$

Using the OPE and dropping the non-singular term, we get the correction [131]

$$\frac{\bar{B}^3}{8L^6} \int d^2 x_1 d^2 x_2 d^2 x_3 : \cos\left(\sqrt{8\pi(1+\delta_B)}\left(\varphi(\vec{x}_1) + \varphi(\vec{x}_2) - \varphi(\vec{x}_3)\right) \right) :$$
$$\times \left(\frac{L^2 |\vec{x}_1 - \vec{x}_2|^2}{|\vec{x}_1 - \vec{x}_3|^2 |\vec{x}_2 - \vec{x}_3|^2} \right)^m.$$

Clearly, the most dominant contributions arise when two coordinates approach each other: either $\vec{x}_1 \to \vec{x}_3$, or $\vec{x}_2 \to \vec{x}_3$. However, these divergences are disconnected and are therefore discarded. Thus, the only singular contribution arises when the three different coordinates approach each other. Taking this into account, we approximate

$$: \cos\left(\sqrt{8\pi(1+\delta_B)}\left(\varphi(\vec{x}_1) + \varphi(\vec{x}_2) - \varphi(\vec{x_3})\right) \right) :\approx: \cos\left(\sqrt{8\pi(1+\delta_B)}\varphi(\vec{x}) \right) :,$$

where $\vec{x}$ is the center of mass coordinate, and therefore

$$\frac{1}{8L^6} \int d^2 x_1 d^2 x_2 d^2 x_3 : \cos\left(\sqrt{8\pi(1+\delta_B)}\varphi(\vec{x}) \right) : \left(\frac{L^2 |\vec{x}_1 - \vec{x}_2|^2}{|\vec{x}_1 - \vec{x}_3|^2 |\vec{x}_2 - \vec{x}_3|^2} \right)^2.$$

Integrating over the relative coordinates, and subtracting disconnected terms, we find the correction [131]

$$\frac{2\pi^2 \bar{B}^3}{L^2} \left[\log\left(\frac{L}{a} \right) \right]^2 \int d^2 x : \cos\left(\sqrt{8\pi(1+\delta_B)}\varphi(\vec{x}) \right) :.$$

Similar considerations show that the $\bar{B}\bar{\Delta}^2$ term provides a contribution of the form

$$\frac{\pi^2 \bar{B}\bar{\Delta}^2}{L^2} \left[\log\left(\frac{L}{a} \right) - 2\left[\log\left(\frac{L}{a} \right) \right]^2 \right] \int d^2 x : \cos\left(\sqrt{8\pi(1+\delta_B)}\varphi(\vec{x}) \right) :.$$

The remaining contribution is of the form S_3^b. The contribution to the B-term is given by

$$2\pi^2 \log \frac{L}{a} \bar{B} \left\{ \bar{B}^2 \left(1 + \delta_B\right) - \bar{\Delta}^2 \left(1 + \delta_\Delta\right) \right\}$$

$$\times \left[\frac{1}{2} \int d^2 x_1 d^2 x_2 \mu^2 \left((\partial_x \varphi(\vec{x}_1))^2 + (\partial_\tau \varphi(\vec{x}_1))^2 \right) : \cos \left(\sqrt{8\pi(1+\delta_B)} \varphi(\vec{x}_2) \right) : \right].$$

Keeping only the third orders in the various scaling parameters, and using the corresponding OPE, we get

$$-2\pi^2 \left(\log \frac{L}{a} \right)^2 \bar{B} \left\{ \bar{B}^2 - \bar{\Delta}^2 \right\} \int d^2 x : \cos \left(\sqrt{8\pi(1+\delta_B)} \left(\varphi(\vec{x}) \right) \right) : .$$

Analogous corrections can be derived for the Δ-field.

Summing the above corrections, we find that the renormalized action is given by

$$S = S_I + 2\pi^2 \log \frac{L}{a} \left\{ \bar{B}^2 \left(1 + \delta_B\right) - \bar{\Delta}^2 \left(1 + \delta_\Delta\right) \right\} \left[\frac{1}{2} \int \left((\partial_x \varphi)^2 + (\partial_\tau \varphi)^2 \right) d^2 x \right]$$

$$+ \frac{\pi^2 \bar{B} \bar{\Delta}^2}{L^2} \log \left(\frac{L}{a} \right) \int d^2 x : \cos \left(\sqrt{8\pi(1+\delta_B)} \varphi(\vec{x}) \right) :$$

$$+ \frac{\pi^2 \bar{\Delta} \bar{B}^2}{L^2} \log \left(\frac{L}{a} \right) \int d^2 x : \cos \left(\sqrt{8\pi(1+\delta_\Delta)} \theta(\vec{x}) \right) : .$$

Based on the above, the RG equations for the coefficients of the cosine terms are given by

$$\frac{d\bar{B}}{dl} = -2\delta_B \bar{B} + \pi^2 \bar{B} \bar{\Delta}^2$$

$$\frac{d\bar{\Delta}}{dl} = -2\delta_\Delta \bar{\Delta} + \pi^2 \bar{\Delta} \bar{B}^2.$$

The correction to the Kinetic term can be eliminated by rescaling the φ and θ-fields. This induces a change in the variables δ_B, δ_Δ, leading to the RG equations:

$$\frac{d\delta_B}{dl} = -2\pi^2 (1 + \delta_B) \left[\bar{B}^2 \left(1 + \delta_B\right) - \bar{\Delta}^2 \left(1 + \delta_\Delta\right) \right]$$

$$\frac{d\delta_\Delta}{dl} = -2\pi^2 (1 + \delta_\Delta) \left[\bar{\Delta}^2 \left(1 + \delta_\Delta\right) - \bar{B}^2 \left(1 + \delta_B\right) \right].$$

Rescaling $\bar{B}' = \pi^2 \bar{B}$, $\bar{\Delta}' = \pi^2 \bar{\Delta}$, we finally write the RG equations

$$\frac{d\bar{B}'}{dl} = -2\delta_B \bar{B}' + \bar{B}' \bar{\Delta}'^2$$

$$\frac{d\bar{\Delta}'}{dl} = -2\delta_\Delta \bar{\Delta}' + \bar{\Delta}' \bar{B}'^2$$
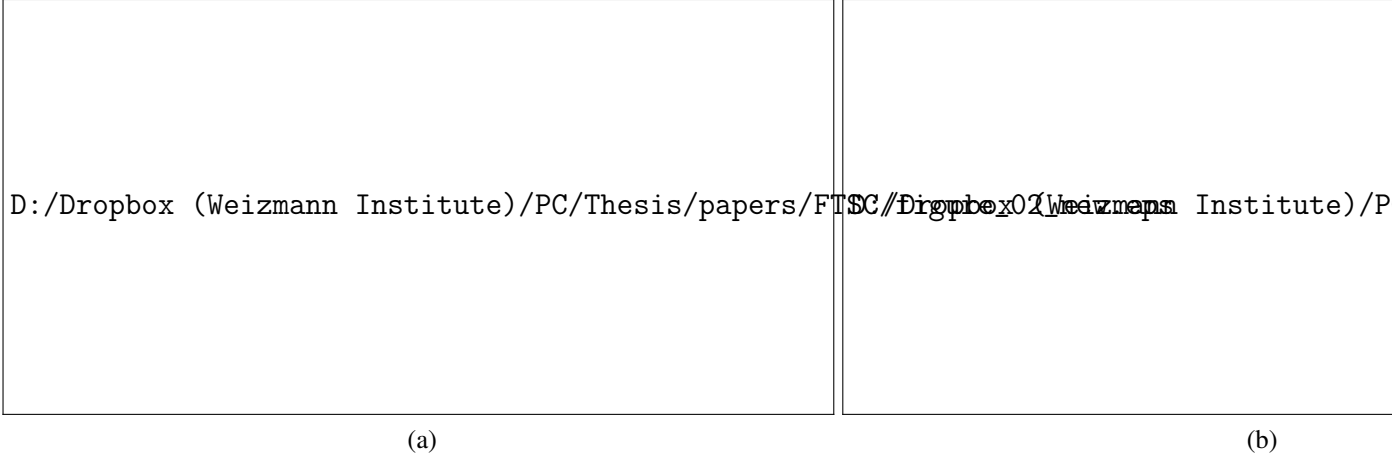
(a)   (b)

Figure A.1: The phase diagrams for (a) $\varepsilon = 0.2$ and (b) $\varepsilon = -0.2$. The red region corresponds to a Δ-dominated phase, the blue region corresponds to a B-terms phase, and the green regions correspond to gapless states.

$$\frac{d\delta_B}{dl} = -2(1+\delta_B)\left[\bar{B}'^2(1+\delta_B) - \bar{\Delta}'^2(1+\delta_\Delta)\right]$$
$$\frac{d\delta_\Delta}{dl} = -2(1+\delta_\Delta)\left[\bar{\Delta}'^2(1+\delta_\Delta) - \bar{B}'^2(1+\delta_B)\right]. \tag{A.6}$$

Fig. A.1 presents the phase diagram resulting from the solution of the RG equations shown in Eq. A.6. Specifically, the different colors represent different phases based on the flow equations: The red regions represent a Δ-dominated phase, the blue region represents a B-dominated phase, and the green regions represent a gapless state. Figure A.1a (A.1b) were generated by studying the properties of the RG equations for various initial values of $\bar{B}', \bar{\Delta}'$ and $\delta_B = \delta_\Delta = \frac{\varepsilon}{2}$, with $\varepsilon = 0.2$ ($\varepsilon = -0.2$) .

A.1.3   Studying the self-dual line

Focusing on the self-dual line $\bar{B}' = \bar{\Delta}' = \bar{\lambda}$, $\delta_B = \delta_\Delta = \varepsilon/2$, we get a single RG equation

$$\frac{d\bar{\lambda}}{dl} = -\varepsilon\bar{\lambda} + \bar{\lambda}^3,$$

accompanied by $\frac{d\varepsilon}{dl} = 0$.

We immediately find a critical point at $\bar{\lambda} = \sqrt{\varepsilon}$, above which a flow to large $\bar{\lambda}$ ensues.

This shows that if the coupling constants in the self-dual theory studied in chapter 6 are large enough, the cosine terms indeed flow to large coupling. In particular, a multicritical point separates the two regimes.

A.2 The scaling dimension of the local electron fields

In this section, we demonstrate that the scaling dimension of the electron fields $\tilde{\alpha}_{nR}(x), \tilde{\beta}_{nL}(x)$ remains $m/2$ in the presence of the intra-wire interacting term, which is taken to the critical point $\tilde{\Delta} = \tilde{B} = \lambda$:

$$\tilde{H}_\Delta + \tilde{H}_B = \lambda i \int dx \tilde{\beta}_{nR} \tilde{\alpha}_{nL}. \tag{A.7}$$

We first note that since $\tilde{\alpha}_{nR}(x)$ and $\tilde{\beta}_{nL}(x)$ commute with the above interacting Hamiltonian, they remain right and left moving fields, respectively. To demonstrate this, we write the equations of motion of $\tilde{\alpha}_{nR}(x)$:

$$\frac{\partial}{\partial \tau} \tilde{\alpha}_{nR}(x, \tau) = [H, \tilde{\alpha}_{nR}(x, \tau)].$$

The Hamiltonian is composed of the kinetic chiral Luttinger liquid Hamiltonian and the interacting Hamiltonian written in Eq. A.7. Since $\tilde{\alpha}_{nR}(x)$ commutes with the latter, we only need to calculate the commutation with the kinetic part,

$$H_K = \frac{v}{4\pi m} \lim_{\varepsilon \to 0} \int \{\partial \eta_{nR}(x)\} \{\partial \eta_{nR}(x+\varepsilon)\},$$

where we have used point splitting regularization. Since, by definition, $\tilde{\alpha}_{nR}(x) = e^{i\eta_{nR}} + e^{-i\eta_{nR}}$, we calculate the commutation relation with each vertex operator separately:

$$\left[H, e^{\pm i\eta_{nR}(x)}\right]$$
$$= \frac{v}{4\pi m} \lim_{\varepsilon \to 0} \int dx' \left[\{\partial \eta_{nR}(x')\} \{\partial \eta_{nR}(x'+\varepsilon)\} e^{\pm i\eta_{nR}(x)} - e^{\pm i\eta_{nR}(x)} \{\partial \eta_{nR}(x')\} \{\partial \eta_{nR}(x'+\varepsilon)\}\right]$$
$$= e^{\pm i\eta_{nR}(x)} \frac{v}{4\pi m} \lim_{\varepsilon \to 0} \int dx' \left[e^{\mp i\eta_{n,R}} \{\partial \eta_{nR}(x')\} \{\partial \eta_{nR}(x'+\varepsilon)\} e^{\pm i\eta_{nR}(x)} - \{\partial \eta_{nR}(x')\} \{\partial \eta_{nR}(x'+\varepsilon)\}\right].$$

Using the commutation relations

$$\left[\eta_{nR}(x), \partial \eta_{nR}(x')\right] = -2\pi i m \delta(x - x')$$

and the Baker-Campbell-Hausdorff formula, we write

$$e^{\mp i\eta_{n,R}} \{\partial \eta_{nR}(x')\} e^{\pm i\eta_{nR}(x)} = \partial \eta_{nR}(x') \mp i \left[\eta_{nR}(x), \partial \eta_{nR}(x')\right] = \partial \eta_{nR}(x') \mp 2\pi m \delta(x - x'),$$

and therefore

$$\left[H, e^{\pm i\eta_{nR}(x)}\right] = \mp v e^{\pm i\eta_{nR}(x)} \partial \eta_{nR}(x) = -iv\partial e^{\pm i\eta_{nR}(x)}.$$

This gives us the equation of motion

$$\frac{\partial}{\partial \tau}\tilde{\alpha}_{nR}(x,\tau) = -iv\frac{\partial}{\partial x}\tilde{\alpha}_{nR}(x,\tau).$$

Defining $z = x + iv\tau$, we may write the above as $\frac{\partial}{\partial\bar{z}}\tilde{\alpha}_{nR}(x,\tau) = 0$.

This shows that $\tilde{\alpha}_{nR}(z)$ remains a right mover in the presence of the interacting Hamiltonian A.7. Similarly, $\tilde{\beta}_{nL}$ satisfies $\frac{\partial}{\partial z}\tilde{\beta}_{nL}(x,\tau) = 0$, and is therefore a left mover. We note that the above analysis cannot be repeated for the fields $\tilde{\alpha}_{nL}$ and $\tilde{\beta}_{nR}$ which do not commute with the interacting Hamiltonian, and are therefore not chiral.

Using the above result, we now turn to calculate the propagator of the remaining chiral fields and show that all corrections to the $\lambda = 0$ limit vanish identically. For example, calculating the propagator $g(z-z') = \langle\tilde{\alpha}_{nR}(z)\tilde{\alpha}_{nR}(z')\rangle$, and treating the interacting Hamiltonian shown in Eq. A.7 perturbatively, we can write the correction to any order p as

$$\delta g_p(z-z') \propto (\lambda i)^p \left\langle \tilde{\alpha}_{nR}(z)\tilde{\alpha}_{nR}(z')\Pi_{i=1}^p \int d^2 z_i \tilde{\beta}_{nR}(z_i,\bar{z}_i)\tilde{\alpha}_{nL}(z_i,\bar{z}_i) \right\rangle_0. \qquad (A.8)$$

Since the expectation value is done with respect to the Kinetic Hamiltonian, we can treat $\tilde{\alpha}_{nL}$ as a function $\bar{z}$ only and $\tilde{\beta}_{nR}$ as a function of z. Furthermore, we can use the symmetries of the Kinetic Hamiltonian: First, we know that under rotations, $z \to ze^{i\theta}, \bar{z} \to \bar{z}e^{-i\theta}$, the fields transform as $\tilde{\alpha}_{nR}(z) \to \tilde{\alpha}_{nR}(z)e^{-i\theta m/2}, \tilde{\alpha}_{nL}(\bar{z}) \to \tilde{\alpha}_{nL}(\bar{z})e^{i\theta m/2}$ (and the same relations for the β-fields). This leads to the condition

$$\delta g_p\left[(z-z')e^{i\theta}\right] = e^{-i\theta m}\delta g_p\left[z-z'\right],$$

which is satisfied if $\delta g_p \propto (z-z')^{-m}$.

Under scale transformations, given by $z \to zd, \bar{z} \to \bar{z}d$, the fields transform as $\tilde{\alpha}_{nR}(z) \to \tilde{\alpha}_{nR}(z)d^{-m/2}, \tilde{\alpha}_{nL}(\bar{z}) \to \tilde{\alpha}_{nL}(\bar{z})d^{-m/2}$ (and similarly for the $\tilde{\beta}$-fields). In this case we get the condition $\delta g_p[(z-z')d] = d^{-m+p(2-m)}\delta g_p[z-z']$, which is satisfied if $\delta g_p \propto (z-z')^{-m+p(2-m)}$. Clearly, we have reached a contradiction, which can only be solved if $\delta g_p[z-z'] = 0$ for any $p > 0$. This shows that all corrections to the propagator calculated in the absence of the interacting term vanish, and the scaling dimension of $\tilde{\alpha}_{nR}$ and $\tilde{\beta}_{nL}$ therefore remains $m/2$.

We note that as the fields $\tilde{\beta}_{nR}$ and $\tilde{\alpha}_{nL}$ are no longer chiral, the full propagator is not a holomorphic (or antiholomorphic) function, and the entire argument fails, as expected.

Appendix B

Appendix: Composite Weyl semimetal as a parent state for three dimensional topologically ordered phases

B.1   Inter-layer coherence through a tractable model

B.1.1   The coupled-wire model

When constructing the QED$_4$ state, we relied on the formation of spontaneous inter-layer coherence, which in turn allowed us to write inter-layer tunneling of dual fermions. In this section, we go beyond the mean-field approach presented in chapter 7 and demonstrate the formation of inter-layer coherence through a tractable coupled-wire model.

The interfaces in our superlattice structure form two-dimensional planes, and will henceforth be referred to as layers. In what follows, each layer is modeled by an array of coupled wires [142]. Each wire hosts a chiral electronic mode, allowed to tunnel between adjacent wires. The interfaces form two-dimensional planes, and will henceforth be referred to as layers. The wires in each layer are enumerated by the index y, the interfaces are enumerated by the index z (see Fig. B.1a), and the electronic annihilation operators are given by $\chi_{y,z}$. The Hamiltonian of the decoupled chiral wires is given by

$$H_{\text{wires}} = -iv\sum_{yz}(-1)^{y+z}\int dx\, \chi_{y,z}^{\dagger}\partial_x \chi_{y,z}, \qquad\qquad (\text{B.1})$$
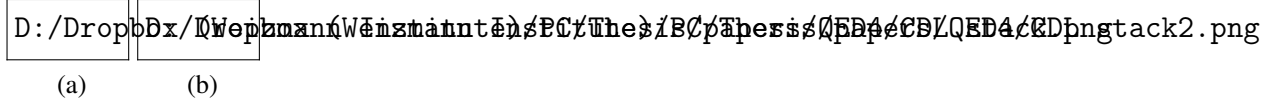
(a)   (b)

Figure B.1: (a) A schematic depiction of our model, where the dual Dirac fermions in each layer are represented by an array of coupled wires. Here, the symbol $\bigcirc$ denotes a left mover, while $\otimes$ denotes a right mover. (b) Coherence between different layers is induced when $\left\langle \tilde{\gamma}_{yz+}^\dagger \tilde{\gamma}_{y,z+1,+} \right\rangle$ (blue) and $\left\langle \tilde{\gamma}_{yz-}^\dagger \tilde{\gamma}_{y,z+1,-} \right\rangle$ (red) acquire expectation values for odd and even z, respectively. Then, four-fermion terms of the form shown by the arrows yield tunneling of $\tilde{\chi}$ across layers.

and the tunneling terms within each layer take the form

$$H_{\text{hop}} = t \sum_{yz} (-1)^{y+z} \int dx \left(\chi_{y,z}^\dagger \chi_{y+1,z} + \text{H.c.} \right). \tag{B.2}$$

Together, H_{wires} and H_{hop} generate a 2D Dirac dispersion in each layer, and can thus be used to model our superlattice system. As demonstrated in Ref. [142], we can explicitly define non-local dual fermion fields, $\tilde{\chi}_{y,z}$, minimally coupled to a dynamical $U(1)$ gauge field, such that each layer is described by a QED$_3$ of dual fermions. For simplicity, we start by ignoring the gauge field. It will be reintroduced in the end of the construction by imposing gauge invariance.

In terms of the dual degrees of freedom, the Hamiltonian of the decoupled layers is given by

$$H_{\text{wires}} = i\tilde{v} \sum_{yz} (-1)^{y+z} \int dx \, \tilde{\chi}_{y,z}^\dagger \partial_x \tilde{\chi}_{y,z}, \tag{B.3}$$

$$H_{\text{hop}} = t \sum_{yz} (-1)^{y+z} \int dx \left(\tilde{\chi}_{y,z}^\dagger \tilde{\chi}_{y+1,z} + \text{H.c.} \right). \tag{B.4}$$

The non-local nature of the dual fermions does not allow us to write inter-layer tunneling.

To simplify the derivation, it is expedient to artificially enlarge the unit cell [61, 142] such that each mode in the original layers is replaced by three chiral fermion modes $\tilde{\gamma}_{y,z,-}, \tilde{\chi}_{y,z}, \tilde{\gamma}_{y,z,+}$ (see Fig. B.1a). The corresponding Hamiltonian is

$$H_{\text{hop}} = \sum_{yz} (-1)^{y+z} \int dx \left[-\tilde{\gamma}_{y,z,-}^\dagger \tilde{\chi}_{y,z} + \tilde{\chi}_{y,z}^\dagger \tilde{\gamma}_{y,z,+} - \tilde{\gamma}_{y,z,+}^\dagger \tilde{\gamma}_{y+1,z,-} + \text{H.c.} \right].$$

As we now demonstrate, interaction terms for the $\tilde{\gamma}$-fields can induce coherence between adjacent layers, which in turn generates inter-layer tunneling of the $\tilde{\chi}$-fields.

B.1.2   Inter-layer coherence

To make adjacent layers coherent, we introduce a local interaction of the form

$$H_{\text{coh}} = \sum_{\text{odd } z} H^{\text{o}}_{\text{coh},z} + \sum_{\text{even } z} H^{\text{e}}_{\text{coh},z},$$

with

$$H^{\text{o}}_{\text{coh},z} = u \sum_y \int dx \left[\tilde{\gamma}^{\dagger}_{yz+} \tilde{\gamma}_{y,z+1,+} \tilde{\gamma}^{\dagger}_{y+1,z+1,+} \tilde{\gamma}_{y+1,z,+} + \text{H.c.} \right],$$

$$H^{\text{e}}_{\text{coh},z} = u \sum_y \int dx \left[\tilde{\gamma}^{\dagger}_{yz-} \tilde{\gamma}_{y,z+1,-} \tilde{\gamma}^{\dagger}_{y+1,z+1,-} \tilde{\gamma}_{y+1,z,-} + \text{H.c.} \right].$$

We start by treating the odd z case in details. To do so, we bosonize the wire degrees of freedom by writing $\tilde{\gamma}_{yz\rho} \propto e^{-i\phi_{yz\rho}}$, in terms of which

$$H^{\text{o}}_{\text{coh,z}} = 2u \sum_y \int dx \cos\left(\phi_{y,z,+} - \phi_{y,z+1,+} + \phi_{y+1,z+1,+} - \phi_{y+1,z,+} \right)$$

$$= 2u \sum_y \int dx \cos\left[2\Delta_y \tilde{\theta}_{y,z,z+1} \right], \tag{B.5}$$

where $\tilde{\theta}_{y,z,z+1} = \frac{\phi_{y,z,+} - \phi_{y,z+1,+}}{2}$, and Δ_y is the discrete derivative defined according to $\Delta_y \tilde{\theta}_{y,z,z+1} = \tilde{\theta}_{y+1,z,z+1} - \tilde{\theta}_{y,z,z+1}$.

If the terms in Eq. (B.5) flow to strong coupling, their arguments can be assumed to weakly fluctuate around the minimum of the cosine. Expanding in these small fluctuations, we obtain a quadratic term of the form $u \sum_y (\Delta_y \tilde{\theta}_{y,z,z+1})^2$. Taking this term together with the quadratic Luttinger-liquid Hamiltonian, the operator $e^{2i\tilde{\theta}_{y,z,z+1}}$ acquires an expectation value. We thus obtain a spontaneous breaking of the $U(1)$ symmetry $\tilde{\theta} \to \tilde{\theta} + \text{const}$. Therefore, at low energies, one can write $\tilde{\theta}_{y,z,z+1} = \tilde{\theta}_0 + \frac{1}{2} a^3_{yz}(x)$, where a^3_{yz} is a slowly varying Goldstone mode.

For even z, we repeat the same analysis in terms of the $\tilde{\gamma}_-$-fields. For these layers, we define $\tilde{\theta}_{y,z,z+1} = \frac{\phi_{y,z,-} - \phi_{y,z+1,-}}{2}$, and find

$$H^{\text{e}}_{\text{coh},z} = 2u \sum_y \int dx \cos\left[2\Delta_y \tilde{\theta}_{y,z,z+1} \right]. \tag{B.6}$$

Following the same arguments as for the odd z case, we again achieve spontaneous symmetry breaking.

Once all the layers are coherent, we generate inter-layer hopping terms for $\tilde{\chi}$. To do so, we write local interaction terms involving correlated tunneling in adjacent layers, as shown in

Fig. B.1b:

$$H_z = \sum_{y,z} \int dx \begin{cases} \tilde{\chi}^\dagger_{y,z} \tilde{\chi}_{y,z+1} \tilde{\gamma}^\dagger_{y,z+1,+} \tilde{\gamma}_{y,z,+} + \text{H.c.} & \text{odd } z \\ \tilde{\chi}^\dagger_{y,z} \tilde{\chi}_{y,z+1} \tilde{\gamma}^\dagger_{y,z+1,-} \tilde{\gamma}_{y,z,-} + \text{H.c.} & \text{even } z \end{cases}. \tag{B.7}$$

Notice that these terms do not involve direct tunneling of dual fermions between different layers. To effectively generate such tunneling, we use the inter-layer coherence and write

$$\tilde{\gamma}^\dagger_{y,z+1,+} \tilde{\gamma}_{y,z,+} \sim e^{-2i\tilde{\theta}_{y,z,z+1}} \sim e^{-ia^3_{yz}(x)} \text{ for odd } z$$
$$\tilde{\gamma}^\dagger_{y,z+1,-} \tilde{\gamma}_{y,z,-} \sim e^{-2i\tilde{\theta}_{y,z,z+1}} \sim e^{-ia^3_{yz}(x)} \text{ for even } z.$$

Therefore, H_z takes the form

$$H_z = \sum_{y,z} \int dx \left[\tilde{\chi}^\dagger_{yz} \tilde{\chi}_{yz+1} e^{-ia^3_{yz}(x)} + \text{H.c.} \right].$$

Thus, despite the non-local nature of the dual fermions, they can tunnel between the layers through the phenomenon of inter-layer coherence.

As noted in chapter 7, the gauge degrees of freedom can be reintroduced by enforcing gauge invariance. However, the inter-layer tunneling terms reduce the gauge symmetry from an independent $U(1)$ symmetry for each interface to a single $U(1)$ symmetry for the entire three dimensional system. This promotes the gauge degrees of freedom to form a truly $3+1$ dimensional $U(1)$ gauge theory, with the Goldstone mode a^3 acting as the fourth component of a.

In the next section, we demonstrate that the inter-layer tunneling terms generate a $3+1$ dimensional Dirac theory, leading to the QED$_4$ parent state.

B.2   Derivation of the QED$_4$ fixed point

In this section, we demonstrate the emergence of the QED$_4$ fixed point. In the absence of coupling between the layers, the action takes the form

$$S_{\text{dual}} = \sum_z \int d^2x dt \left[i\bar{\tilde{\Psi}}_z \gamma_{\mu z} \left(\partial^\mu - ia^\mu_z \right) \tilde{\Psi}_z + \mathscr{L}_{\text{Maxwell}} \left[a^\mu_z \right] \right] \tag{B.8}$$

in the dual formulation, where $\mathscr{L}_{\text{Maxwell}}$ denotes the $2+1$-dimensional Maxwell term in each layer.

Upon inducing inter-layer coherence, we effectively generate tunneling terms of the form

$$S_{\text{int}} = \chi_0 \sum_z \sum_{\alpha=\uparrow,\downarrow} \int d^2x dt \left(e^{-ia_z^3} \tilde{\psi}_{z,\alpha}^\dagger \tilde{\psi}_{z+1,\alpha} + \text{H.c.} \right). \tag{B.9}$$

Next, we note that in the absence of gauge fluctuations the inter-layer action [Eq. (B.9)] is associated with the spectrum $E = 2\chi_0 \cos k_z$, which gives rise to low-energy fermion excitations around $k_z = \pm\frac{\pi}{2}$. Focusing on these low energy degrees of freedom, we write

$$\tilde{\Psi}_z = \tilde{\Psi}_{z,+} e^{i\frac{\pi z}{2}} + \tilde{\Psi}_{z,-} e^{-i\frac{\pi z}{2}}. \tag{B.10}$$

Notice that in this mean field approximation the unit cell consists of two layers, meaning the Brillouin zone is defined for k_z between $-\pi/2$ and $\pi/2$, and the above low energy degrees of freedom coincide at the edge of the Brillouin zone.

Inserting this into Eqs. (B.8) and (B.9) and dropping the spatially oscillating terms, which do not affect the low energy description, we obtain

$$\begin{aligned} S = \sum_z \int d^2x dt \Bigg\{ & \sum_{\rho=\pm} \left[\left(i\chi_0\rho e^{-ia_z^3} \tilde{\Psi}_{z,\rho}^\dagger \tilde{\Psi}_{z+1,\rho} + \text{H.c.} \right) \right. \\ & + i\tilde{\Psi}_{z\rho}^\dagger \left(\partial^0 - ia_z^0 \right) \tilde{\Psi}_{z\rho} \Big] \\ & + i\tilde{\Psi}_{z+}^\dagger \sigma_3 \left(\partial^1 - ia_z^1 \right) \tilde{\Psi}_{z-} + \text{H.c.} \\ & + i\tilde{\Psi}_{z+}^\dagger \sigma_2 \left(\partial^2 - ia_z^2 \right) \tilde{\Psi}_{z-} + \text{H.c.} \Bigg\}. \end{aligned} \tag{B.11}$$

Defining the four-component spinor $\Psi' = \begin{pmatrix} \Psi_{\uparrow+} & \Psi_{\uparrow-} & \Psi_{\downarrow+} & \Psi_{\downarrow-} \end{pmatrix}$, we take the natural continuum limit and obtain

$$S = i \int d^3x dt \, \bar{\Psi}' \Gamma_\mu \left(\partial^\mu - ia^\mu \right) \Psi', \tag{B.12}$$

where $\Gamma_0 = \sigma_1\tau_1, \Gamma_1 = -i\sigma_2, \Gamma_2 = i\sigma_3, \Gamma_3 = -i\sigma_1\tau_2$, and the τ_i-matrices are the Pauli matrices acting on the $\rho = \pm$ space. It can easily be verified that the Γ-matrices satisfy the Clifford algebra, indicating that the action in Eq. (B.12) indeed describes Dirac fermions coupled to a $U(1)$ gauge field in $3+1$-dimensions. Notice that in moving from Eq. (B.11) to Eq. (B.12), we have rescaled spacetime to make the Dirac action appear isotropic.

The kinetic action of the dynamical gauge field a_μ generically consists of all gauge invariant terms. The most relevant among these is the Maxwell term $\mathcal{L}_{\text{Maxwell}} = -\frac{1}{4e^2} F_{\mu\nu} F^{\mu\nu}$ with $\mu, \nu = 0, \cdots, 3$. Notice that due to the anisotropic nature of our realization, we generally expect an anisotropic version of the Maxwell action.

B.3   The composite Weyl semimetal phase

With the addition of the mass term

$$S_m = m \sum_z \int d^2x dt \left(\tilde{\psi}_{z,\uparrow}^\dagger \tilde{\psi}_{z,\downarrow} + H.c. \right), \tag{B.13}$$

it can easily be checked that the spectrum generated by Eqs. (B.9) and (B.13) hosts low-energy excitations around four points of the form $\vec{k} = (0,0,k_z)$. Defining $k_0 = \cos^{-1}\left(\frac{|m|}{2\chi_0} \right)$, two of these points are located at $k_z = \pm k_0$ and associated with the wavefunction $\frac{1}{\sqrt{2}} \begin{pmatrix} 1 & -1 \end{pmatrix}^T$, while the other two, located at $k_z = \pm(\pi - k_0)$, are associated with $\frac{1}{\sqrt{2}} \begin{pmatrix} 1 & 1 \end{pmatrix}^T$.

We therefore write at low energies

$$\tilde{\Psi}_z = \frac{1}{\sqrt{2}} \left[\left(\tilde{\psi}_{z,++} e^{ik_0 z} + \tilde{\psi}_{z,-+} e^{-ik_0 z} \right) \begin{pmatrix} 1 \\ -1 \end{pmatrix} \right. \tag{B.14}$$
$$\left. + (-1)^z \left(\tilde{\psi}_{z,--} e^{-ik_0 z} + \tilde{\psi}_{z,+-} e^{ik_0 z} \right) \begin{pmatrix} 1 \\ 1 \end{pmatrix} \right].$$

Inserting this into the action in Eqs. (B.8),(B.9), and (B.13), we obtain

$$S = \sum_z \sum_{\beta = \pm} \int d^2x dt \left\{ \sum_\gamma \left[\left(i\tilde{\chi}_0 \beta \gamma e^{-ia_z^3} \tilde{\psi}_{z,\beta\gamma}^\dagger \tilde{\psi}_{z+1,\beta\gamma} + H.c. \right) \right. \right.$$
$$+ i\tilde{\psi}_{z\beta\gamma}^\dagger \left(\partial^0 - ia_z^0 \right) \tilde{\psi}_{z\beta\gamma} \Big]$$
$$+ i\tilde{\psi}_{z\beta-}^\dagger \left(\partial^1 - ia_z^1 \right) \tilde{\psi}_{z,\beta+} + H.c.$$
$$\left. - \tilde{\psi}_{z\beta-}^\dagger \left(\partial^2 - ia_z^2 \right) \tilde{\psi}_{z,\beta+} + H.c. \right\}, \tag{B.15}$$

with $\tilde{\chi}_0 = \sqrt{\chi_0^2 - \frac{m^2}{4}}$.

Taking the continuum limit by assuming $\tilde{\psi}_{z,\beta\gamma}$ to vary slowly in the z direction, we get the low-energy action

$$S = i \sum_{\beta = \pm 1} \int d^3x dt \tilde{\Psi}_\beta^\dagger \sigma_\mu^\beta \left(\partial^\mu - ia_j^\mu \right) \tilde{\Psi}_\beta,$$

where σ_μ are the Pauli matrices acting on the γ-indices, $\sigma_\mu^\beta = \sigma_\mu$ for $\mu = 0,1,2$ and $\sigma_3^\beta = \beta\sigma_3$. The resulting theory indeed describes two separate Weyl theories coupled to a gauge field. As pointed out in chapter 7, a generally acquires a mass through the Higgs mechanism, thus

leaving only Weyl fermions at low energies. Notice that while these two Weyl theories are technically equivalent to a single Dirac theory, they are associated with degrees of freedom located at different points in the Brillouin zone, prompting us to regard them as separate theories.

B.4 The monopole propagator

In Sec. B.2, we obtained an effective QED_4 theory, with the action

$$S_{\text{QED}_4} = \int d^4x \left(-\frac{1}{4e^2} F_{\mu\nu} F^{\mu\nu} + i\bar{\tilde{\Psi}}\gamma^\mu \left(\partial_\mu - ia_\mu \right) \tilde{\Psi} \right). \tag{B.16}$$

In what follows, we calculate the monopole propagator within this theory,

$$C(\vec{x},t) = \left\langle M(\vec{x}_t,t)M^\dagger(\vec{x}_0,0) \right\rangle, \tag{B.17}$$

where $M^\dagger$ is an operator that creates a 4π monopole. To calculate this propagator, we first employ the asymptotic freedom of QED_4 at low energies to neglect the coupling to the dual Dirac theory. This allows us calculate Eq. (B.17) within the free Maxwell theory (i.e., the first term of Eq. (B.16)). Second, we use the electromagnetic duality of the Maxwell theory to the calculate the propagator of the electronic charge instead, and argue that the result should be identical in the magnetic case.

Within the Maxwell theory, the charge propagator can be written as a path integral

$$C(\vec{x}_{\text{f}} - \vec{x}_{\text{i}}, t_{\text{f}} - t_{\text{i}}) = \int_{\vec{x}_{\text{i}}(t_{\text{i}})}^{\vec{x}_{\text{f}}(t_{\text{f}})} \mathscr{D}\vec{x} \int \mathscr{D}a_\mu e^{i\mathscr{S}(x,a)},$$

where $S = \int \left[-\frac{1}{4e^2} F_{\mu\nu} F^{\mu\nu} + a_\mu J^\mu \right]$, with $J^\mu = qv^\mu \delta(\vec{x} - \vec{x}(t))$ and $v^\mu = \frac{dx^\mu}{dt} = (1, d\vec{x}/dt)$. We integrate over all the paths starting at $\vec{x}_{\text{i}}$ and ending at $\vec{x}_{\text{f}}$, with the dynamics determined only by the coupling to the electromagnetic field.

Defining the photon propagator $G_{\mu\nu}(x)$, we integrate out the electromagnetic field and obtain the effective action

$$C(\vec{x}_{\text{f}} - \vec{x}_{\text{i}}, t_{\text{f}} - t_{\text{i}}) \equiv \int_{\vec{x}_{\text{i}}(t_{\text{i}})}^{\vec{x}_{\text{f}}(t_{\text{f}})} \mathscr{D}\vec{x} e^{\mathscr{S}_{\text{eff}}[x]},$$

where

$$S_{\text{eff}}[x] = q^2 \int dt dt' v^\mu(t) v^\nu(t') G^{\mu\nu}\left[\vec{x}(t) - \vec{x}(t'), t - t'\right].$$

Adopting the Feynman gauge, we have $G_{\mu\nu}(x) \propto \frac{e^2 \eta_{\mu\nu}}{x^2}$, with x a four-vector. Plugging this in, we obtain

$$S_{\text{eff}} = \frac{(qe)^2}{8\pi^2} \int dt dt' v^\mu(t) v^\nu(t') \eta_{\mu\nu} \frac{1}{(t - t')^2 - (\vec{x}(t) - \vec{x}(t'))^2} \tag{B.18}$$

$$= \frac{(qe)^2}{8\pi^2} \int dx^\mu dx'^\nu \eta_{\mu\nu} \frac{1}{(x - x')^2}, \tag{B.19}$$

with x, x' four-vectors.

The effective action can now be cast as

$$S_{\text{eff}} = \frac{(qe)^2}{8\pi^2} \int d\tau d\tau' \frac{dx^\mu}{d\tau} \frac{dx'^\nu}{d\tau'} \eta_{\mu\nu} \frac{1}{(x(\tau) - x(\tau'))^2}, \tag{B.20}$$

in terms of the (Lorentz invariant) proper time τ along the path. We now split the integral over τ into infinitely many infinitesimal segments, each of which is Lorentz invariant. Therefore, for each τ we can choose to write the corresponding segment in an inertial frame of reference comoving with $x^\mu(\tau)$ (Notice that for each point τ on the path we use a distinct frame of reference). In this case, $\frac{dx^\mu}{d\tau} = (1, 0, 0, 0)$, and we get

$$\frac{dx^\mu}{d\tau} \frac{dx'^\nu}{d\tau'} \eta_{\mu\nu} = \frac{dt'}{d\tau'}.$$

As can be seen by examining the denominator of Eq. (B.20), the dominant contributions arise from the vicinity of $\tau' = \tau$. Therefore, to leading order in $\tau - \tau'$ we take

$$x^\mu(\tau) - x^\mu(\tau') = \frac{dx^\mu(\tau)}{d\tau}(\tau' - \tau) = \delta_0^\mu(\tau - \tau')$$

$$dt' = d\tau' = d\tau.$$

This results in

$$\mathscr{S}_{\text{eff}} = \frac{(qe)^2}{8\pi^2} \int_0^T d\tau \int_0^T d\tau' \frac{1}{(\tau - \tau')^2},$$

with T the proper time at the end of the path. To regularize the integral we introduce a cutoff:

$$
\begin{aligned}
S_{\text{eff}} &= \frac{(qe)^2}{8\pi^2} \int_0^T d\tau \int_0^T d\tau' \frac{1}{(\tau - \tau' + i\varepsilon)^2} \\
&= \frac{(qe)^2}{8\pi^2} \left[2\log\frac{\varepsilon}{T} - \log\left(1 + \left(\frac{\varepsilon}{T}\right)^2\right) \right] \approx \frac{(qe)^2}{4\pi^2} \log\frac{\varepsilon}{T}.
\end{aligned}
$$

This finally gives us the propagator

$$
C(x_{\text{f}} - x_{\text{i}}) \propto e^{\frac{(qe)^2}{4\pi^2} \log\frac{\varepsilon}{|x_{\text{f}} - x_{\text{i}}|}} \propto \left(|x_{\text{f}} - x_{\text{i}}|\right)^{-\frac{(qe)^2}{4\pi^2}}.
$$

B.5   Distinction between gapped phases

In this section we comment on the distinction between the two gapped phases discussed in chapter 7 (in the absence of additional discrete symmetries).

As discussed in chapter 7, for $m = \Delta = 0$, one finds two dual Weyl nodes located at the edge of the Brillouin zone at $k_z = \pm\frac{\pi}{2}$ (and $k_x = k_y = 0$), thus forming the parent Dirac theory.

Introducing $m, \Delta \neq 0$, the nodes are shifted to $k_z = \pm k_0$, with

$$
k_0 = \cos^{-1}\left(\frac{\sqrt{m^2 - \Delta^2}}{2\chi_0}\right). \tag{B.21}
$$

It is evident that m pushes the nodes toward the origin at $k_z = 0$, while Δ pushes them toward the edge of the Brillouin zone. If the cones meet at either of these points, they generically annihilate each other, leading to completely gapped phases. Depending on where the cones meet, we obtain two distinct gapped phases.

One can understand the distinction between the two phases by examining the Bloch Hamiltonian at fixed values of k_z: $H_{k_z}(k_x, k_y)$. Given k_z, these two-dimensional Hamiltonians can be associated with an integer Chern number $C(k_z)$. Notice that the Chern number is defined in the BDG formulation, and therefore counts the number of chiral Majorana edge modes for the effective two-dimensional models. In particular, $C = 2$ corresponds to a single chiral fermion on the edge (i.e., two Majorana modes).

In our model, this Chern number is given by

$$
C(k_z) = \begin{cases} 0 & |k_z| < k_0 \\ 2 & |k_z| > k_0 \end{cases}.
$$

Indeed, the points where the Chern number transitions from one value to another and the gap must therefore close, correspond to the locations of the Weyl nodes.

From Eq. (B.21), we see that the Weyl cones survive as long as $|\Delta| < |m|$ and $m^2 < 4\chi_0^2 + \Delta^2$. If Δ is increased such that $|\Delta| = |m|$, the nodes meet at the edge of the Brillouin zone. As they move toward the edge of the Brillouin zone, the region of non-zero C shrinks, and eventually vanishes, leaving us with $C = 0$ throughout the Brillouin zone when they meet. For $|\Delta| > |m|$, the two cones gap out, leading to a trivially gapped state with $C = 0$ for all k_z.

On the other hand, if we increase m instead of Δ, the nodes are shifted toward the origin of the Brillouin zone, thus enlarging the non-trivial region of $C = 2$. Eventually, at $m^2 = 4\chi_0^2 + \Delta^2$, the two cones meet at the origin, and the non-trivial region of $C = 2$ covers the entire Brillouin zone. For larger values of m, the cones annihilate out and we end up with a gapped phase associated with a Chern number $C = 2$ for each k_z. Such a phase is adiabatically connectable to a stack of Chern insulators (with a single chiral fermionic edge mode) forming a 3D quantum Hall state of dual fermions. While such a state has no electronic response, it possesses a thermal Hall conductivity, and is thus referred to as a thermal Hall insulator.

As we discussed in chapter 7, additional scenarios arise where Δ is not identical in all layers. Generically, each of the Weyl cones splits into two Majorana-Weyl cones [160], located at $k_z = -k_2, -k_1, k_1, k_2$. In this case, the Chern number is given by

$$C(k_z) = \begin{cases} 0 & |k_z| < k_1 \\ 1 & k_1 < |k_z| < k_2 \\ 2 & |k_z| > k_2 \end{cases}.$$

A distinct gapped phase can be stabilized if k_2 is shifted toward the edge of the Brillouin zone, while k_1 is shifted toward the origin. This results in a gapped phase associated with $C = 1$ for all k_z. Such a phase is adiabatically connectable to a stack of dual-fermion $p + ip$ superconductors associated with each two-layer unit cell.

Appendix C

Appendix: Spin liquids from Majorana Zero Modes in a Cooper Box

The Response Function

In chapter 8, we proposed that the critical nature of our 1D spin models can be revealed by studying the effect of perturbations of the form $H_{\text{pert}} = f(t)S^z(x_0)$, with $f(t) = V_0 \cos(\omega t + \phi_0)$. To do that, we would like to compute the average value of S^z at a distant point x and later times.

Performing linear response, this can be written as

$$\langle S^z(x,t) \rangle = \int dt' f(t') \chi(t-t', x-x_0), \tag{C.1}$$

with χ being the dynamic susceptibility: $\chi(t-t', x-x') = i \langle [S^z(x,t), S^z(x',t')] \rangle \Theta(t-t')$. In our case, the function f is harmonic, meaning we may write

$$\begin{aligned}
\langle S^z(x,t) \rangle &= V_0 \Re \left\{ e^{i\phi_0} \int dt' e^{i\omega t'} \chi(t-t', x-x_0) \right\} \\
&= V_0 \Re \left\{ e^{i\omega t} e^{i\phi_0} \chi(\omega, x-x_0) \right\}, \tag{C.2}
\end{aligned}$$

where $\chi(\omega, x) = \int dt e^{-i\omega t} \chi(t,x)$ is the frequency domain form of the dynamic susceptibility.

The susceptibility can be written in terms of the time-ordered propagator as

$$\chi(t,x) = -2\Theta(t)\text{Im}\{G(t,x)\}.$$

The time ordered propagators of one-dimensional CFTs can generally be written as

$$G(t,x) = \frac{\alpha^{2(h+\bar{h})}}{[x - vt + i\varepsilon \operatorname{sign}(t)]^{2h} [x + vt - i\varepsilon \operatorname{sign}(t)]^{2\bar{h}}},$$

where $h, \bar{h}$ are the conformal dimensions of the corresponding field. For a non-chiral field, we have $h = \bar{h}$. For a chiral field, one of these vanishes.

Non-chiral fields

For non-chiral fields, the susceptibility is given by

$$\chi(t,x) = -2\Theta(t)\alpha^{4h} \operatorname{Im} \left\{ \frac{1}{[x - vt + i\varepsilon]^{2h} [x + vt - i\varepsilon]^{2h}} \right\}$$
$$= -2\Theta(t)\alpha^{4h} \operatorname{Im} \left\{ e^{-2h \log A} \right\},$$

where we follow Ref. [182] in defining

$$A = (x - vt + i\varepsilon)(x + vt - i\varepsilon)$$
$$= x^2 - v^2 t^2 + 2i\varepsilon t.$$

If we put the branch cut of the log along the negative real axis, we get an imaginary part only for $x^2 - v^2 t^2 < 0$, i.e. $t > \frac{|x|}{v}$, and we get

$$e^{-2h \log A} = e^{-2h \log \left| x^2 - v^2 t^2 \right| - 2\pi i h \Theta\left(t + \frac{x}{v}\right)\Theta\left(t - \frac{x}{v}\right)}.$$

We therefore obtain

$$\chi(t,x) = -2\sin(2\pi h)\, \alpha^{4h} \frac{\Theta(t)\Theta\left(t + \frac{x}{v}\right)\Theta\left(t - \frac{x}{v}\right)}{\left(v^2 t^2 - x^2\right)^{2h}}. \tag{C.3}$$

If $h = 1/2$, this expression vanishes. This result is non-physical, and indeed, the case

$h = 1/2$ requires special attention. In this case, we can explicitly write

$$
\begin{aligned}
\chi(t,x) &= -2\Theta(t)\alpha^2 \mathrm{Im}\left\{\left(\frac{1}{x-vt+i\varepsilon}\right)\left(\frac{1}{x+vt-i\varepsilon}\right)\right\} \\
&= -2\Theta(t)\alpha^2 \mathrm{Im}\left\{\left[\mathscr{P}\frac{1}{x-vt}-i\pi\delta\left(x-vt\right)\right]\left[\mathscr{P}\frac{1}{x+vt}+i\pi\delta\left(x+vt\right)\right]\right\} \\
&= -2\pi\Theta(t)\alpha^2\left[\frac{1}{x-vt}\delta\left(x+vt\right)-\frac{1}{x+vt}\delta\left(x-vt\right)\right],
\end{aligned}
\tag{C.4}
$$

where $\mathscr{P}$ denotes the principal value.

In order to evaluate Eq. C.2 for a general h, we wish to get the frequency domain form of $\chi(t,x)$ in Eq. C.3:

$$
\begin{aligned}
\chi(\omega,x) &= 2\alpha^{4h}\sin\left(2\pi h\right)\int_{\frac{|x|}{v}}^{\infty}dt\,\frac{e^{-i\omega t}}{\left(v^2t^2-x^2\right)^{2h}} \\
&= \frac{2\alpha^{4h}\sin\left(2\pi h\right)}{v\,|x|^{4h-1}}\int_{1}^{\infty}dT\,\frac{e^{-i\frac{\omega|x|}{v}T}}{\left(T^2-1\right)^{2h}},
\end{aligned}
$$

where we have defined $T = \frac{vt}{|x|}$. Performing the integral, we obtain

$$
\chi(\omega,x) = B\alpha^{4h}v^{-2h-\frac{1}{2}}\left(\frac{\omega}{|x|}\right)^{2h-\frac{1}{2}}K_{\frac{1}{2}-2h}\left[i\frac{\omega\,|x|}{v}\right],
\tag{C.5}
$$

with $B = \frac{2\sin(2\pi h)\Gamma(1-2h)(-2i)^{\frac{1}{2}-2h}}{\sqrt{\pi}}$. Notice that while Eq. C.3 vanishes for $h = 1/2$, Eq. C.5 has a finite limit for $h \to 1/2$. In this case, since $\sin\left(2\pi h\right)\Gamma\left(1-2h\right) \to const$ as $h \to 1/2$, and $K_{-\frac{1}{2}}[z] = \sqrt{\frac{\pi}{2}}\frac{e^{-z}}{\sqrt{z}}$, we get

$$
\chi(\omega,x) \propto \alpha^2\frac{e^{-i\frac{\omega|x|}{v}}}{v\,|x|}.
$$

We can obtain this result directly from Eq. C.4. In this case

$$
\begin{aligned}
\chi(\omega,x) &= -2\pi\alpha^2\int_{0}^{\infty}dt\left[\frac{1}{x-vt}\delta\left(x+vt\right)-\frac{1}{x+vt}\delta\left(x-vt\right)\right]e^{-i\omega t} \\
&= \frac{\pi\alpha^2}{v}\left[-\frac{1}{x}\Theta(-x)e^{i\omega\frac{x}{v}}+\frac{1}{x}\Theta(x)e^{-i\omega\frac{x}{v}}\right] = \frac{\pi\alpha^2}{v}\frac{e^{-i\omega\frac{|x|}{v}}}{|x|}.
\end{aligned}
$$

Chiral fields

For chiral (right moving) fields, the susceptibility is given by

$$\chi(t,x) = -2\alpha^{2h}\Theta(t)\mathrm{Im}\left\{\frac{1}{[x-vt+i\varepsilon]^{2h}}\right\}$$
$$= -2\alpha^{2h}\Theta(t)\mathrm{Im}\left\{e^{-2h\log A}\right\},$$

where now

$$A = x - vt + i\varepsilon.$$

The same analysis as in the non-chiral case indicates that

$$e^{-2h\log A} = e^{-2h\log|x-vt|-2\pi ih\Theta\left(t-\frac{x}{v}\right)},$$

and therefore

$$\chi(t,x) = -2\sin(2\pi h)\,\alpha^{2h}\frac{\Theta(t)\Theta\left(t-\frac{x}{v}\right)}{(vt-x)^{2h}}. \tag{C.6}$$

Calculating the Fourier transform, we obtain

$$\chi(\omega,x) = \frac{2\alpha^{2h}\sin(2\pi h)}{v\cdot x^{2h-1}}\int_1^\infty dT\,\frac{e^{-i\frac{\omega x}{v}T}}{(T-1)^{2h}}$$
$$= C\frac{\omega^{2h-1}\alpha^{2h}}{v^{2h}}e^{-i\frac{\omega x}{v}},$$

with $C = 2\sin(2\pi h)\,i^{2h-1}\Gamma(1-2h)$.